

NO-A182 891

VISCOUS/INVISCID INTERACTION ANALYSIS OF THE
AERODYNAMIC PERFORMANCE OF THE NACA 65-213 AIRFOIL(U)
NAVAL POSTGRADUATE SCHOOL MONTEREY CA P H SUBROTO

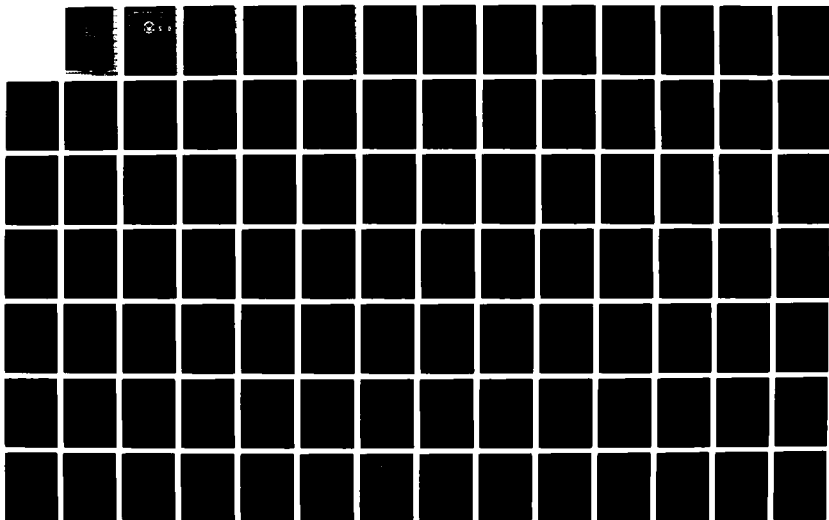
1/2

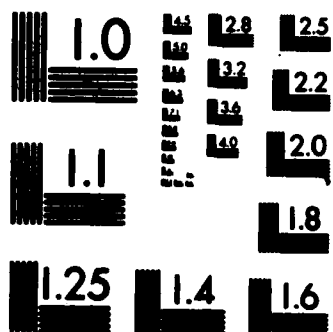
UNCLASSIFIED

MAR 87

F/G 28/4

NL





MICROCOPY RESOLUTION TEST CHART
NATIONAL BUREAU OF STANDARDS-1963-A

AD-A182 091

NAVAL POSTGRADUATE SCHOOL

Monterey, California

DTIC FILE COPY



DTIC
ELECTE
JUL 09 1987
S D

THESIS

VISCOUS/INVISCID INTERACTION ANALYSIS
OF THE AERODYNAMIC PERFORMANCE OF
THE NACA 65-213 AIRFOIL

by

Phutut H. Subroto

March 1987

Thesis Advisor

M. F. Platzer

Approved for public release; distribution is unlimited.

UNCLASSIFIED

AD A162091

REPORT DOCUMENTATION PAGE

1. REPORT SECURITY CLASSIFICATION Unclassified		2. RESTRICTIVE MARKINGS	
3. DECLASSIFICATION/DOWNGRADING SCHEDULE		4. DISTRIBUTION/AVAILABILITY OF REPORT Approved for public release ; distribution is unlimited	
5. PERFORMING ORGANIZATION REPORT NUMBER(S)		6. MONITORING ORGANIZATION REPORT NUMBER(S)	
7a. NAME OF PERFORMING ORGANIZATION Naval Postgraduate School	7b. OFFICE SYMBOL (If applicable) Code 67	8. NAME OF MONITORING ORGANIZATION Naval Postgraduate School	
9a. ADDRESS (City, State, and ZIP Code) Monterey, California 93943-5000		9b. ADDRESS (City, State, and ZIP Code) Monterey, California 93943-5000	
10a. NAME OF FUNDING SPONSORING ORGANIZATION	10b. OFFICE SYMBOL (If applicable)	11. PROCUREMENT INSTRUMENT IDENTIFICATION NUMBER	
12. ADDRESS (City, State, and ZIP Code)		13. SOURCE OF FUNDING NUMBERS PROGRAM ELEMENT NO PROJECT NO TASK NO WORK UNIT ACCESS OR NO	
14. INCLUDE SECURITY CLASSIFICATION Viscous/Inviscid Interaction Analysis of the Aerodynamic Performance of the NACA 65-213 Airfoil.			
15. PERSONAL AUTHOR(S) Subroto, Phutut Hadi			
16. TYPE OF REPORT Master's Thesis	17. TIME COVERED FROM TO	18. DATE OF REPORT (Year Month Day) 1987, March	19. PAGE COUNT 112
20. SUPPLEMENTARY NOTATION			
21. COSAT CODES FIELD GROUP SUB-GROUP		22. SUBJECT TERMS (Continue on reverse if necessary and identify by block number) Viscous/Inviscid Interaction Method Airfoil Flows	
23. ABSTRACT (Continue on reverse if necessary and identify by block number) → Cebeci's viscous/inviscid interaction program was applied to the analysis of steady two-dimensional incompressible flow past a NACA 65-213 airfoil at zero angle of attack at a Reynolds number of 240,000. Predicted boundary layer characteristics were found to be quite sensitive to the choice of boundary layer transition begin and length. Good agreement with the experimental results of Hoheisel et al could be obtained by proper choice of both transition begin and length. Keywords: Airfoil Flows, Viscous			
24. DISTRIBUTION/AVAILABILITY OF ABSTRACT <input checked="" type="checkbox"/> UNCLASSIFIED/UNLIMITED <input type="checkbox"/> SAME AS RPT <input type="checkbox"/> DTIC USERS		25. ABSTRACT SECURITY CLASSIFICATION Unclassified	
26. NAME OF RESPONSIBLE INDIVIDUAL Prof. Max F. Platzer		27a. TELEPHONE (Include Area Code) (408) 646-2944	27b. OFFICE SYMBOL 67P1

FORM 1473, 84 MAR

83 APR edition may be used until exhausted
All other editions are obsolete

SECURITY CLASSIFICATION OF THIS PAGE

UNCLASSIFIED

Approved for public release; distribution is unlimited.

— Viscous/Inviscid Interaction Analysis
of the Aerodynamic Performance of
the NACA 65-213 Airfoil

by

Phutut H. Subroto
Captain, Indonesian Air Force
B.S., Indonesian Air Force Academy, 1975

Submitted in partial fulfillment of the
requirements for the degree of

MASTER OF SCIENCE IN AERONAUTICAL ENGINEERING

from the

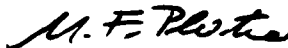
NAVAL POSTGRADUATE SCHOOL
March 1987

Author:

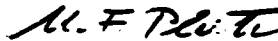


Phutut H. Subroto

Approved by:



M. F. Platzer, Thesis Advisor



M. F. Platzer, Chairman,
Department of Aeronautics



Gordon E. Schacher,
Dean of Science and Engineering

ABSTRACT

Cebeci's viscous-inviscid interaction program was applied to the analysis of steady two dimensional incompressible flow past a NACA 65-213 airfoil at zero angle of attack at a Reynolds number of 240,000. Predicted boundary layer characteristics were found to be quite sensitive to the choice of boundary layer transition begin and length. Good agreement with the experimental results of *Hoheisel et al* could be obtained by proper choice of both transition begin and length.

Accession For	
NTIS	CRA&I <input checked="" type="checkbox"/>
DTIC	TAB <input type="checkbox"/>
Unannounced	<input type="checkbox"/>
Justification	
By	
Distribution /	
Availability Codes	
Dist	Avail and/or Special
A-1	

TABLE OF CONTENTS

I.	INTRODUCTION	10
II.	FUNDAMENTAL EQUATIONS	11
A.	CONSERVATION OF MASS	11
B.	CONSERVATION OF MOMENTUM	13
C.	INVISCID FLOW EQUATION	18
1.	Potential Flow	18
2.	Governing Equation for irrotational, incompressible flow : Laplace Equation.	20
D.	BOUNDARY LAYER EQUATION	20
E.	TURBULENT FLOW EQUATION	22
III.	PANEL METHOD	24
A.	INTRODUCTION	24
1.	Single Source and Source Panel	24
2.	Single Vortex and Vortex Panel	25
B.	SOURCE AND VORTEX DISTRIBUTION	27
1.	Flow Tangency Condition	31
2.	Concept of the Influence Coefficient	32
3.	Computation of Total Disturbance Velocity V	33
4.	Kutta Condition	35
5.	Determination of the vortex strength	35
6.	Determination of the source strength	37
7.	Calculation of 'on body' velocities	37
C.	LINEARLY VARYING VORTEX DISTRIBUTION	38
1.	Kutta Condition	42
2.	Calculation of the 'on body' velocities	43
3.	Calculation of C_p, C_L, C_D and C_M	44
D.	DISCUSSION OF THE PROGRAM PANEL	44
1.	Input Data	46

2. Program output	46
E. DISCUSSION OF THE RESULTS	46
IV. VISCOUS FLOW METHOD	49
A. DIRECT BOUNDARY LAYER METHOD	50
1. The Box Method	51
2. Newton's Method	54
3. Keller's Block Elimination Method	56
B. INTERACTIVE BOUNDARY LAYER METHOD	57
C. INTERACTION MODEL	65
D. TURBULENCE MODELLING	75
E. DISCUSSION OF THE COMPUTER PROGRAM	77
1. Inviscid Flow Method	77
2. Interactive Viscous Flow Method	78
F. DISCUSSION OF THE RESULTS	80
1. High Reynolds Number Flows	80
2. Low Reynolds Number Flows	80
V. CONCLUSION AND RECOMMENDATION	97
APPENDIX A: FORTRAN PROGRAM	98
APPENDIX B: PROGRAM OUTPUT	103
APPENDIX C: TABLE I	104
APPENDIX D: TABLE II	105
APPENDIX E: TABLE III	106
APPENDIX F: TABLE IV	107
LIST OF REFERENCES	108
INITIAL DISTRIBUTION LIST	110

LIST OF TABLES

1. DESCRIPTION OF THE PROGRAM OUTPUT	46
2. EFFECT OF GGTR AND XTRU ON THE BUBBLE LENGTH	104
3. EFFECT OF GGTR AND XTRU ON THE SHAPE FACTOR(H) AT POINT OF ZERO SKIN FRICTION	105
4. EFFECT OF GGTR AND XTRU ON THE DRAG COEFFICIENT (CD)	106
5. EFFECT OF GGTR AND XTRU ON THE LIFT COEFFICIENT (CL)	107

LIST OF FIGURES

2.1	Sketch illustrating the velocity and the density for mass flow balance through a fixed volume in 2-D	12
2.2	Stresses acting on a 2-D element of fluid.	15
3.1	Vortex Sheet Representation	26
3.2	Discretization: a). Actual airfoil b). Airfoil after discretization	29
3.3	Representation of i-th and j-th panels in the Panel Method	30
3.4	Replacement of an airfoil by vortex panels of linearly varying vortex strength	40
3.5	Source and Vortex Panel Method	45
3.6	Comparison of pressure distributions on the NACA 23012 airfoil using the original Smith-Hess-panel method (source and vortex panels) and the vortex panel method.	47
4.1	Net rectangle for finite difference approximation	53
4.2	Direct, Inverse and Semi Inverse method	66
4.2d	Viscous-Inviscid Interaction Method	68
4.3	Concept of blowing velocity	69
4.4	Application of the Direct and Interactive Method	71
4.5	Lift curves of the Wortmann FX 60-126 airfoil at $Re = 700,000$, $1,000,000$ and $2,000,000$ (source of experimental results: Ref.18)	79
4.6	Phenomenological features of the boundary layer on the low Reynolds Number airfoil	81
4.7	Experimental result for the NACA 65-213 (by Hoheisel et al.) $Ma =$	82
4.8	Skin friction distribution on the NACA 65-213 for $G_{ytr} = 120$ and $XTRU = 0.64$	84
4.9	Effect of variation of $XTRU$ for $G_{ytr} = 20$ on the velocity distribution	85
4.10	Effect of variation of $XTRU$ for $G_{ytr} = 40$ on the velocity distribution	86
4.11	Effect of variation of G_{ytr} for $XTRU = 0.68$ on the distributions of skin friction and intermittency factor	87
4.12	Effect of variation of $XTRU$ (begin of transition) for $G_{ytr} = 20$ on the distributions of skin friction and intermittency factor	88
4.13	Velocity profiles in front of the bubble at $x/c = 0.367, 0.483$ and 0.609	89
4.14	Velocity profiles in the bubble region at $x/c = 0.739$ and 0.774	90

4.15	Comparison of δ^* at 1θ with experimental results	91
4.16	Boundary layer profiles on the NACA 65-213 at $Re = 240,000$ AOA = 0 deg and $G_{ytr} = 10$	92
4.17	Boundary layer profile on the NACA 65-213 at $Re = 240,000$ AOA = 0 deg and $G_{ytr} = 20$	93
4.18	Boundary layer profile on the NACA 65-213 at $Re = 240,000$ AOA = 0 deg and $G_{ytr} = 30$	94
4.19	Boundary layer profile on the NACA 65-213 at $Re = 240,000$ AOA = 0 deg and $G_{ytr} = 40$	95
4.20	Boundary layer profile on the NACA 65-213 at $Re = 240,000$ AOA = 0 deg and $G_{ytr} = 50$	96

ACKNOWLEDGEMENTS

The author gratefully acknowledges Prof. M.F. Platzer for his excellent guidance. And Mr. Andreas Krainer who helped to make this program run smoothly. This thesis is also dedicated to my wife Hernawatie, my daughter Cerri and my son Ganis. Thanks for their patience.

I. INTRODUCTION

The prediction of the stall characteristics is of major importance in aeronautical engineering to determine the operating limits of an aircraft. Therefore, the development of reliable and accurate numerical methods for predicting separated flow regions is one of the most challenging problems in *Computational Fluid Dynamics (CFD)*.

In this thesis we limit ourselves to the problem of incompressible two-dimensional airfoil flows. Two basic methods are available to compute viscous flows which include regions of flow separation. The first approach is based upon a solution of the full *Navier-Stokes* equations (or some approximate form, such as the parabolized Navier-Stokes equations). This approach has the disadvantage of being very expensive and time consuming. The second approach is based upon the so-called *Viscous-Inviscid Interaction Method*. The outer flow is computed using the inviscid flow equations. The inner flow (close to the airfoil) is obtained from a numerical solution of the Prandtl's boundary layer equation. However, in contrast to the well-known classical boundary layer computations the pressure cannot be prescribed a priori, but must be found iteratively (i.e., by viscous-inviscid interaction). This approach has the advantage of being much faster and more efficient than the Navier-Stokes solutions.

The approach chosen in this thesis is based upon the viscous-inviscid interaction method developed by T. Cebeci and collaborators at the *Douglas Aircraft Company*. In chapter 2 the fundamental equations are summarized. Chapter 3 is devoted to a discussion of the inviscid flow method, especially the so-called *Panel Method* first introduced [Ref. 4] by Hess and Smith. In chapter 4 the direct and interactive boundary layer methods are discussed, followed by a brief explanation of the turbulence model used. Finally, the computer program is explained and computed results are presented for the NACA 65-213 airfoil and compared with detailed measurements by Hoheisel et al. [Ref. 14].

II. FUNDAMENTAL EQUATIONS

This chapter presents the equations used in our analysis, which involve the development of:

1. Conservation of mass (Continuity equation)
2. Conservation of momentum (Newton's Second Law)
3. Inviscid flow equations
4. Boundary layer equation
5. Turbulence model

With these equations we can predict the behavior of a body moving through the fluid. In our case we are dealing with an airfoil in two dimensional, steady, inviscid and viscous flow.

A. CONSERVATION OF MASS

Let us apply the principle of conservation of mass to a small volume of space through which the fluid can move freely. For convenience, we shall use a cartesian coordinate system (x, y, z) . Furthermore, in the interest of simplicity, we shall treat a 2-D flow, that is, one in which there is no flow along the z -axis. Flow patterns are the same for any x - y plane. As indicated in the sketch of Figure 2.1, the component of the fluid velocity in the x direction will be designated by u , and in the y direction by v . The net outflow of mass through the surface surrounding the volume must be equal to the decrease of mass within the volume. The mass flow rate through the surface bounding the element is equal to the product of the density, the velocity component normal to the surface, and area of that surface.

A first-order Taylor series expansion is used to evaluate the flow properties at the faces of the element [Ref. 3] since the properties are a function of position. Consider the flow out of the volume as positive, then the net outflow of mass per-unit time is the summation of

$$\left[\rho u - \frac{\partial}{\partial x}(\rho u) \frac{\Delta x}{2} \right] \Delta y + \left[\rho u + \frac{\partial}{\partial x}(\rho u) \frac{\Delta x}{2} \right] \Delta y + \left[\rho v + \frac{\partial}{\partial y}(\rho v) \frac{\Delta y}{2} \right] \Delta x + \left[\rho v - \frac{\partial}{\partial y}(\rho v) \frac{\Delta y}{2} \right] \Delta x \quad (2.1)$$

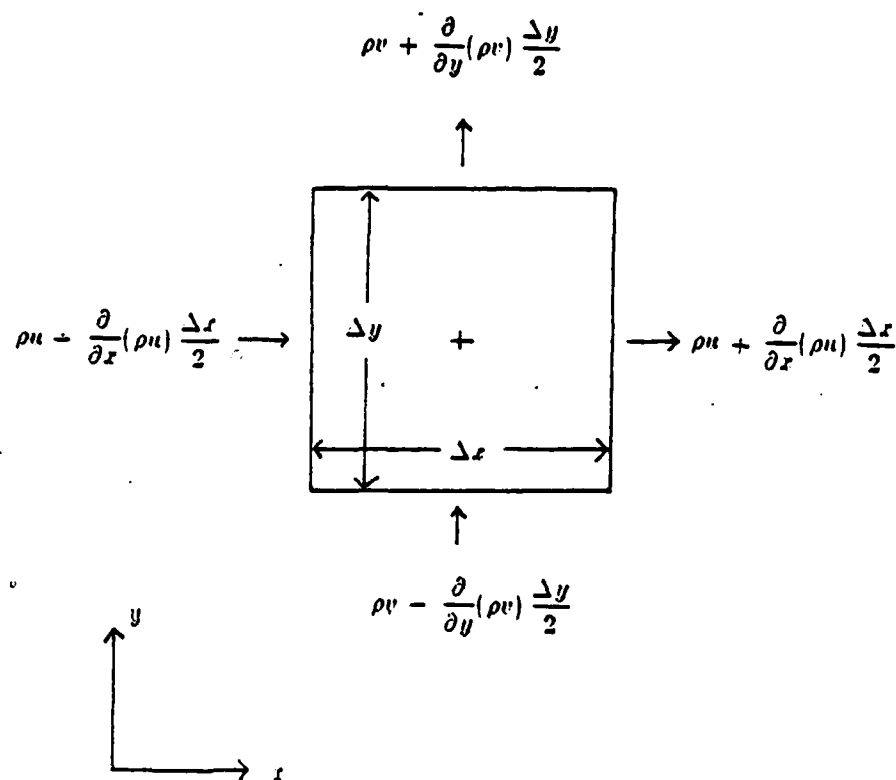


Figure 2.1 Sketch illustrating the velocity and the density for mass flow balance through a fixed volume in 2-D.

which must equal the rate at which the mass contained within the element decreases

$$- \frac{\partial \rho}{\partial t} \Delta x \Delta y \quad (2.2)$$

Combining equation 2.1 and 2.2, dividing by $\Delta x \Delta y$, one gets

$$\frac{\partial \rho}{\partial t} + \frac{\partial}{\partial x}(\rho u) + \frac{\partial}{\partial y}(\rho v) = 0 \quad (2.3)$$

In vector form, equation 2.3 is

$$\frac{\partial \rho}{\partial t} + \nabla \cdot (\rho \vec{v}) = 0 \quad (2.4)$$

Because the pressure variations that occur in relatively low speed flow are sufficiently small, the density is essentially constant. For these incompressible flows, the continuity equation becomes

$$\frac{\partial u}{\partial x} + \frac{\partial v}{\partial y} = 0 \quad (2.5)$$

$$\text{or, in vector form } \nabla \cdot \vec{v} = 0 \quad (2.6)$$

B. CONSERVATION OF MOMENTUM

The equation of the conservation of linear momentum is obtained by applying Newton's 2nd Law [Ref. 3] where the net force acting on a fluid particle is equal to the time rate of change of the linear momentum of the fluid particle. As the fluid moves in space, its shape and volume may change, but its mass is conserved. Thus, using a coordinate system that is neither accelerating nor rotating, called an inertial coordinate system, we may write

$$\vec{F} = m \frac{D\vec{V}}{Dt} \quad (2.7)$$

The velocity \vec{V} of a fluid particle is, in general, an explicit function of time t as well as of its position x, y . Furthermore, the position coordinates x, y of the fluid particle are themselves a function of time. Since the time differentiation of equation 2.7 follows a given particle in its motion, the derivative is frequently termed the particle or substantial derivative of \vec{V} , since $\vec{V}(x, y, t)$ and $x(t), y(t)$.

$$\frac{D\vec{V}}{Dt} = u \frac{\partial \vec{V}}{\partial x} + v \frac{\partial \vec{V}}{\partial y} + \frac{\partial \vec{V}}{\partial t} \quad (2.8)$$

where, $u = \frac{dx}{dt}$ and $v = \frac{dy}{dt}$

Therefore, the acceleration of a fluid particle is

$$\frac{D\vec{V}}{Dt} = \frac{\partial \vec{V}}{\partial t} + (\vec{V} \cdot \nabla) \vec{V} \quad (2.9)$$

Thus, the substantial derivative is the sum of the local, time dependent changes that occur at a point in the flow field and of the convection in space. When the local, time dependent changes are zero, $\partial \vec{V} / \partial t = 0$, such flows are known as steady-state flows. The principal forces that act on the body are those which act directly on the mass of the fluid element, the *body forces*, and those which act on its surface, the *pressure forces and shear forces* known as *surface forces*. The stress system acting on an element of the surface is illustrated in Figure 2-2. The stress components τ acting on the small cube are assigned subscripts. The first subscript indicates the direction of the normal direction to the surface on which the stress acts and the second subscript indicates the direction in which the stress acts. Thus, τ_{xy} denotes a stress acting in the y direction on the surface whose normal points in the x direction. The properties of most fluids have no preferred direction in space; that is, fluids are isotropic.

Again, the stresses on the fluid element can be obtained from a Taylor series expansion. In general, the various stresses change from point to point. Thus, they

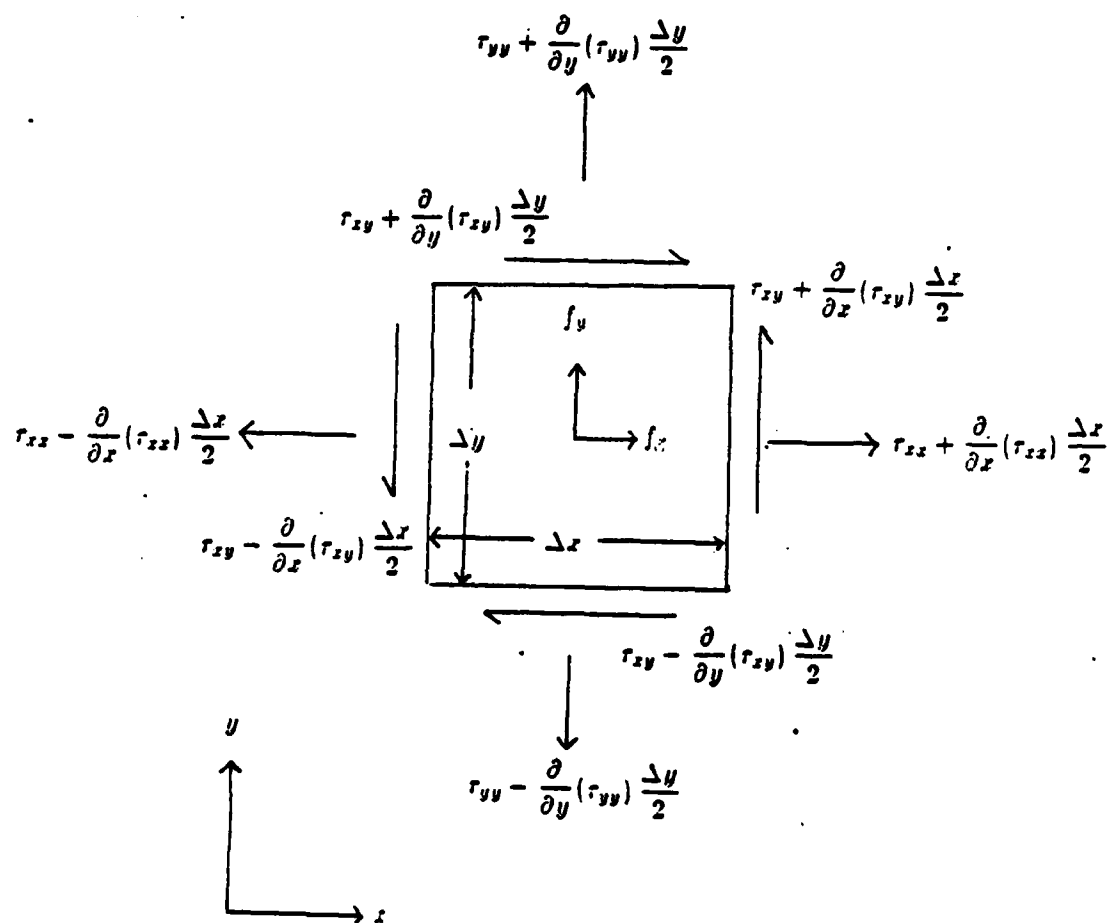


Figure 2.2 Stresses acting on a 2-D element of fluid.

produce net forces on the fluid particle, which cause it to accelerate. The forces acting on each surface are obtained by taking into account the variations of stress with position, by using the center of the element as a reference point.

To simplify the illustration of the force balance on the fluid particle we shall again consider a 2-D flow, as indicated in Figure 2-2. The resultant force in the x -direction, for one unit length in z is

$$F_x = \rho f_x \Delta x \Delta y + \frac{\partial}{\partial x}(\tau_{xx}) \Delta x \Delta y + \frac{\partial}{\partial y}(\tau_{xy}) \Delta x \Delta y \quad (2.10)$$

Where f_x is the body force per-unit mass in the x direction. The most common body force for the flow fields is that of gravity. Equation 2.10 is the left hand side of equation 2.7. For the right hand side, combine mass term with equation 2.10 in the x direction

$$m \frac{Du}{Dt} = (\rho \Delta x \Delta y) \left[\frac{\partial u}{\partial t} + (\vec{V} \cdot \nabla) u \right] \quad (2.11)$$

From equation 2.10 and 2.11, substitute into equation 2.7 divided by $\Delta x \Delta y$ we have

$$\rho f_x + \frac{\partial}{\partial x} \tau_{xx} + \frac{\partial}{\partial y} \tau_{xy} = \rho \left[\frac{\partial u}{\partial t} + (\vec{V} \cdot \nabla) u \right] \quad (2.12)$$

similarly in the y direction

$$\rho f_y + \frac{\partial}{\partial x} \tau_{xy} + \frac{\partial}{\partial y} \tau_{yy} = \rho \left[\frac{\partial v}{\partial t} + (\vec{V} \cdot \nabla) v \right] \quad (2.13)$$

Next, we need a relation between the stresses and the motion of the fluid. For a fluid at rest or for inviscid fluid motion, there is no shearing stress and the normal stress is in the nature of a pressure. For fluid particles, the stress is related to the rate of strain by a physical law based on the following assumptions:

1. Stress components may be expressed as a linear function of the components of the rate of the strain. The friction law for 1-D flow of a *Newtonian fluid* is a special case of this linear stress/rate of strain relation, i.e., $\tau = \mu (\partial u / \partial y)$, where μ is the fluid viscosity.
2. The relation between the stress components and strain rate components must be invariant to a coordinate transformation consisting of either a rotation or a mirror reflection of axes, since a physical law cannot depend upon the choice of the coordinate system.
3. When all velocity gradients are zero (i.e., the shear stress, vanishes), the stress components must reduce to the hydrostatic pressure p .

For a fluid that satisfies these criteria, in two dimensional flow

$$\tau_{xx} = -p + 2\mu \frac{\partial u}{\partial x} - \frac{2}{3}\mu(\nabla \cdot \vec{v}) \quad (2.14)$$

$$\tau_{yy} = -p + 2\mu \frac{\partial v}{\partial y} - \frac{2}{3}\mu(\nabla \cdot \vec{v}) \quad (2.15)$$

$$\tau_{xy} = \mu \left[\frac{\partial u}{\partial y} + \frac{\partial v}{\partial x} \right] \quad (2.16)$$

with the appropriate expressions for the surface stresses, substitute into equation 2.12 and 2.13, we have

$$\rho \left[\frac{\partial u}{\partial t} + (\vec{v} \cdot \nabla)u \right] = \rho f_x - \frac{\partial p}{\partial x} + \frac{\partial}{\partial x} \left[2\mu \frac{\partial u}{\partial x} - \frac{2}{3}\mu(\nabla \cdot \vec{v}) \right] + \frac{\partial}{\partial y} \left[\mu \left(\frac{\partial u}{\partial y} + \frac{\partial v}{\partial x} \right) \right] \quad (2.17)$$

$$\rho \left[\frac{\partial v}{\partial t} + (\vec{v} \cdot \nabla)v \right] = \rho f_y - \frac{\partial p}{\partial y} + \frac{\partial}{\partial x} \left[\mu \left(\frac{\partial u}{\partial y} + \frac{\partial v}{\partial x} \right) \right] + \frac{\partial}{\partial y} \left[2\mu \frac{\partial v}{\partial y} - \frac{2}{3}\mu(\nabla \cdot \vec{v}) \right] \quad (2.18)$$

These general differential equations for the conservation of linear momentum are known as the *Navier - Stokes* equations. When we are dealing with incompressible and 2-D flow, then from equation 2.6, $\nabla \cdot \vec{V} = 0$, and the body forces are neglected, and $\tau_{xx} + \tau_{yy} = -2p$. Therefore equation 2.17 and 2.18 can be written as

$$u \frac{\partial u}{\partial x} + v \frac{\partial u}{\partial y} + \frac{\partial u}{\partial t} = -\frac{1}{\rho} \frac{\partial p}{\partial x} + \nu \left[\frac{\partial^2 u}{\partial x^2} + \frac{\partial^2 u}{\partial y^2} \right] \quad (2.19)$$

$$u \frac{\partial v}{\partial x} + v \frac{\partial v}{\partial y} + \frac{\partial v}{\partial t} = -\frac{1}{\rho} \frac{\partial p}{\partial y} + \nu \left[\frac{\partial^2 v}{\partial x^2} + \frac{\partial^2 v}{\partial y^2} \right] \quad (2.20)$$

These are the well known *Navier - Stokes equation for 2-D, incompressible, viscous flow*.

C. INVISCID FLOW EQUATION

Inviscid flow represents an ideal flow, where the effects of viscosity are zero. In reality, this is not true because every medium has viscosity, even though it may be very small.

Why is the inviscid flow important in dealing with a body moving in the viscous fluid?

In 1904 L. Prandtl came up with the answer. For high Reynolds Number on a body moving in a viscous fluid, two regions can be distinguished. The effect of viscosity can be neglected outside a very thin region near the body which is called boundary layer. Inside the boundary layer the viscous effects are important (further discussion in viscous flow section). This is the reason why the inviscid flow remains important in the computation of fluid dynamics, even though it represents an ideal case.

1. Potential Flow

Since the flow upstream of the body is uniform then it is also irrotational (in inviscid flow).

$$\xi = \nabla \times \vec{V} \quad (2.21)$$

Consider the following vector identity, if ϕ is a scalar function, then

$$\vec{r} \times (\nabla \varphi) = 0 \quad (2.22)$$

i.e., the curl of the gradient of a scalar function is identically zero. Comparing equation 2.21 and 2.22, we see that

$$\vec{r} = \nabla \varphi \quad (2.23)$$

Equation 2.23 states that for an irrotational flow there exists a scalar function φ such that the velocity is given by the gradient of φ . We denote φ as the *velocity potential*. φ is a function of the spatial coordinates, i.e., $\varphi = \varphi(x, y)$. And from the definition of the gradient in cartesian coordinates, equation 2.23 can be written as

$$u = \frac{\partial \varphi}{\partial x} \quad \text{and} \quad v = \frac{\partial \varphi}{\partial y} \quad (2.24)$$

Thus, φ has the property that its partial derivative in any direction is the velocity component in that direction. It follows that the existence of φ is the sole criterion for irrotationality. The usefulness of the velocity potential in flows of practical significance derives from the circumstance that, for a body in relative motion in an originally irrotational flow, the circulation vanishes around any contour that does not include the body or does not intersect the boundary layer or the wake, therefore, a velocity potential can be found to describe the flow everywhere outside the boundary layer or the wake. When a flow field is irrotational, hence allowing the velocity potential to be defined, there is a tremendous simplification. Instead of dealing with the velocity components (say, u, v and w) as the unknowns, hence requiring three equations for three unknowns, we can instead deal with the velocity potential as one unknown, therefore, requiring the solution of only one equation for the flow field and the velocity components can be obtained from equation 2.24. Because irrotational flows can be described by the velocity potential φ such flows are called *potential flows*.

2. Governing Equation for irrotational, incompressible flow : Laplace Equation.

We have seen from equation 2.6, that the conservation of mass for an incompressible flow takes the form $\nabla \cdot \vec{V} = 0$. In addition, for irrotational flow we have seen in equation 2.23, $\vec{V} = \nabla \phi$. Therefore, for a flow that is both incompressible and also irrotational, equations 2.6 and 2.23 can be combined to yield,

$$\nabla^2 \phi = 0. \quad \text{or} \quad \frac{\partial^2 u}{\partial x^2} + \frac{\partial^2 v}{\partial y^2} = 0 \quad (2.25)$$

Equation 2.25 is called *Laplace's Equation*, one of the most extensively studied equations in mathematical physics.

Note that Laplace's equation is a second order linear partial differential equation. The fact that it is *linear* is particularly important, because the superposition of any particular solution of a linear differential equation is also a solution of the equation. For example, if $\phi_1, \phi_2, \phi_3, \dots, \phi_n$ represent n separate solutions of equation 2.25, then the sum $\phi = \phi_1 + \phi_2 + \dots + \phi_n$ is also a solution of equation 2.25.

Since irrotational, incompressible flow is governed by Laplace's equation and Laplace's equation is linear, we conclude that a complicated flow pattern for an irrotational, incompressible flow can be synthesized by superposition of elementary flows which are also irrotational and incompressible. The singularity (or panel) methods presented in the next chapter are based on this idea.

D. BOUNDARY LAYER EQUATION

Up to this point, we have been dealing with flow outside the boundary layer, where viscous effects remain small. In the region within the boundary layer, velocity gradients are high even with very small viscosity. Therefore, it becomes very important to deal with a real fluid. Before the boundary layer can be analyzed further, we have to know what governing equations can be used in the practical analysis. The objective is to predict viscous flows by means of the boundary layer method, instead of solving the complete Navier-Stokes equations.

From the previous derivations, equations 2.5, 2.19 and 2.20 are used here. In order to simplify these equations we have to make some assumptions: two-dimensional, steady, constant fluid properties, and no body forces. Another important

assumption is that the boundary layer thickness is very small compared to the length of the body (airfoil in this case). With these assumptions, L. Prandtl in 1904 introduced the "order of magnitude" estimate into equation 2.5, 2.19 and 2.20. In order to do this, all linear dimensions will be referenced to the characteristic length l and all velocities will be referenced to U , therefore l and U can be said to have order of magnitude of one (written as $O(1)$) and with the above assumptions, y will correspond to the boundary layer thickness (δ). Then the continuity equation 2.5 can be written as

$$\left(\frac{U}{l}\right) \left(\frac{v}{\delta}\right) \quad \text{and} \quad (v) = O\left(\frac{U\delta}{l}\right)$$

Because δ is very small, from the above relation we can imply that v , the velocity in the y direction must be very small. Therefore, the continuity equation still holds in the boundary layer. From the Navier-Stokes equation in the x direction (eqn 2.19)

$$u \frac{\partial u}{\partial x} + v \frac{\partial u}{\partial y} = -\frac{1}{\rho} \frac{\partial p}{\partial x} + \nu \left[\frac{\partial^2 u}{\partial x^2} + \frac{\partial^2 u}{\partial y^2} \right] \quad (2.19)$$

Introducing the order of magnitude in the above equation, we have

$$\left(\frac{U^2}{l}\right) \cdot \left(\frac{U^2}{l}\right) \cdot \left(-\frac{P}{\rho l}\right) \cdot \left(\nu \frac{U}{l^2}\right) \cdot \left(\nu \frac{U}{\delta^2}\right)$$

If all above terms multiplied by $\left(\frac{l}{U^2}\right)$ then

$$(1) \cdot (1) \cdot \left(-\frac{P}{\rho U^2}\right) \cdot \left(\frac{1}{U l / \nu}\right) \cdot \left(\frac{l^2 / \delta^2}{U l / \nu}\right)$$

If the Reynolds Number is high, the fourth term

$$\frac{1}{U l / \nu} = O(\text{zero})$$

$$\frac{l^2 / \delta^2}{U l / \nu} = \frac{\text{very large}}{\text{large}} \neq \text{zero} \equiv O(1)$$

$$\text{therefore } \frac{l^2}{\delta^2} = O(R_e)$$

$$\frac{\delta}{x} = O\left(\sqrt{\frac{1}{R_e}}\right)$$

So, equation 2.19 becomes:

$$u \frac{\partial u}{\partial x} + v \frac{\partial u}{\partial y} = -\frac{1}{\rho} \frac{\partial p}{\partial x} + \nu \frac{\partial^2 u}{\partial y^2} \quad (2.26)$$

For the y direction (equation 2.20) in terms of order of magnitude we obtain

$$\left(\frac{U^2 \delta}{l^2} \right) \cdot \left(\frac{U^2 \delta}{l^2} \right) \cdot \left(-\frac{1}{\rho} \frac{\partial p}{\partial y} \right) \cdot \left(\nu \frac{U \delta}{l^3} \right) \cdot \left(\nu \frac{U}{\delta l} \right)$$

all above terms multiplied by $\left(\frac{\delta}{U l^2} \right)$ then

$$\left(\frac{\delta^2}{l^2} \right) \cdot \left(\frac{\delta^2}{l^2} \right) \cdot \left(-\frac{1}{\rho} \frac{\delta}{U^2} \frac{P}{\delta} \right) \cdot \left(\nu \frac{U \delta^2}{l^3 U^2} \right) \cdot \left(\nu \frac{U \delta}{\delta l U^2} \right)$$

$$\left(\frac{\delta^2}{l^2} \right) \cdot \left(\frac{\delta^2}{l^2} \right) \cdot \left(-\frac{1}{\rho} \frac{P}{U^2} \right) \cdot \left(\frac{\delta^2}{U l^2 / \nu} \right) \cdot \left(\frac{1}{U l / \nu} \right)$$

$$O\left(\frac{1}{Re}\right) \cdot O\left(\frac{1}{Re}\right) \cdot \left(-\frac{P}{\rho U^2}\right) \cdot O\left(\frac{1}{Re^2}\right) \cdot O\left(\frac{1}{Re}\right)$$

The only term left is the pressure term, because all other terms are of higher order

$$\frac{\partial p}{\partial y} = 0 \quad (2.27)$$

This is very important because it tells us that the pressure across the boundary layer remains constant. The triplet of equations (2.5 , 2.26 and 2.27) and the boundary condition of zero normal and tangential velocity are known as the *Prandtl's boundary layer equations*.

E. TURBULENT FLOW EQUATION

Since the continuity equation (2.5) and the Navier-Stokes equation (2.19) make no assumptions regarding the type of flow, they are instantaneously valid in both the *laminar* and *turbulent* flow regimes. However, it is too difficult to deal with instantaneous properties in turbulent flow. Therefore we introduce the time-averaged

properties. In our notation, prime denotes the fluctuation quantity, and bar denotes the mean value.

$$u = \bar{u} + u'$$

$$v = \bar{v} + v'$$

$$p = \bar{p} + p'$$

Introducing these properties into the continuity equation and averaging, we have

$$\overline{\frac{\partial}{\partial x}(\bar{u} + u') + \frac{\partial}{\partial y}(\bar{v} + v')} = 0$$

Carrying out the integration term by term (details are in [Ref. 17]), yields:

$$\overline{\frac{\partial}{\partial x}(\bar{u} + u')} + \overline{\frac{\partial}{\partial y}(\bar{v} + v')} = 0$$

$$\text{or} \quad \overline{\frac{\partial}{\partial x}(\bar{u})} + \overline{\frac{\partial}{\partial x}(u')} + \overline{\frac{\partial}{\partial y}(\bar{v})} + \overline{\frac{\partial}{\partial y}(v')} = 0$$

$$\text{since} \quad \overline{\frac{\partial}{\partial x}(\bar{u})} = \frac{\partial}{\partial x}(\bar{u}) = \frac{\partial}{\partial x}(\bar{u}) \quad \text{and} \quad \overline{\frac{\partial}{\partial x}(u')} = \frac{\partial}{\partial x}(\overline{u'}) = 0$$

Therefore the continuity equation for turbulent flow becomes;

$$\frac{\partial}{\partial x}(\bar{u}) + \frac{\partial}{\partial y}(\bar{v}) = 0 \quad (2.28)$$

A similar procedure can be applied to the Navier-Stokes Equation

$$\bar{u} \frac{\partial}{\partial x}(\bar{u}) + \bar{v} \frac{\partial}{\partial y}(\bar{u}) = -\frac{1}{\rho} \frac{\partial \bar{p}}{\partial x} + \nu \left[\frac{\partial^2 \bar{u}}{\partial x^2} + \frac{\partial^2 \bar{u}}{\partial y^2} \right] - \frac{\partial}{\partial x}(\overline{u'u'}) - \frac{\partial}{\partial y}(\overline{u'v'}) \quad (2.29)$$

The last two terms correspond to the normal and shear stress terms respectively, which we call the *Reynolds Stresses* or *Turbulent Stresses*.

III. PANEL METHOD

A. INTRODUCTION

The thin airfoil theory is just what it says, it applies only to a thin airfoil at small angle of attack. It is not much used these days for the analysis or design of single element airfoils. It does give fairly good results for airfoils of 12 % thickness or less. On the other hand, the determination of the aerodynamic characteristics of thick, highly cambered, slotted surfaces, with single or multiple flaps and mutual interference effects among wings, fuselage, nacelles, and so forth, requires, in general, the use of numerical methods.

In the 1960's Hess and Smith at McDonnell Douglas introduced a method, the so called *Panel Method* [Ref. 4], as a numerical approach for 2-D flows which can be extended to 3-D potential flow problems. Such methods are called panel methods because the body surface is approximated by a collection of *panels*. There are a number of ways to set up the panel method. To begin with, there are choices even as to the type of singularity used, sources, doublets, vortices or a combination of source and vortex distributions.

Panel methods as a numerical approach for predicting forces and moments acting on the body gave good agreement with the reliable published data. The application of the panel method requires that the problem can be formulated such that

1. the body can be represented by a closed polygon of a finite number of elements, called panels connected by nodes.
2. the flow tangency condition is satisfied in the middle of the panels (control points) to avoid the inaccuracies of thin airfoil theory.
3. the singularity distribution of each element is approximated by some kind of analytical function. Also, the singularities should be distributed on the body surface rather than on the chord line or any other line within the body.

Before we discuss further details, it is necessary to know about the basic formulation for source and vortex distribution as a singularity parameter.

1. Single Source and Source Panel

A flowfield where all streamlines are straight lines emanating from a source point, is called a source flow. On the other hand, when the flow direction is inward, it

is called sink flow. $\nabla \cdot \mathbf{V} = 0$ at every point except at the origin where $\nabla \cdot \mathbf{V}$ becomes infinite. The source flow is irrotational at every point. Its velocity potential is defined as

$$\text{single source} \quad \varphi(x, y) = \frac{\Lambda}{2\pi} \ln r \quad (3.1)$$

where Λ is defined as the source strength and r is the distance from the considered point (x, y) to the source. When we are dealing with non-lifting flows over a body, we can superimpose elementary source flows in order to obtain a complete solution. This method is called source panel method.

$$\text{source panel} \quad \varphi(x, y) = \frac{\Lambda}{2\pi} \int_0^l \ln r \, ds \quad (3.2)$$

where l is the panel length.

2. Single Vortex and Vortex Panel

The flow where all streamlines are concentric circles about a given point is defined as single vortex flow. The velocity along any given circular streamline is constant, but varies from streamline to streamline. Its velocity potential can be written as

$$\text{single vortex} \quad \varphi(x, y) = -\frac{\Gamma}{2\pi} \theta \quad (3.3)$$

where $\theta = \arctan \left[\frac{y - y_v}{x - x_v} \right]$, with (x_v, y_v) as the center of vortex

Let us imagine a straight line perpendicular to the page (Figure 3.1). This line is a straight vortex filament of strength Γ and the flow induced in any planes perpendicular to the vortex of strength Γ , i.e., the flows in the plane \perp to the vortex filament at o and o' are identical to each other and are identical to the flow induced by a point vortex of strength Γ .

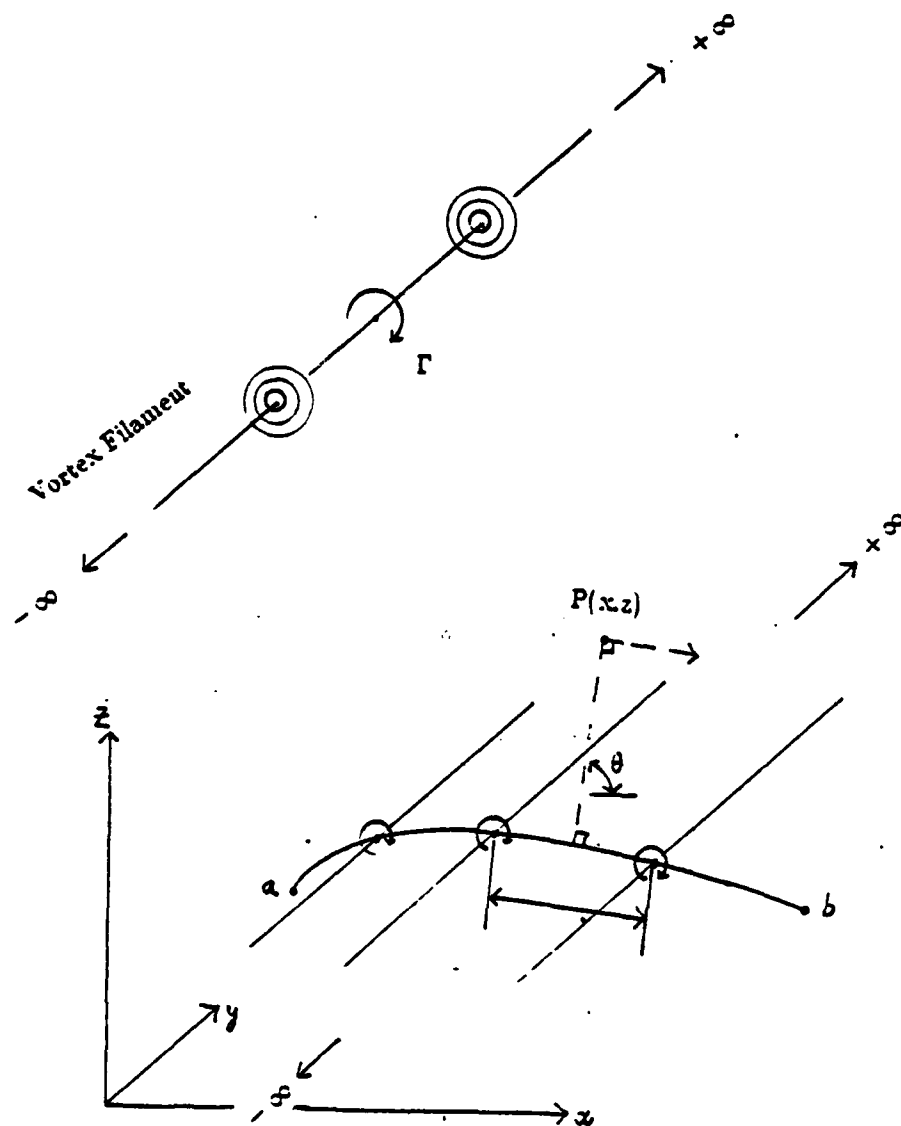


Figure 3.1 Vortex Sheet Representation.

Refer to Figure 3.1, imagine an infinite number of straight vortex filaments side by side, where the strength of each filament is infinitesimally small. Define $\gamma = \gamma(s)$ as the strength of the vortex sheet per unit length along s , then the strength of the infinitesimal portion ds of the sheet is γds and the small section of the vortex sheet of strength γds induces an infinitesimally small velocity dv at point $P(x, z)$

$$dv = -\gamma \frac{ds}{2\pi} \quad r, \perp \text{ to } r \quad (3.4)$$

It is sometimes more convenient to use the velocity potential ϕ , and the increment in velocity potential $d\phi$ induced at $P(x, z)$ by elemental vortex γds

$$d\phi = -\frac{\gamma ds}{2\pi} \theta \quad (3.5)$$

For the entire vortex sheet, from a to b

$$\phi(x, y) = -\frac{1}{2\pi} \int_a^b \theta \gamma ds \quad (3.6)$$

Equation 3.5 is useful in classical thin airfoil theory and equation 3.6 is important for the numerical vortex panel method.

B. SOURCE AND VORTEX DISTRIBUTION

Having introduced the basic idea of the panel method, we can use these singularities either alone or in combination. This method is due to *Hess and Smith*. Thus, the potential may be decomposed in a manner such that

$$\phi = \phi_0 + \phi_s + \phi_v \quad (3.7)$$

with ϕ_0 being the potential of the uniform onset flow, and ϕ_s and ϕ_v the potentials due to source and vortex distributions respectively, hence

$$\phi_s = \int \frac{\sigma(s)}{2\pi} \ln r ds \quad (3.8)$$

$$\varphi_v = - \int \frac{\gamma(s)}{2\pi} \theta ds \quad (3.9)$$

in which the integrations are to be performed over the body surface. Because of the superposition principle, this φ automatically satisfies Laplace's Equation (see equation 2.25) and the boundary condition at infinity. It will be the solution we seek, if $\sigma(s)$ and $\gamma(s)$ are determined so as to meet the boundary condition of flow tangency and the *Kutta condition* (to be discussed in the next section).

Hess and Smith assumed the vortex strength to be constant over the body surface and the source strength must vary over the surface. Since the Kutta condition involves only the trailing edge, the vortex strength can be represented by a single number. Thus, if one distributes on or within the body surface, vortices whose net strength is the correct circulation, the problem is solved if sources can be distributed over the body surface so as to make the total velocity field (comprised of the onset flow and the velocity fields due to sources and vortices) tangent to the body surface, regardless of how the vortices are distributed. However, the integrals in equations 3.8 and 3.9 are hard to evaluate, even for simple forms of the source and vortex strength, unless the surface on which the sources and vortices are distributed, is a straight line. Thus, we select a certain number of points on the body contour, called nodes, and connect the nodes with straight lines, which become the panels of the method (see Figure 3.2)

We then distribute the sources and vortices on the straight line panels, so that the potential given by equation 3.7 can be written as:

$$\varphi = V_0(x \cos \alpha + y \sin \alpha) + \sum_{j=1}^N \int_{l_j} \left(\frac{\sigma_j}{2\pi} \ln r - \frac{\gamma_j}{2\pi} \theta \right) ds \quad (3.10)$$

In most cases, equation 3.10 still allows an exact solution of the flow problem. The exceptional cases are those in which the sources and vortices must be distributed exactly on the body surface ; to be mathematically precise, in which the potential cannot be *continued analytically* across the body surface. By increasing the panel density, the body shape can be better approximated. This is the only major approximation of the panel method, one that becomes more accurate as the number of panels increases.

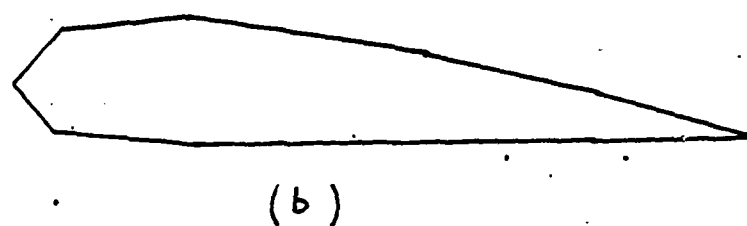
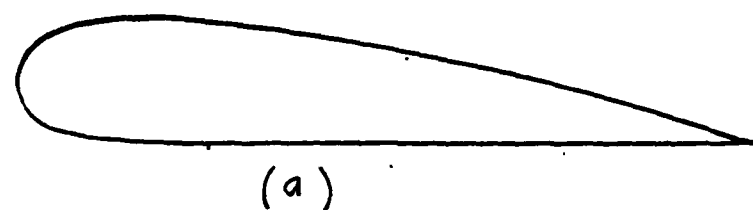


Figure 3.2 Discretization: a). Actual airfoil
b). Airfoil after discretization.

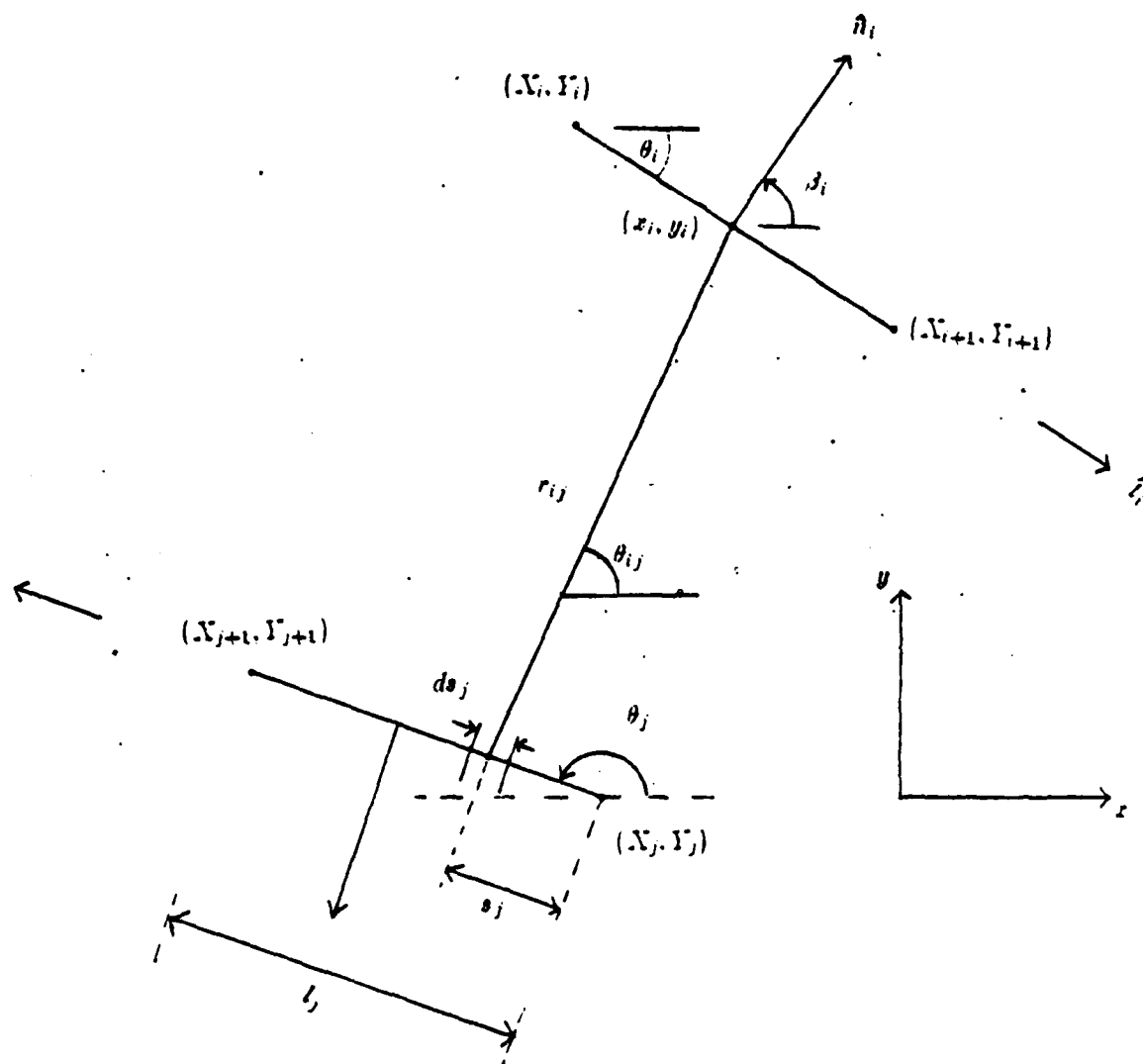


Figure 3.3 Representation of i -th and j -th panels in the Panel Method.

To implement this method, we need a nomenclature. Let the i -th panel be defined as the one between the i -th and $(i+1)$ th nodes, and its inclination to the x axis be θ_i . Therefore the relation between midpoints and boundary points

$$x_i = \frac{(X_i + X_{i+1})}{2}$$

$$y_i = \frac{(Y_i + Y_{i+1})}{2}$$

and the computation of the angle θ

$$\theta_i = \arctan \left[\frac{Y_{i+1} - Y_i}{X_{i+1} - X_i} \right]$$

From the geometry in Figure 3.3 a relation for angle and distance between two panels can be obtained

$$r_{ij} = \sqrt{(x_i - x_j)^2 + (y_i - y_j)^2}$$

$$\theta_{ij} = \arctan \left[\frac{(y_i - y_j)}{(x_i - x_j)} \right]$$

2. Flow Tangency Condition

The flow tangency condition in the case of no blowing or suction, is satisfied at the middle of each panel sometimes called *the no penetration condition*. To obtain this condition, differentiate equation 3.10 with respect to the normal vector for each panel.

$$\frac{\partial \varphi(x_i, y_i)}{\partial n_i} = \vec{v}_b \cdot \vec{n}_i = 0 \quad (3.11)$$

$$\sum_{j=1}^N AA_{ij} \sigma_j + \gamma \sum_{j=1}^N BB_{ij} = \sin(\theta_i - \alpha) \quad (3.12)$$

where,

$$AA_{ij} = \frac{1}{2\pi} \int_{l_j} \frac{\partial}{\partial n_i} \ln \sqrt{(x_i - x_j)^2 + (y_i - y_j)^2} ds_j$$

$$BB_{ij} = -\frac{1}{2\pi} \int_{l_j} \frac{\partial}{\partial n_i} \arctan \left[\frac{(y_i - y_j)}{(x_i - x_j)} \right] ds_j$$

AA_{ij} ... The influence coefficient or normal velocity (normalized with V_0) at the midpoint of the i -th panel due to a source distribution at the j -th panel.

BB_{ij} ... The influence coefficient or normal velocity (normalized with V_0) at the midpoint of the i -th panel due to a vortex distribution at the j -th panel.

x_i, y_i ... Coordinates of panel midpoint of i -th panel

x_j, y_j ... Coordinates of panel midpoint of j -th panel

l_j ... length of j -th panel

2. Concept of the Influence Coefficient

Equation 3.12 can be evaluated by integration. To obtain this, we have to relate the coordinate of a point in the j -th panel with the known coordinates of the boundary points and panel angles. From the geometry in Figure 3.2, one obtains

$$\frac{\partial x_i}{\partial n_i} = \cos \beta_i \quad (3.13)$$

$$\frac{\partial y_i}{\partial n_i} = \sin \beta_i \quad (3.14)$$

but, $\cos \beta_i = -\sin \theta_i$ and $\sin \beta_i = \cos \theta_i$, therefore equation 3.13 and 3.14 become

$$\frac{\partial x_i}{\partial n_i} = -\sin \theta_i \quad (3.15)$$

$$\frac{\partial y_i}{\partial n_i} = \cos \theta_i \quad (3.16)$$

On the other hand,

$$x_j = X_j + s_j \cos \theta_j \quad (3.17)$$

$$y_j = Y_j + s_j \sin \theta_j \quad (3.18)$$

And the influence coefficients can be obtained in terms of

$$AA_{ij} = \frac{1}{2\pi} \left[\frac{1}{2} CF - DG \right] \quad (3.19)$$

$$BB_{ij} = \frac{1}{2\pi} \left[\frac{1}{2} DF - CG \right] \quad (3.20)$$

where,

$$A = -(x_i - X_j) \cos \theta_j - (y_i - Y_j) \sin \theta_j$$

$$B = (x_i - X_j)^2 + (y_i - Y_j)^2$$

$$C = \sin(\theta_i - \theta_j)$$

$$D = \cos(\theta_i - \theta_j)$$

$$E = \sqrt{B - A^2} = (x_i - X_j) \sin \theta_j - (y_i - Y_j) \cos \theta_j$$

$$F = \ln \left[1 + \frac{l_i^2 + 2Al_j}{B} \right]$$

$$G = \arctan \left[\frac{El_i}{B + Al_j} \right]$$

when $i = j$ $AA_{ii} = \frac{1}{2}$ and $BB_{ii} = 0$

3. Computation of Total Disturbance Velocity V

The computation of the total disturbance velocity in x and y direction can be obtained by differentiating in the x and y direction.

$$\vec{V} = V_x \vec{i} + V_y \vec{j} = \text{grad } \varphi \quad (3.21)$$

$$V_x = \sum_{j=1}^N AA'_{ij} \sigma_j + \gamma \sum_{j=1}^N BB'_{ij} \quad (3.22)$$

$$V_y = \sum_{j=1}^N AA''_{ij} \sigma_j + \gamma \sum_{j=1}^N BB''_{ij} \quad (3.23)$$

where,

$$AA_{ij}^x = \frac{1}{2\pi} \int_{l_j} \frac{\partial}{\partial x_i} \ln \sqrt{(x_i - x_j)^2 + (y_i - y_j)^2} ds_j$$

$$BB_{ij}^x = -\frac{1}{2\pi} \int_{l_j} \frac{\partial}{\partial x_i} \arctan \left[\frac{(y_i - y_j)}{(x_i - x_j)} \right] ds_j$$

$$AA_{ij}^y = \frac{1}{2\pi} \int_{l_j} \frac{\partial}{\partial y_i} \ln \sqrt{(x_i - x_j)^2 + (y_i - y_j)^2} ds_j$$

$$BB_{ij}^y = -\frac{1}{2\pi} \int_{l_j} \frac{\partial}{\partial y_i} \arctan \left[\frac{(y_i - y_j)}{(x_i - x_j)} \right] ds_j$$

AA_{ij}^x . The horizontal velocity component at midpoint of i -th panel due to a unit source distribution at the j -th panel.

AA_{ij}^y . The vertical velocity component at midpoint of i -th panel due to a unit source distribution at the j -th panel.

BB_{ij}^x . The horizontal velocity component at midpoint of i -th panel due to a unit vortex distribution at the j -th panel.

BB_{ij}^y . The vertical velocity component at midpoint of i -th panel due to a unit vortex distribution at the j -th panel.

These influence coefficients can be obtained by integrating equation 3.12 and introducing equations 3.15 thru 3.18 into equation 3.12

$$AA_{ij}^x = \frac{1}{2\pi} \left[-\frac{1}{2} \cos \theta_j F + \sin \theta_j G \right] \quad (3.24)$$

$$BB_{ij}^x = \frac{1}{2\pi} \left[-\frac{1}{2} \sin \theta_j F - \cos \theta_j G \right] \quad (3.25)$$

$$AA_{ij}^y = BB_{ij}^x \quad (3.26)$$

$$BB_{ij}^y = -AA_{ij}^x \quad (3.27)$$

when $i = j$

$$AA_{ii}^x = -\frac{1}{2} \sin \theta_i$$

$$BB_{ii}^x = \frac{1}{2} \cos \theta_i$$

$$AA_{ii}^y = BB_{ii}^x$$

$$BB_{ii}^y = -AA_{ii}^x$$

4. Kutta Condition

As in all problems concerning airfoils in inviscid flows, an auxiliary condition needs to be invoked to ensure that a unique solution is obtained. This condition, known as *Kutta Condition*, relate to assumptions about the flow characteristics at, or at least in the neighbourhood of, the trailing edge. When the surface velocities are made equal at the midpoints of the trailing edge elements then, by the *Bernoulli Equation*, the pressures at these points are also equal, so the Kutta condition can be represented as the condition of zero loading in the region of the trailing edge [Ref. 1] which is physically realistic. Therefore the Kutta condition can be summerized as follows:

1. For a given angle of attack, the value of circulation Γ around the airfoil is such that the flow leaves the trailing edge smoothly.
2. If the trailing edge angle is finite, then the trailing edge is a stagnation point.
3. If the trailing edge angle is cusped, then the velocities leaving the top and the bottom surfaces at the trailing edge are finite and equal in magnitude and direction.

These are the basic principles of the Kutta condition. In the actual computation we are using in the code, there is no restriction whether the trailing edge angle is cusped or not as mentioned in item 3, but, rather, two tangential velocities in the last control points assume have the same magnitude but in opposite direction.

In the numerical solutions, the actual trailing edge is not a stagnation point. Furthermore, it is found that the velocities at the midpoint of the trailing edge elements differ significantly from stagnation values; they are more likely to be closer to the free stream velocities.

5. Determination of the vortex strength

The Kutta condition is used to determine the vortex strength γ . From equation 3-12, set $\gamma = 1.0$ and obtain the expression of σ_j in terms of the influence coefficient

$$\sum_{j=1}^N A_{i,j} \sigma_j = 1 \left[\sum_{j=1}^N B B_{i,j} \right] - \left[\sin(\theta_i - \alpha) \right] \quad (3.28)$$

This equation can be solved by using Gaussian elimination. The result can be substituted into equation 3.19 and 3.20. By letting $i=1$ and $i=N$ for the trailing edge panel, we can compute horizontal and vertical velocities for i -th and N -th panel as $V_{x,i}$, $V_{y,i}$, $V_{x,N}$ and $V_{y,N}$. Introducing these values into the Kutta condition, produces a quadratic equation in γ . This method is not the best way to satisfy the Kutta condition in steady flow calculation, but by using this method the code can be extended to the unsteady case.

$$e\gamma^2 + 2p\gamma + q = 0 \quad (3.29)$$

$$\begin{aligned} \text{where. } e &= (a_1^x)^2 + (a_1^y)^2 - (a_N^x)^2 - (a_N^y)^2 \\ p &= (a_1^x)(b_1^x) + (a_1^y)(b_1^y) - (a_N^x)(b_N^x) - (a_N^y)(b_N^y) - [(a_N^x) - (a_1^x)] \cos \alpha \\ &\quad - [(a_N^y) - (a_1^y)] \sin \alpha \\ q &= (b_1^x)^2 + (b_1^y)^2 - (b_N^x)^2 - (b_N^y)^2 - 2[(b_N^x) - (b_1^x)] \cos \alpha - 2[(b_N^y) - (b_1^y)] \sin \alpha \end{aligned}$$

$$\left. \begin{aligned} a_i^x &= \sum_{j=1}^N A_{i,j}^x \alpha_j + \sum_{j=1}^N B B_{i,j}^x & a_i^y &= \sum_{j=1}^N A_{i,j}^y \alpha_j + \sum_{j=1}^N B B_{i,j}^y \\ b_i^x &= \sum_{j=1}^N A_{i,j}^x \beta_j & b_i^y &= \sum_{j=1}^N A_{i,j}^y \beta_j \end{aligned} \right\} \begin{array}{l} \text{for } i=1 \\ \text{and } i=N \end{array}$$

$$\begin{Bmatrix} \alpha_1 \\ \alpha_2 \\ \vdots \\ \alpha_i \\ \vdots \\ \alpha_N \end{Bmatrix} = \begin{bmatrix} A_{11} & A_{12} & \dots & A_{1N} \\ A_{21} & & & A_{2N} \\ \vdots & \vdots & & \vdots \\ A_{i1} & A_{i2} & \dots & A_{iN} \\ \vdots & \vdots & & \vdots \\ A_{N1} & A_{N2} & \dots & A_{NN} \end{bmatrix}^{-1} \begin{Bmatrix} \sum_{j=1}^N B B_{1,j} \\ \vdots \\ \sum_{j=1}^N B B_{N,j} \end{Bmatrix}$$

$$\begin{Bmatrix} \beta_1 \\ \beta_2 \\ \vdots \\ \beta_i \\ \vdots \\ \beta_N \end{Bmatrix} = \begin{bmatrix} A_{11} & A_{12} & \dots & A_{1N} \\ A_{21} & & & A_{2N} \\ \vdots & \vdots & & \vdots \\ A_{i1} & A_{i2} & \dots & A_{iN} \\ \vdots & \vdots & & \vdots \\ A_{N1} & A_{N2} & \dots & A_{NN} \end{bmatrix}^{-1} \begin{Bmatrix} -\sin(\theta_1 - \alpha) \\ -\sin(\theta_2 - \alpha) \\ \vdots \\ -\sin(\theta_i - \alpha) \\ \vdots \\ -\sin(\theta_N - \alpha) \end{Bmatrix}$$

α_j and β_j are the result obtained from equation 3.28. From equation 3.29, there are two values of vortex strength γ , but only one value is used in the further calculation. These values relate to the angle of attack. If the angle of attack is positive, use the negative value of γ . If angle of attack is negative use the positive value.

6. Determination of the source strength

Once vortex strength has been determined using equation 3.12, the source strength σ can be obtained from

$$[\sigma_j] = \gamma[\alpha_j] + [\beta_j] \quad (3.30)$$

7. Calculation of 'on body' velocities

The velocity at midpoint of the i -th panel can be obtained by a spatial derivative of the velocity potential in the tangential direction.

$$V_i = \frac{\partial}{\partial t_i} [\varphi(x_i, y_i)] \quad (3.31)$$

$$V_i = \sum_{j=1}^N AT_{ij} \sigma_j + \gamma \sum_{j=1}^N BT_{ij} + \cos(\theta_i - \alpha) \quad (3.32)$$

$$\text{where } AT_{ij} = \frac{1}{2\pi} \left[-CG - \frac{1}{2}DF \right] \quad (3.33)$$

$$BT_{ij} = \frac{1}{2\pi} \left[-DG + \frac{1}{2}CF \right] \quad (3.34)$$

$$\text{when } i = j \quad AT_{ii} = 0.0 \quad (3.35)$$

$$BT_{ii} = \frac{1}{2} \quad (3.36)$$

AT_{ij} is the influence coefficient of tangential direction at the midpoint of the i -th panel due to a unit source at j -th panel, and BT_{ij} is the influence coefficient of tangential direction at the midpoint of the i -th panel due to a unit vortex at j -th panel.

a. Calculation of Pressure Coefficients

Once the velocity on the body has been calculated, we can easily obtain the pressure coefficients by the Bernoulli equation

$$\frac{p_i - p_0}{\frac{1}{2}\rho V_0^2} = 1 - V_i^2 \quad (3.37)$$

where V_i is the dimensionless velocity (normalized by V_0) at the midpoint of the i -th panel. Furthermore, as soon as the pressure coefficients are known other coefficients such as Lift Coefficient(CL), Drag Coefficient(CD) and Moment Coefficient about the leading edge (CM) can be obtained by using pressure integration along the body contour which is approximated by a closed polygon.

$$C_x = \sum_{i=1}^N C_{pi} [(Y_{i+1} - Y_i)] \quad (3.38)$$

$$C_y = \sum_{i=1}^N -C_{pi} [(X_{i+1} - X_i)] \quad (3.39)$$

$$CM = \sum_{i=1}^N C_{pi} [(X_{i+1} - X_i)x_i + (Y_{i+1} - Y_i)y_i] \quad (3.40)$$

$$CD = C_x \cos \alpha + C_y \sin \alpha \quad (3.41)$$

$$CL = C_y \cos \alpha - C_x \sin \alpha \quad (3.42)$$

C. LINEARLY VARYING VORTEX DISTRIBUTION

The following method is only one variation of the use of the panel method [Ref. 7] ; it involves representation of the airfoil by a closed polygon of the vortex

panels. The vortex-panel method introduced here has the feature that the circulation density on each panel varies linearly from one corner to the other and is continuous across the corner as indicated in Figure 3.4. The airfoil and wing problems can be solved by means of a vortex-panel distribution alone, but calculation of fuselage and nacelle characteristics and their interference flows dictate the use of source and, possibly, doublet as well as vortex-panels. For steady flows, it has been found that the use of piecewise constant, discontinuous distributions of vorticity can lead to inaccuracies such as oscillating values of the vorticity on successive panels. The use of a linearly varying, continuous distribution of vorticity eliminates this problem.

In the presence of uniform flow V_0 at an angle of attack α and m vortex panels, the velocity potential at the i -th control point (x_i, y_i) is defined as

$$\varphi = \varphi_0 + \varphi_v \quad (3.43)$$

$$\varphi(x_i, y_i) = V_0(x_i \cos \alpha + y_i \sin \alpha) - \sum_{j=1}^N \int_{s_j} \frac{\gamma(s_j)}{2\pi} \arctan \left[\frac{(y_i - y_j)}{(x_i - x_j)} \right] ds_j \quad (3.44)$$

$$\text{where} \quad \gamma(s_j) = \gamma_j + (\gamma_{j+1} - \gamma_j) \frac{s_j}{l_j} \quad (3.45)$$

is the vortex distribution which is linear along the panel and continuous across the boundary points.

The panels, N in number, are assumed planar and are named in the clockwise direction, starting from the trailing edge, and boundary points selected on the surface of the airfoil, are the intersections of continuous vortexpanels. The $(N+1)$ values of γ_j at boundary points are the unknowns to be determined numerically. The condition that the airfoil be a streamline is met approximately at *control points*. The boundary condition requires that the velocity in the direction outward normal vector n_i be vanishing at the i -th control point, such that

$$\frac{\partial}{\partial n_i} \varphi(x_i, y_i) = 0 \quad \text{for } i = 1, 2, 3, \dots, N \quad (3.46)$$

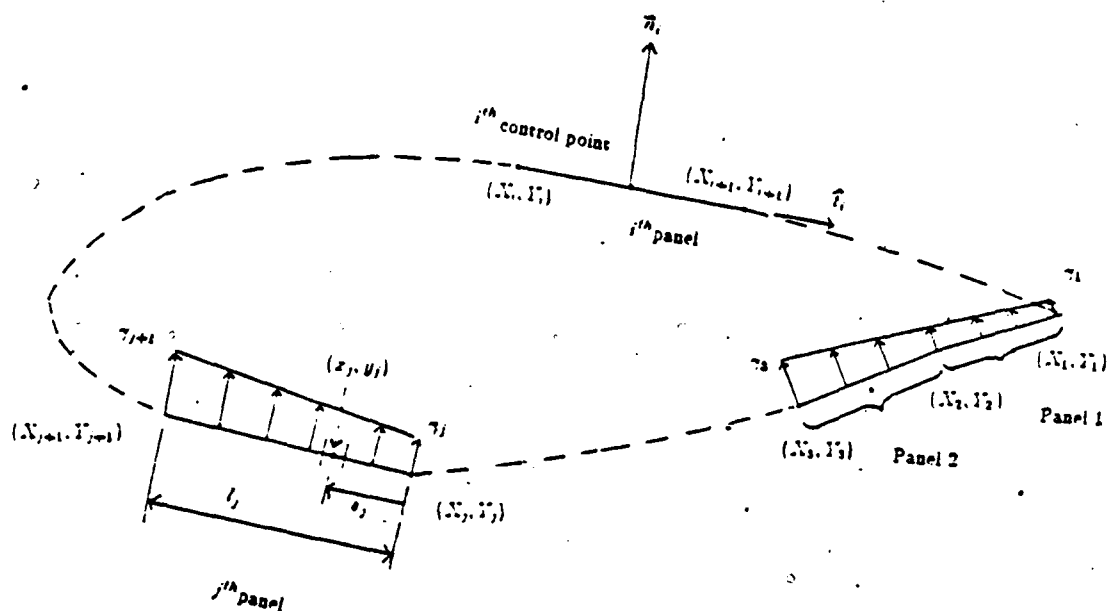


Figure 3.4 Replacement of an airfoil by vortex panels of linearly varying vortex strength.

Carrying out the calculation of equation 3.44 and normalizing the vortex strengths by $2\pi V_0$ we have

$$\sum_{j=1}^N \int_0^{l_j} \left[\gamma'_j + (\gamma'_{j+1} - \gamma'_j) \frac{s_j}{l_j} \right] \frac{\partial}{\partial n_i} \arctan \left[\frac{(y_i - y_j)}{(x_i - x_j)} \right] ds_j = -\sin(\theta_i - \alpha) \quad (3.47)$$

and from differentiation and integration we get

$$\sum_{j=1}^N [CN_{1,j} \gamma'_j + CN_{2,j} \gamma'_{j+1}] = \sin(\theta_i - \alpha) \quad (3.48)$$

where, $\gamma' = \gamma/2\pi V_0$ is a dimensionless vortex strength. The coefficients in the parentheses are

$$CN_{1,j} = \frac{1}{2}DF + CG - CN_{2,j}$$

$$CN_{2,j} = D + \frac{1}{2} \frac{QF}{l_j} - [AC - DZ] \frac{G}{l_j}$$

where

$$A = -(x_i - x_j) \cos \theta_j - (y_i - y_j) \sin \theta_j$$

$$B = (x_i - x_j)^2 + (y_i - y_j)^2$$

$$C = \sin(\theta_i - \theta_j)$$

$$D = \cos(\theta_i - \theta_j)$$

$$E = (x_i - x_j) \sin \theta_j - (y_i - y_j) \cos \theta_j$$

$$F = \ln \left[1 + \frac{l_j^2 + 2Al_j}{B} \right]$$

$$G = \arctan \left[\frac{El_j}{B + Al_j} \right]$$

$$Q = (x_i - x_j) \cos(\theta_i - 2\theta_j) - (y_i - y_j) \sin(\theta_i - 2\theta_j)$$

The expressions in the parentheses on the left side of equation 3.48 represent the normal velocity at the i -th control point induced by the linear distribution of vortices

on the j -th panel, called *influence coefficient* of normal velocity (except for $i = m+1$). When $i = j$, the coefficients have simplified values

$$\begin{aligned} CN_{1,i} &= -1 \\ CN_{2,i} &= 1 \end{aligned}$$

which describe the self-induced normal velocity at the i -th control point.

1. Kutta Condition

In order to apply the *Kutta condition* in the theoretical analysis, we need to be more precise about the nature of the flow at the trailing edge. It was mentioned before that the trailing edge can have a finite angle or it can be cusped. The statement of the Kutta condition in terms of the vortex sheet is $\gamma(TE) = V_n - V_l$ where V_n and V_l are the tangential velocities at the upper and lower side of the trailing edge. However, for the finite-angle trailing edge, the velocities at the upper and lower surface have same magnitude. Thus the Kutta condition becomes $\gamma(TE) = 0$,

$$\gamma'_1 + \gamma'_{N+1} = 0 \quad (3.49)$$

For computer programming, equation 3.48 can be arranged such that the equation is easy to formulate in matrix form

$$\sum_{j=1}^N A_{ij} \gamma'_j = RHS_i, \quad i=1,2,3,\dots,N+1 \quad (3.50)$$

After combining equation 3.49 and 3.50 they are sufficient to solve for the $(N+1)$ unknown γ'_j values, in which the influence coefficients can be classified as

$$\begin{aligned} \text{for } i < N+1: \quad & A_{i1} = CN_{1,i} \\ & A_{ij} = CN_{1,j} + CN_{2,j}, \quad j = 2,3,\dots,N \\ & A_{i,N+1} = CN_{2,i} \\ & RHS_i = \sin(\theta_i - \alpha) \\ \text{for } i = N+1: \quad & A_{i1} = A_{i,N+1} = 1 \\ & A_{ij} = 0, \quad j = 2,3,\dots,N \\ & RHS_i = 0 \end{aligned}$$

From the above equation, it can be expressed in matrix form

$$\begin{bmatrix} \Delta V_{11} & \Delta V_{12} & \dots & \Delta V_{1,N} & \Delta V_{1,N+1} \\ \Delta V_{21} & & & & \Delta V_{2,N+1} \\ \vdots & & \ddots & & \vdots \\ \Delta V_{N1} & & & & \Delta V_{N,N+1} \\ 1 & 0 & \dots & 0 & 1 \end{bmatrix} \begin{Bmatrix} \gamma'_1 \\ \gamma'_2 \\ \vdots \\ \gamma'_N \\ \gamma'_{N+1} \end{Bmatrix} = \begin{Bmatrix} \sin(\theta_1 - \alpha) \\ \sin(\theta_2 - \alpha) \\ \vdots \\ \sin(\theta_N - \alpha) \\ 0 \end{Bmatrix} \quad (3.51)$$

To obtain the unknown γ'_j values, the above expression can be solved by using the Gaussian Elimination method or any other linear equation algorithm.

2. Calculation of the 'on body' velocities

The unknown vortex strength having been determined, we can proceed to compute the velocities and pressures at every control point. Recall the *no penetration condition* at the control point. Hence the disturbance velocity induced at control points is only the tangential velocity. The velocity can be obtained by differentiating equation 3.44 in the direction of the tangential vector on the i -th panel, hence

$$V_{t_i} = \frac{\partial}{\partial t_i} \varphi(x_i, y_i) \quad (3.52)$$

$$V_{t_i} = \cos(\theta_i - \alpha) + \sum_{j=1}^N [CT_{1,j} \gamma'_j + CT_{2,j} \gamma'_{j+1}] \quad i = 1, 2, 3, \dots, N \quad (3.53)$$

in which the coefficients in the parentheses are defined as

$$CT_{1,i} = \frac{1}{2}CF - DG - CT_{2,i}$$

$$CT_{2,i} = C + \frac{1}{2} \frac{PF}{l_j} + [AD - CE] \frac{G}{l_j}$$

$$\text{when } i = j \quad CT_{1,ii} = CT_{1,ii} = \frac{1}{2}\pi$$

The expression in the parentheses following the summation symbol has the physical meaning of the tangential velocity at the i -th control point induced by the vortices distributed in the j -th panel. Equation 3.53 can be simplified further, to facilitate computer programming,

$$V_{t_i} = \cos(\theta_i - \alpha) + \sum_{j=1}^N AT_{ij} \gamma'_j \quad i = 1.2.3. \dots N \quad (3.54)$$

and AT_{ij} is defined as $AT_{i1} = CT_{i1}$

$$AT_{ij} = CT_{1,j} + CT_{2,j} \quad j = 2.3. \dots N$$

$$AT_{1,N+1} = CT_{2,N}$$

in convenient matrix, the tangential velocity can be written as

$$\begin{Bmatrix} V_{t_1} \\ V_{t_2} \\ \vdots \\ V_{t_N} \end{Bmatrix} = \begin{Bmatrix} \cos(\theta_1 - \alpha) \\ \cos(\theta_2 - \alpha) \\ \vdots \\ \cos(\theta_N - \alpha) \end{Bmatrix} + \begin{bmatrix} AT_{11} & AT_{12} & \dots & AT_{1,N} & AT_{1,N+1} \\ AT_{21} & & & & AT_{2,N+1} \\ \vdots & & \ddots & & \vdots \\ AT_{N1} & & & & AT_{N,N+1} \end{bmatrix} \begin{Bmatrix} \gamma'_1 \\ \gamma'_2 \\ \vdots \\ \gamma'_N \end{Bmatrix} \quad (3.55)$$

3. Calculation of C_p , CL , CD and CM

After the velocities at control points have been determined, one can obtain the pressure coefficients at the i -th control point using the *Bernoulli* equation 3.37. Similarly, other coefficients can be obtained easily by pressure integration along the body contour.

D. DISCUSSION OF THE PROGRAM PANEL

The Panel program used in this analysis consists of two FORTRAN programs which involve the implementation of source and vortex distributions, and the implementation of linear vortex distributions. Only the first program is included in this thesis (see Appendix A) as a sample program. The panel methods used here are basically the same as the Hess and Smith method [Ref. 4] where the source is located on the mid-point of each panel, constant along the panel but different from panel to panel. On the other hand, the vortex is considered constant for all the panels. To satisfy the Kutta condition at the trailing edge, the velocity components are computed by differentiating the velocity potential in the horizontal and vertical direction. And introducing these values into the Kutta condition, we can solve for the unknown vortex strength and subsequently for the source strength.

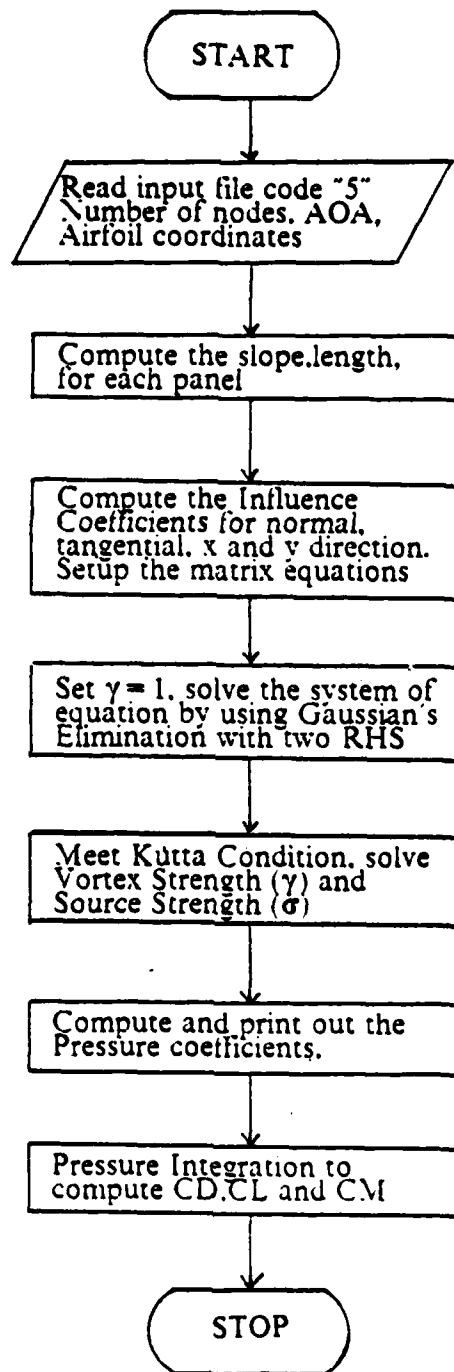


Figure 3.5 Source and Vortex Panel Method.

In the second method, only vortices are used as singularity distributions. The only difference here is, that the vortices are distributed linearly along the panel and continuous from one panel to the other.

1. Input Data

The input data for the program PANEL must be arranged in the following order:

1. Header card. The header card consists of the input for the number of coordinate points (column 1-10; integer) and input for angle of attack (column 11-20 real)
2. Coordinates of the airfoil. The arrangement for the body coordinates must be inputted in the following sequence: start from the trailing edge, progress on the lower surface to the leading edge, return through the upper surface and finish at the trailing edge, so that the trailing edge coordinate will be accounted twice.

2. Program output

The output from this program (see Appendix B) can be arranged as follows:

TABLE 1
DESCRIPTION OF THE PROGRAM OUTPUT

- | | |
|-------------|------------------------------------------------------------------------------------------------------------|
| 1. PNL(I) | : is the panel number |
| 2. X(I) | : x coordinate of control points (mid-points) |
| 3. Y(I) | : y coordinate of control points (mid-points) |
| 4. VEL(I) | : is the dimensionless velocity for each control point
(total velocity divided by free stream velocity) |
| 5. GAMMA(I) | : vortex strength(must be the same for the each panels) |
| 6. SIGMA(I) | : source strength for each control point |
| 7. CP(I) | : pressure coefficients for each control point |
| 8. CL,CD,CM | : coefficient of lift, drag and moment respectively |

E. DISCUSSION OF THE RESULTS

Figure 3.6 shows some results from the present computation for various angles of attack. In general, both methods give very good agreement in pressure distribution, although there are slight differences in the region of minimum pressure and at the

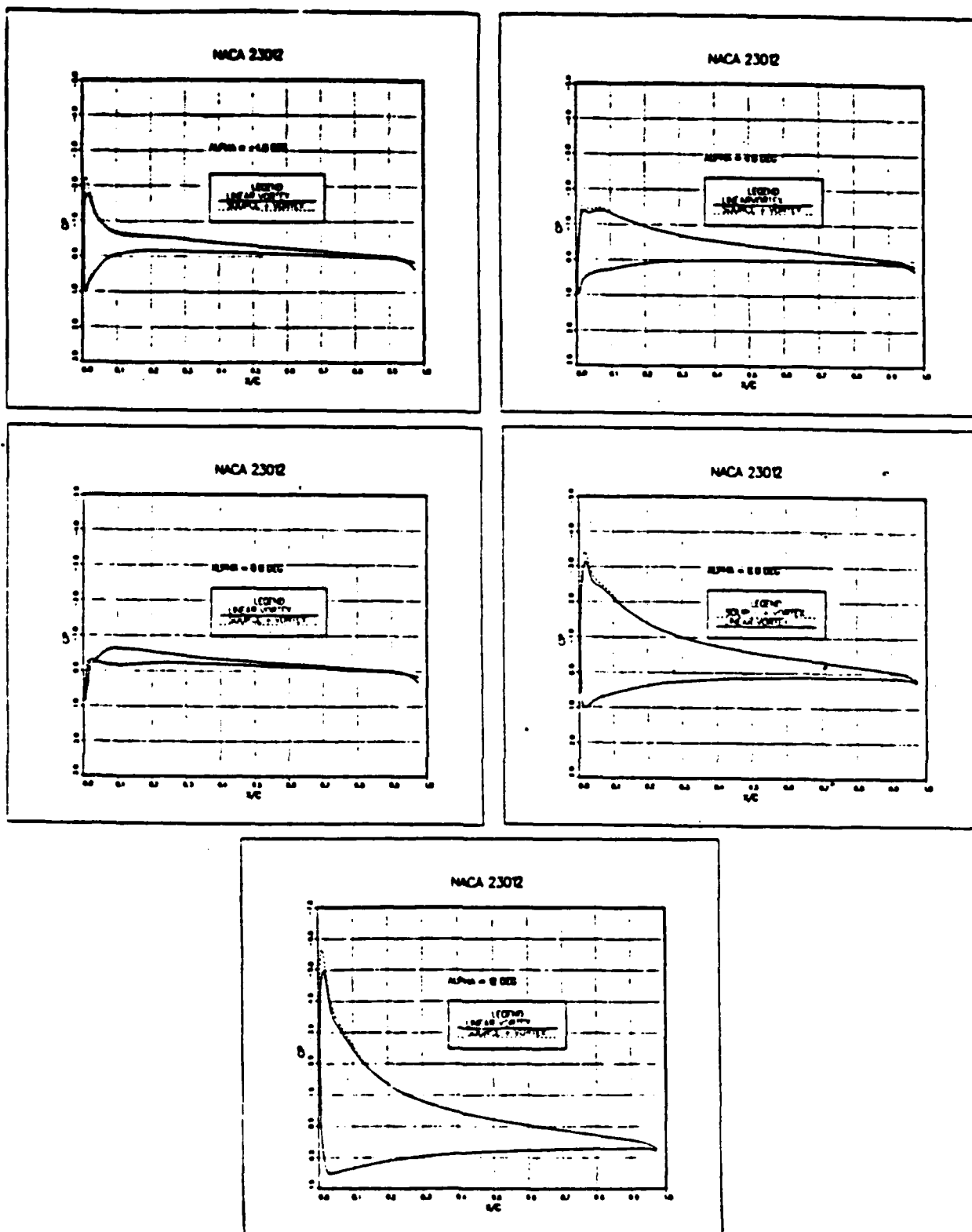


Figure 3.6 Comparison of pressure distributions on the NACA 23012 airfoil using the original Smuth-Hess-panel method (source and vortex panels) and the vortex panel method..

trailing edge. In the leading edge neighborhood , the source strength may give a significant effect in the region where the velocity changes rapidly. On the other hand, the different implementation of the Kutta conditions at the trailing edge also give slight differences in the pressure distribution. Recall that the first method using both velocities at the first and last panels are the same in magnitude but in the opposite direction, while the second method is using the condition of zero vortex strength at the trailing edge.

From the above conditions, the conclusions can be obtained from the present computations. Both methods, can be used to predict forces and moments around the airfoil as long as the fluid assumed remains inviscid and is not changing with time. Experience dictated that the second method gave less execution time than the first method might be true because in the second method solve only one unknown (γ) instead of two ($\dot{\gamma}$ and σ) for the first method. On the other hand, the second method is more complicated in the numerical formulation than the first one, because of the varying vortex strength throughout the airfoil contour.

IV. VISCOUS FLOW METHOD

In fluids, momentum is transferred by internal stresses, namely the hydrostatic pressure and the viscous stresses. When fluids are affected only by pressure and not by viscous stresses, their behavior is relatively easy to predict by standard inviscid flow methods as described in chapter 3.

A variation of velocity in the direction normal to the direction of the velocity itself is called a *shear*. Especially in high Reynolds Number flows this shear layer is very thin.

The most common type of a shear layer is the *boundary layer* between a stream and a solid surface. On the solid surface, the fluid velocity is reduced to zero (*no slip condition*), but there is no direct constraint on the velocity gradient at the surface. At the outer edge, the velocity tends asymptotically to the free stream values.

As mentioned before, in 1904 L. Prandtl came up with his well known theory of boundary layers. Prandtl's hypothesis divides the flowfield past a body into two separate regions, namely:

1. The region very close to the body where viscous effects are important.
2. The remaining region where inertia terms are more dominant than viscous terms, so that this region can be treated as inviscid flow.

These assumptions allow us to deal with the parabolic boundary layer equations, instead of the elliptic Navier-Stokes equations. The prior experience indicates that parabolic equations can be solved very rapidly and efficiently. Numerically, the change of characteristics means a change from a field procedure to a marching method, which integrates the boundary layer equation for given initial conditions step by step, proceeding in the downstream direction. Depending on the boundary conditions, boundary layer methods fall into three types:

1. The direct boundary layer method. This method employs the 'no slip condition', requiring zero normal and zero tangential velocity at the surface, and a prescription of the external velocity at the edge of the boundary layer.
2. The inverse boundary layer method. The prescription of wall shear or displacement thickness replaces the above edge boundary condition.

3. The interactive boundary layer method. The edge boundary condition prescribes a combination of displacement thickness and external velocity. Further discussion will focus on the first and the third method, since the computer code uses those.

A. DIRECT BOUNDARY LAYER METHOD

Direct methods are used in the region where the viscous effects remain small. The current code applies this method in the region near the leading edge. Direct methods allow the generation of initial conditions at the stagnation point and the efficient integration around the leading edge. The numerical approach features a finite difference method, which recasts the continuity and momentum equation as a system of linear algebraic equations [Ref. 13.] To begin with, we consider 2-D, steady flows of incompressible fluids, described in a curvilinear coordinate system with x directing along the airfoil surface and y perpendicular to the airfoil surface. The velocity components u and v shall be determined such that they satisfy anywhere in the flow field the continuity equation (4.1) and the momentum equation (4.2)

$$\frac{\partial u}{\partial x} + \frac{\partial v}{\partial y} = 0 \quad (4.1)$$

$$u \frac{\partial u}{\partial x} + v \frac{\partial u}{\partial y} = u_e \frac{du_e}{dx} + \nu \frac{\partial}{\partial y} \left(b \frac{\partial u}{\partial y} \right) \quad (4.2)$$

where 3 boundary conditions are needed at the boundaries of the flowfield,

$$y = 0: \quad u(x, 0) = 0, \quad v(x, 0) = 0$$

$$y = y_e: \quad u(x, y_e) = u_e(x)$$

with $b = 1 + v_t/v$. These equations are referred to as *boundary layer* or *thin shear layer* equations. To solve these equations, it is convenient to introduce a stream function ($u = \partial \psi / \partial y$ and $v = -\partial \psi / \partial x$), which reduces the number of dependent variables. Since the stream function automatically satisfies the continuity equation, only the momentum equation is left

$$\frac{\partial u}{\partial y} \frac{\partial^2 \psi}{\partial x \partial y} - \frac{\partial u}{\partial x} \frac{\partial^2 \psi}{\partial y^2} = u_e \frac{du_e}{dx} + \nu \frac{\partial}{\partial y} \left(b \frac{\partial^2 \psi}{\partial y^2} \right) \quad (4.3)$$

This equation is subjected to the *Falkner-Skan* transformation, which scales the normal coordinate y and the stream function ψ with reference to the external velocity.

$$\eta = \sqrt{\frac{u_e}{\nu x}} y$$

$$f(x, \eta) = \frac{1}{\sqrt{\frac{u_e}{\nu x}}} \psi(x, y)$$

With these transformations, the momentum equation becomes

$$(bf''')' + \frac{m+1}{2} f f'' + m[1 - (f')^2] = x \left(f' \frac{\partial f'}{\partial x} - f'' \frac{\partial f}{\partial x} \right) \quad (4.4)$$

and the boundary conditions are

$$\eta = 0: \quad f'(x, 0) = 0, \quad f(x, 0) = 0$$

$$\eta = \eta_e: \quad f'(x, \eta_e) = 1$$

where m is defined as a dimensionless pressure gradient parameter ($m = (x u_e)(du_e/dx)$), and prime denotes differentiation with respect to η . This is a third order partial differential equation. The solutions of this PDE are called non-similar flows, because they depend on both x and η . In contrast, if the right hand side of equation 4.4 vanishes, and therefore the solutions depend on η only, they are known as similar flows.

1. The Box Method

One of the most flexible methods in solving non-linear differential equations is the box method developed by Keller [Ref. 13] in 1970. The basic steps of the box method are the conversion of the governing equations into a first order system, the discretization of the differential equation by using central differences and two point averages, the linearization, and the solution of the resulting algebraic system. The introduction of two additional dependent variables U and V converts the third order momentum equation (4.4) into a first order system

$$f' = U \quad (4.5)$$

$$U' = V \quad (4.6)$$

$$(bV)' + \frac{m+1}{2} fV + m(1-V^2) = x \left(U \frac{\partial U}{\partial x} - V \frac{\partial f}{\partial x} \right) \quad (4.7)$$

and the boundary conditions become

$$\begin{aligned} \eta = 0: \quad U(x, 0) &= 0, \quad f(x, 0) = 0 \\ \eta = \eta_e: \quad U(x, \eta_e) &= 1 \end{aligned}$$

Instead of dealing with continuous functions f , U , and V , we use a set of discrete values of these flow properties. Let the solution domain $0 \leq x \leq x_I$, $0 \leq \eta \leq \eta_J$ be covered by a rectangular mesh (Figure 4.1)

$$x_1 = 0, \quad x_i = x_{i-1} + k_i \quad \text{with} \quad 2 \leq i \leq I$$

$$\eta_1 = 0, \quad \eta_j = \eta_{j-1} + h_j \quad \text{with} \quad 2 \leq j \leq J \quad \text{and} \quad \eta_J = \eta_e$$

We approximate all quantities whether it is a function or its derivative or a parameter like 'b', in terms of nodal values and coordinate of the network. The stream function and its first and second derivatives with respect to η are abbreviated at the nodes of network by

$$\{f(x_i, \eta_j), U(x_i, \eta_j), V(x_i, \eta_j)\} = \{f_i^j, U_i^j, V_i^j\}$$

The solution of the parabolic boundary layer equation at a certain streamline position, say x_i , depends solely on the solution of upstream positions say x_{i-1} , x_{i-2} , ... while no downstream influence has to be considered. The overall solution can be obtained step by step with the calculation propagating from the stagnation point into the downstream direction. The advantage of using first order equations and central differences is that we can reduce the domain of dependence from all upstream x -stations to the immediate preceding one, hence one step of the solution procedure writes the governing equations for a column of net rectangles (boxes) residing in the subdomain

$$x_{i-1} \leq x \leq x_i \quad \text{and} \quad 0 \leq \eta \leq \eta_J$$

and solves subsequently for the nodal values of the downstream face of the rectangular shaped subdomain. The x -station being currently solved holds therefore the superscript "i", while "i-1" denotes the known flow properties of the adjacent upstream location. As indicated by the term central differences the equations are satisfied midway between the nodes.

The two ODE's are centered about $(x_i, \eta_{j-1/2})$

And the PDE is centered about $(x_{i-1/2}, \eta_{j-1/2})$

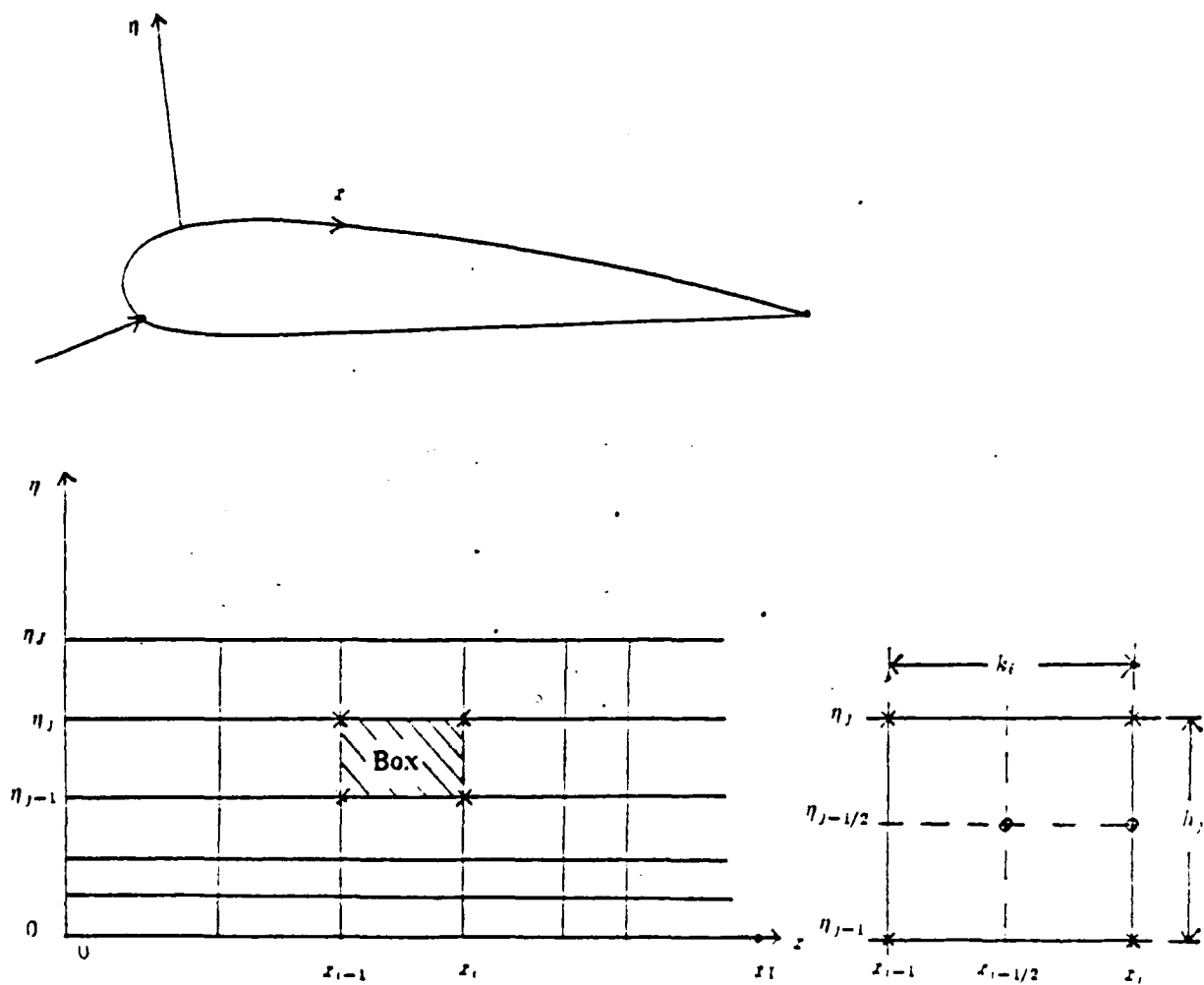


Figure 4.1 Net rectangle for finite difference approximation.

So equations 4.5, 4.6 and 4.7 can be written in terms of finite differences

$$\frac{f_j^i - f_{j-1}^i}{h_j} = \frac{1}{2}(U_j^i + U_{j-1}^i) \quad (4.8)$$

$$\frac{U_j^i - U_{j-1}^i}{h_j} = \frac{1}{2}(V_j^i + V_{j-1}^i) \quad (4.9)$$

$$\begin{aligned} & \frac{(\delta V^i)_j^{i-1/2} - (\delta V^i)_{j-1}^{i-1/2}}{h_j} + \frac{m^{i-1/2} + 1}{2} (f^i)_{j-1/2}^{i-1/2} + m^{i-1/2} \left[1 - (U_{j-1/2}^{i-1/2})^2 \right] \\ & = \varepsilon_{i-1/2} \left[U_{j-1/2}^{i-1/2} \frac{U_{j-1/2}^i - U_{j-1/2}^{i-1}}{k_i} - V_{j-1/2}^{i-1/2} \frac{f_{j-1/2}^i - f_{j-1/2}^{i-1}}{k_i} \right] \end{aligned} \quad (4.10)$$

and the boundary conditions take the form

$$\begin{aligned} U_1^i &= 0, & f_1^i &= 0 \\ U_j^i &= 1 \end{aligned}$$

The subdomain under consideration consists of $J-1$ net rectangles, the flow quantities of each being related by a momentum equation. The equations 4.8 and 4.9 link the dependent variables to their η -derivatives.

2. Newton's Method.

Unfortunately, the unknowns appear in nonlinear combinations. Therefore we introduce *Newton's Method* to solve this nonlinear system. The solution involves an iterative procedure, in which the variables are linearized around their values of the preceding iteration

$$\begin{aligned} f_j^{i,k} &= f_j^{i,k-1} + \delta f_j^{i,k} & \text{for } k \geq 2, & & f_j^{i,1} &= f_j^{i-1} + \delta f_j^{i,1} & \text{where } \delta f_j^{i,k} < f_j^{i,k-1} \\ U_j^{i,k} &= U_j^{i,k-1} + \delta U_j^{i,k} & \text{for } k \geq 2, & & U_j^{i,1} &= U_j^{i-1} + \delta U_j^{i,1} & \text{where } \delta U_j^{i,k} < U_j^{i,k-1} \\ V_j^{i,k} &= V_j^{i,k-1} + \delta V_j^{i,k} & \text{for } k \geq 2, & & V_j^{i,1} &= V_j^{i-1} + \delta V_j^{i,1} & \text{where } \delta V_j^{i,k} < V_j^{i,k-1} \end{aligned}$$

where k denotes the iteration counter. Substitution of these values into equations 4.8, 4.9 and 4.10, and dropping the quadratic terms in $(\delta f_j^{i,k}, \delta U_j^{i,k}, \delta V_j^{i,k})$ lead to a linear system in the unknowns $\delta f_j^{i,k}, \delta U_j^{i,k}, \delta V_j^{i,k}$

$$\delta f_j^{i,\kappa} - \delta f_{j-1}^{i,\kappa} - \frac{h_j}{2} (\delta U_j^{i,\kappa} + \delta U_{j-1}^{i,\kappa}) = f_{j-1}^{i,\kappa-1} - f_j^{i,\kappa-1} + h_j U_{j-1/2}^{i,\kappa-1} \quad (4.11)$$

$$\delta U_j^{i,\kappa} - \delta U_{j-1}^{i,\kappa} - \frac{h_j}{2} (\delta V_j^{i,\kappa} + \delta V_{j-1}^{i,\kappa}) = U_{j-1}^{i,\kappa-1} - U_j^{i,\kappa-1} + h_j V_{j-1/2}^{i,\kappa-1} \quad (4.12)$$

$$\begin{aligned} (s_1)_j^{i,\kappa} \delta V_j^{i,\kappa} + (s_2)_j^{i,\kappa} \delta V_{j-1}^{i,\kappa} + (s_3)_j^{i,\kappa} \delta f_j^{i,\kappa} + (s_4)_j^{i,\kappa} \delta f_{j-1}^{i,\kappa} \\ + (s_5)_j^{i,\kappa} \delta U_j^{i,\kappa} + (s_6)_j^{i,\kappa} \delta U_{j-1}^{i,\kappa} = (r_2)_j^{i,\kappa} \end{aligned} \quad (4.13)$$

where the coefficients in the bracket are defined as

$$\begin{aligned} (s_1)_j^{i,\kappa} &= \frac{\delta_j^{i,\kappa-1}}{h_j} + \frac{x_{i-1/2}}{2k_i} (f_{j-1/2}^{i,\kappa-1} - f_{j-1/2}^{i-1}) + \frac{m^i+1}{4} f_j^{i,\kappa-1} \\ (s_2)_j^{i,\kappa} &= -\frac{\delta_j^{i,\kappa-1}}{h_j} + \frac{x_{i-1/2}}{2k_i} (f_{j-1/2}^{i,\kappa-1} - f_{j-1/2}^{i-1}) + \frac{m^i+1}{4} f_{j-1}^{i,\kappa-1} \\ (s_3)_j^{i,\kappa} &= \frac{x_{i-1/2}}{2k_i} (V_{j-1/2}^{i,\kappa-1} + V_{j-1/2}^{i-1}) + \frac{m^i+1}{4} V_j^{i,\kappa-1} \\ (s_4)_j^{i,\kappa} &= \frac{x_{i-1/2}}{2k_i} (V_{j-1/2}^{i,\kappa-1} + V_{j-1/2}^{i-1}) + \frac{m^i+1}{4} V_{j-1}^{i,\kappa-1} \\ (s_5)_j^{i,\kappa} &= -\left(\frac{x_{i-1/2}}{k_i} + m^i\right) U_j^{i,\kappa-1} \\ (s_6)_j^{i,\kappa} &= -\left(\frac{x_{i-1/2}}{k_i} + m^i\right) U_{j-1}^{i,\kappa-1} \\ (r_2)_j^{i,\kappa} &= -\left\{ \frac{(bV^*)_{j-1}^{i,\kappa-1} - (bV^*)_{j-1}^{i-1}}{h_j} + \frac{m^i+1}{2} (fV^*)_{j-1/2}^{i,\kappa-1} - \left(\frac{x_{i-1/2}}{k_i} + m^i\right) (U_{j-1/2}^{i,\kappa-1})^2 \right. \\ &\quad \left. + \frac{x_{i-1/2}}{k_i} (V_{j-1/2}^{i,\kappa-1} f_{j-1/2}^{i,\kappa-1} + V_{j-1/2}^{i-1} f_{j-1/2}^{i,\kappa-1} - f_{j-1/2}^{i-1} V_{j-1/2}^{i,\kappa-1}) \right\} \\ &\quad - \left\{ \frac{(bV^*)_j^{i-1} - (bV^*)_{j-1}^{i-1}}{h_j} + \frac{m^{i-1}+1}{2} (fV^*)_{j-1/2}^{i-1} + \left(\frac{x_{i-1/2}}{k_i} - m^{i-1}\right) (U_{j-1/2}^{i-1})^2 \right. \\ &\quad \left. - \frac{x_{i-1/2}}{k_i} V_{j-1/2}^{i-1} f_{j-1/2}^{i-1} + 2m^{i-1/2} \right\} \end{aligned}$$

3. Keller's Block Elimination Method

Together with the boundary conditions this system is repeatedly solved until $\delta f_j^{i,\kappa}, \delta U_j^{i,\kappa}, \delta V_j^{i,\kappa}$ are small enough to be neglected. Equation 4.11, 4.12, and 4.13 can be solved by *Keller's Block Elimination Method*. Block-tridiagonal matrices are composed of submatrices, called *blocks*, of which only those residing on main and both adjacent diagonals have non-zero entries.

$$\begin{bmatrix} [A_1^{i,\kappa}] & [C_1^{i,\kappa}] & & & \\ [B_2^{i,\kappa}] & [A_2^{i,\kappa}] & [C_2^{i,\kappa}] & & \\ & \ddots & \ddots & \ddots & \\ & [B_j^{i,\kappa}] & [A_j^{i,\kappa}] & [C_j^{i,\kappa}] & \\ & & \ddots & \ddots & \ddots \\ & & [B_{j-1}^{i,\kappa}] & [A_{j-1}^{i,\kappa}] & [C_{j-1}^{i,\kappa}] \\ & & & [B_j^{i,\kappa}] & [A_j^{i,\kappa}] \end{bmatrix} \begin{Bmatrix} \{\delta_1^{i,\kappa}\} \\ \{\delta_2^{i,\kappa}\} \\ \vdots \\ \{\delta_j^{i,\kappa}\} \\ \vdots \\ \{\delta_{j-1}^{i,\kappa}\} \\ \{\delta_j^{i,\kappa}\} \end{Bmatrix} = \begin{Bmatrix} \{r_1^{i,\kappa}\} \\ \{r_2^{i,\kappa}\} \\ \vdots \\ \{r_j^{i,\kappa}\} \\ \vdots \\ \{r_{j-1}^{i,\kappa}\} \\ \{r_j^{i,\kappa}\} \end{Bmatrix} \quad (4.14)$$

where the blocks are 3×3 -matrices being defined as

$$[A_j^{i,\kappa}] = \begin{bmatrix} 1 & -h_j/2 & 0 \\ (s_3)_j^{i,\kappa} & (s_3)_j^{i,\kappa} & (s_1)_j^{i,\kappa} \\ 0 & -1 & -h_{j+1}/2 \end{bmatrix} \quad \text{for } 2 \leq j \leq J-1$$

$$[B_j^{i,\kappa}] = \begin{bmatrix} -1 & -h_j/2 & 0 \\ (s_4)_j^{i,\kappa} & (s_4)_j^{i,\kappa} & (s_2)_j^{i,\kappa} \\ 0 & 0 & 0 \end{bmatrix} \quad \text{for } 2 \leq j \leq J$$

$$[C_j^{i,\kappa}] = \begin{bmatrix} 0 & 0 & 0 \\ 0 & 0 & 0 \\ 0 & 1 & -h_{j+1}/2 \end{bmatrix} \quad \text{for } 1 \leq j \leq J-1$$

$$[A_1^{i,\kappa}] = \begin{bmatrix} 1 & 0 & 0 \\ 0 & 1 & 0 \\ 0 & -1 & -h_2/2 \end{bmatrix}$$

$$[A_J^{i,\kappa}] = \begin{bmatrix} 1 & -h_J/2 & 0 \\ (s_3)_J^{i,\kappa} & (s_3)_J^{i,\kappa} & (s_1)_J^{i,\kappa} \\ 0 & 1 & 0 \end{bmatrix}$$

and where the right hand sides are obtained from

$$(r_1)_j^{i,k} = f_{j-1}^{i,k-1} - f_j^{i,k-1} + h_j U_{j-1/2}^{i,k-1} \quad \text{for } 2 \leq j \leq J$$

$$(r_2)_j^{i,k} = \begin{cases} \text{as given by} \\ \text{momentum equation} \end{cases} \quad \text{for } 2 \leq j \leq J$$

$$(r_3)_j^{i,k} = U_j^{i,k-1} - U_{j-1}^{i,k-1} + h_{j+1} V_{j+1/2}^{i,k-1} \quad \text{for } 1 \leq j \leq J-1$$

$$(r_1)_1^{i,k} = 0, \quad (r_2)_1^{i,k} = 0, \quad (r_3)_J^{i,k} = 0$$

The unknowns of the linear equations are the Newton iterates of the stream function ($f_j^{i,k}$), its first derivative ($U_j^{i,k}$) and its second derivative ($V_j^{i,k}$). This method is very effective and it consists primarily of two steps:

1. The forward step eliminates the lower diagonal of submatrices.
2. The backward step solves the remaining system from bottom to top.

B. INTERACTIVE BOUNDARY LAYER METHOD.

The application of the direct method is restricted to regions where the viscous effects remain small. Integration of the boundary layer equations will break down at the point of zero skin friction. To avoid this break down, we need a method that is able to integrate the boundary layer equations through the point of zero skin friction. Further, these methods are required to account for strong interaction effects, arising from boundary layer separation or the rapid flow acceleration downstream of the trailing edge, both of which cause substantial changes in the external velocity distribution.

In contrast with direct and inverse methods, the interactive method treats the external velocity and displacement thickness as unknown quantities, reflecting the elliptic character of the outer flows. This introduces apparently one additional unknown into the viscous flow problem, whose solution can be obtained by using two methods:

1. The eigenvalue method, or
2. The Mechul function method.

The second method is being preferred here, since the first method involves non-linear eigenvalue problems. The edge boundary condition of the direct problem is supplemented by the so-called *interactive boundary condition*, which relates the unknown external velocity with its inviscid and "displacement-perturbation-related" contributions. Boundary layer equations in the following constitute a system in the unknown functions $u(x,y)$, $v(x,y)$ and $u_e(x,y)$

$$-\frac{\partial u}{\partial x} + \frac{\partial v}{\partial y} = 0 \quad (4.15)$$

$$u \frac{\partial u}{\partial x} + v \frac{\partial u}{\partial y} = u_e \frac{\partial u_e}{\partial x} + \nu \frac{\partial}{\partial y} \left(b \frac{\partial u}{\partial y} \right) \quad (4.16)$$

$$0 = \frac{\partial u_e}{\partial y} \quad (4.17)$$

These equations consist of *continuity equation* (4.15), *momentum equation in x-direction* (4.16) and the seemingly unnecessary *momentum equation in y-direction* (4.17), where the pressure term has been expressed in terms of the external velocity. The Mechul function approach assumes that the external velocity be a function of two arguments, resulting in the need for the trivial y-momentum equation. The reason for considering $u_e(x, y)$ rather than $u_e(x)$ is for purely numerical reasons, i.e., such a provision allows an easy setup of the finite difference equations avoiding the eigenvalue technique.

The governing equations are complemented by proper boundary conditions. The velocity components u and v are required to satisfy the no-slip conditions at the surface of the airfoil and the horizontal component must merge smoothly into the outer flow at the boundary layer edge.

$$y = 0: \quad u(x, 0) = 0, \quad v(x, 0) = 0$$

$$y = y_e: \quad u(x, y_e) = u_e(x, y_e), \quad u_e(x, y_e) = u_{ef}(x) + \frac{1}{\pi} \int \frac{d}{d\xi} (u_e \delta^*) \frac{d\xi}{x - \xi}$$

with $u_f(x)$ denoting the inviscid velocity distribution and the second term, called *Hilbert integral*, approximating the perturbation velocity due to viscous effects. The interactive method can be applied to attached and separated flow regions, while direct method cannot do so because of their breakdown related to the *Goldstein* singularity, nor inverse methods because of their poor convergence rates. Therefore the interactive methods are being preferred on the main parts of the airfoil. Only at the stagnation point this method cannot be applied.

The steps which turn the partial differential equations of the interactive problem into a linear system of algebraic equations resemble those of the direct method, so that only major steps and their results will be repeated here. After the introduction of a

stream function ($u = \partial\psi / \partial y$ and $v = -\partial\psi / \partial x$), the equations undergo a transformation, which scales the normal coordinate y , stream function ψ , and the external velocity u_e with reference to the constant velocity u_0 and the local streamwise coordinate x

$$\eta = \sqrt{\frac{u_0}{\nu x}} y$$

$$f(x, \eta) = \frac{1}{\sqrt{u_0 \nu x}} \psi(x, y)$$

$$\Pi(x, \eta) = \frac{u_e(x, y)}{u_0}$$

where u_0 is taken as the free stream velocity. The concept of constant boundary layer thickness, attained by *Falkner-Skan* variables with u_e as reference velocity, has to be abandoned because the external velocity is *unknown* in the interactive calculations. Provided that the integration of the boundary layer equations does not start in the immediate neighborhood of the stagnation point, the growth of the boundary layer thickness can be kept limited. In terms of these so called *semi-transformed coordinates* the boundary layer equations, written as a first order system by means of two additional dependent variables U and V , and the boundary conditions take the form

$$f' = U \quad (4.18)$$

$$U' = V \quad (4.19)$$

$$(bV')' + \frac{1}{2} fV' + x\Pi \frac{\partial \Pi}{\partial x} = x \left(U \frac{\partial U}{\partial x} - V \frac{\partial f}{\partial x} \right) \quad (4.20)$$

$$\Pi' = 0 \quad (4.21)$$

$$\eta = 0: \quad U(x, 0) = 0, \quad f(x, 0) = 0$$

$$\eta = \eta_e: \quad U(x, \eta_e) = \Pi(x, \eta_e)$$

$$\Pi(x, \eta_e) = \frac{u_{ef}(x)}{u_0} + \frac{1}{\pi} \int \frac{d}{d\xi} \left\{ \sqrt{\frac{\nu \xi}{u_0}} \left[\Pi(\xi, \eta_e) \eta_e - f(\xi, \eta_e) \right] \right\} \frac{d\xi}{x - \xi}$$

The discretization of the flow field follows closely the above outlined procedure of the direct method, covering the generation of an orthogonal grid and the introduction of central differences and two-point-averages. The overall solution proceeds in the downstream direction, accounting for downstream travelling disturbances only. On the

assumption that backflow velocities are comparatively small, a stable integration can be carried out by adopting the FLARE approximation (*Flugge-Lotz and Reyhner*). The purpose of a FLARE approximation is to permit the use of a downstream-marching algorithm in regions of backflow. This is accomplished by setting the streamwise convection term $u \partial u / \partial x$ equal to zero in regions of backflow. With

$$\psi_{j-1/2}^i = \begin{cases} 1 & \text{if } U_{j-1/2}^i \geq 0 \\ 0 & \text{if } U_{j-1/2}^i < 0 \end{cases}$$

designating an "on-off switch" of the streamwise convection term, the finite difference equations of the interactive boundary layer problem become

$$\frac{f_j^i - f_{j-1}^i}{h_j} = \frac{1}{2}(U_j^i + U_{j-1}^i) \quad (4.22)$$

$$\frac{U_j^i - U_{j-1}^i}{h_j} = \frac{1}{2}(V_j^i + V_{j-1}^i) \quad (4.23)$$

$$\begin{aligned} & \frac{(bV_j^i)^{i-1/2} - (bV_{j-1}^i)^{i-1/2}}{h_j} + \frac{1}{2}(f_j^i)^{i-1/2} + x_{i-1/2} \frac{\pi_{j-1/2}^{i-1/2} - \pi_{j-1/2}^{i-1}}{k_i} \\ & = x_{i-1/2} \left[\psi_{j-1/2}^i U_{j-1/2}^{i-1/2} \frac{U_{j-1/2}^i - U_{j-1/2}^{i-1}}{k_i} - V_{j-1/2}^{i-1/2} \frac{f_{j-1/2}^i - f_{j-1/2}^{i-1}}{k_i} \right] \end{aligned} \quad (4.24)$$

$$\frac{\pi_j^i - \pi_{j-1}^i}{h_j} = 0 \quad (4.25)$$

Boundary conditions are expressed in terms of nodal values, whereby the evaluation of the integral occurring in the interactive boundary condition involves an approximation in the fashion of the panel method approach, leading to

$$\begin{aligned} U_1^i &= 0, & f_1^i &= 0 \\ U_j^i &= \pi_j^i, & \pi_j^i &= \tilde{g}_i + \tilde{c}_{ii}(\pi_j^i \eta_j - f_j^i) \end{aligned}$$

where \tilde{g}_i and \tilde{c}_{ii} denote a parameter and the diagonal element of the interaction matrix, resulting from a discrete approximation to the Hilbert integral. Averaging as well as

centering is supposed to obey the principle that the number of generated terms approaches a minimum. This entails ordinary differential equations, like the y-momentum equation, being centered about the middle of the downstream face and partial differential equations, like the x-momentum equation, being centered about the middle of the box.

A balance of unknowns, which occur here as vectors in four components, $\{f_j^i, U_j^i, V_j^i, \Pi_j^i\}^T$ confirms the principal solvability of the system. The J quadruplets of unknowns match with a total of $4J$ equations, including $2(J-1)$ auxiliary relations, $(J-1)$ x-momentum and $(J-1)$ y-momentum equations, each of which corresponding to one of the $(J-1)$ net rectangles, and 4 boundary conditions. After linearizing this system around the values of the preceding iteration (iteration counter " $k-1$ "), respectively around the solution of the adjacent upstream x-station in case of the first iteration, we arrive at a linear system in the *Newton iterates* $\delta f_j^{i,k}, \delta U_j^{i,k}, \delta V_j^{i,k}, \delta \Pi_j^{i,k}$

$$\delta f_j^{i,k} - \delta f_{j-1}^{i,k} - \frac{h_j}{2} (\delta U_j^{i,k} + \delta U_{j-1}^{i,k}) = f_{j-1}^{i,k-1} - f_j^{i,k-1} + h_j U_{j-1/2}^{i,k-1} \quad (4.26)$$

$$\delta U_j^{i,k} - \delta U_{j-1}^{i,k} - \frac{h_j}{2} (\delta V_j^{i,k} + \delta V_{j-1}^{i,k}) = U_{j-1}^{i,k-1} - U_j^{i,k-1} + h_j V_{j-1/2}^{i,k-1} \quad (4.27)$$

$$(g_1)_j^{i,k} \delta V_j^{i,k} + (g_2)_j^{i,k} \delta V_{j-1}^{i,k} + (g_3)_j^{i,k} \delta f_j^{i,k} + (g_4)_j^{i,k} \delta f_{j-1}^{i,k} + (g_5)_j^{i,k} \delta U_j^{i,k} + (g_6)_j^{i,k} \delta U_{j-1}^{i,k} + (g_7)_j^{i,k} \delta \Pi_j^{i,k} + (g_8)_j^{i,k} \delta \Pi_{j-1}^{i,k} = (r_2)_j^{i,k} \quad (4.28)$$

$$\delta \Pi_j^{i,k} - \delta \Pi_{j-1}^{i,k} = \Pi_{j-1}^{i,k-1} - \Pi_j^{i,k-1} \quad (4.29)$$

supplemented by the two components of no-slip condition, edge and interactive boundary condition

$$\begin{aligned} \delta U_1^{i,k} &= 0, \quad \delta f_1^{i,k} = 0 \\ \delta U_j^{i,k} - \delta \Pi_j^{i,k} &= 0 \\ \delta f_j^{i,k} + \left(\frac{1}{c_{ii}} - \eta_j \right) \delta \Pi_j^{i,k} &= \frac{\tilde{g}_i}{c_{ii}} - f_j^{i,k-1} - \left(\frac{1}{c_{ii}} - \eta_j \right) \Pi_j^{i,k-1} \end{aligned}$$

Terms have been grouped such that known quantities reside on the right hand sides, while unknown quantities appear left of the equal sign. The abbreviated coefficients in the momentum equation are defined by

$$\begin{aligned}
 (s_1)_j^{i,\kappa} &= \frac{b_j^{i,\kappa-1}}{h_j} + \frac{x_{i-1/2}}{2k_i} (f_{j-1/2}^{i,\kappa-1} - f_{j-1/2}^{i-1}) + \frac{1}{4} f_j^{i,\kappa-1} \\
 (s_2)_j^{i,\kappa} &= -\frac{b_j^{i,\kappa-1}}{h_j} + \frac{x_{i-1/2}}{2k_i} (f_{j-1/2}^{i,\kappa-1} - f_{j-1/2}^{i-1}) + \frac{1}{4} f_{j-1}^{i,\kappa-1} \\
 (s_3)_j^{i,\kappa} &= \frac{x_{i-1/2}}{2k_i} (v_{j-1/2}^{i,\kappa-1} + v_{j-1/2}^{i-1}) + \frac{1}{4} v_j^{i,\kappa-1} \\
 (s_4)_j^{i,\kappa} &= \frac{x_{i-1/2}}{2k_i} (v_{j-1/2}^{i,\kappa-1} + v_{j-1/2}^{i-1}) + \frac{1}{4} v_{j-1}^{i,\kappa-1} \\
 (s_5)_j^{i,\kappa} &= -\frac{x_{i-1/2}}{k_i} U_j^{i,\kappa-1} v_{j-1/2}^i \\
 (s_6)_j^{i,\kappa} &= -\frac{x_{i-1/2}}{k_i} U_{j-1}^{i,\kappa-1} v_{j-1/2}^i \\
 (s_7)_j^{i,\kappa} &= \frac{x_{i-1/2}}{k_i} w_{j-1/2}^{i,\kappa-1} \\
 (s_8)_j^{i,\kappa} &= \frac{x_{i-1/2}}{k_i} w_{j-1/2}^{i,\kappa-1}
 \end{aligned}$$

and the right hand side of equation (4.28)

$$\begin{aligned}
 (r_2)_j^{i,\kappa} &= -\left\{ \frac{(bV)_j^{i,\kappa-1} - (bV)_{j-1}^{i,\kappa-1}}{h_j} + \frac{1}{2} (fV)_{j-1/2}^{i,\kappa-1} + \frac{x_{i-1/2}}{k_i} \left[(w_{j-1/2}^{i,\kappa-1})^2 \right. \right. \\
 &\quad \left. \left. - (U_{j-1/2}^{i,\kappa-1})^2 v_{j-1/2}^i + v_{j-1/2}^{i,\kappa-1} f_{j-1/2}^{i,\kappa-1} + v_{j-1/2}^{i-1} f_{j-1/2}^{i,\kappa-1} - f_{j-1/2}^{i-1} v_{j-1/2}^{i,\kappa-1} \right] \right\} \\
 &\quad - \left\{ \frac{(bV)_j^{i-1} - (bV)_{j-1}^{i-1}}{h_j} + \frac{1}{2} (fV)_{j-1/2}^{i-1} - \frac{x_{i-1/2}}{k_i} \left[(w_{j-1/2}^{i-1})^2 - (U_{j-1/2}^{i-1})^2 v_{j-1/2}^i \right. \right. \\
 &\quad \left. \left. + v_{j-1/2}^{i-1} f_{j-1/2}^{i-1} \right] \right\}
 \end{aligned}$$

Since the overall procedure involves a repetitive linear pattern to approach the solution of the nonlinear system, the linear equation solver has to be as fast as possible. Fast algorithms take advantage of specific matrix structures, one of which is the block-tridiagonal structure, which can be enforced in this method by the following arrangement of equations and boundary conditions :

1. First set of equations (index $j = 1$)
 1. Wall boundary condition prescribing no penetration
 2. Wall boundary condition prescribing zero tangential velocity

3. Second auxiliary relation (linking U'' and V) of the first box
4. Trivial y-momentum equation of the first box
2. Intermediate sets of equations (index $2 \leq j \leq J-1$)
 1. First auxiliary relation (linking f' and U) of the $(j-1)$ -st box
 2. Momentum equation of the $(j-1)$ -st box
 3. Second auxiliary relation (linking U'' and V) of the j -th box
 4. Trivial y-momentum equation of the j -th box
3. Last set of equations (index $j = J$)
 1. First auxiliary relation (linking f' and U) of the last box
 2. Momentum equation of the last box
 3. Interactive boundary condition
 4. Edge boundary condition.

Following these instructions equations and boundary conditions can be arranged in matrix-vector form.

$$\begin{bmatrix}
 [A_1^{i,\kappa}] & [C_1^{i,\kappa}] & & & \\
 [B_2^{i,\kappa}] & [A_2^{i,\kappa}] & [C_2^{i,\kappa}] & & \\
 & \ddots & \ddots & \ddots & \\
 & [B_j^{i,\kappa}] & [A_j^{i,\kappa}] & [C_j^{i,\kappa}] & \\
 & & \ddots & \ddots & \ddots \\
 & & [B_{J-1}^{i,\kappa}] & [A_{J-1}^{i,\kappa}] & [C_{J-1}^{i,\kappa}] \\
 & & & [B_J^{i,\kappa}] & [A_J^{i,\kappa}]
 \end{bmatrix}
 \begin{Bmatrix}
 \{\delta_1^{i,\kappa}\} \\
 \{\delta_2^{i,\kappa}\} \\
 \vdots \\
 \{\delta_j^{i,\kappa}\} \\
 \vdots \\
 \{\delta_{J-1}^{i,\kappa}\} \\
 \{\delta_J^{i,\kappa}\}
 \end{Bmatrix}
 =
 \begin{Bmatrix}
 \{r_1^{i,\kappa}\} \\
 \{r_2^{i,\kappa}\} \\
 \vdots \\
 \{r_j^{i,\kappa}\} \\
 \vdots \\
 \{r_{J-1}^{i,\kappa}\} \\
 \{r_J^{i,\kappa}\}
 \end{Bmatrix} \quad (4.30)$$

where $\{\delta_j^{i,\kappa}\} = \{\delta f_j^{i,\kappa}, \delta U_j^{i,\kappa}, \delta V_j^{i,\kappa}, \delta W_j^{i,\kappa}\}^T$ and $\{r_j^{i,\kappa}\} = \{(r_1)_j^{i,\kappa}, (r_2)_j^{i,\kappa}, (r_3)_j^{i,\kappa}, (r_4)_j^{i,\kappa}\}^T$ are four dimensional vectors of the unknown Newton iterates and the known right hand sides, respectively. The blocks in the three diagonals of the above matrix are 4×4 and can be obtained from

$$[A_j^{i,\kappa}] = \begin{bmatrix}
 1 & -h_j/2 & 0 & 0 \\
 (g_3)_j^{i,\kappa} & (g_3)_j^{i,\kappa} & (g_1)_j^{i,\kappa} & (g_7)_j^{i,\kappa} \\
 0 & -1 & -h_{j+1}/2 & 0 \\
 0 & 0 & 0 & -1
 \end{bmatrix} \quad \text{for } 2 \leq j \leq J-1$$

$$[B_j^{i,\kappa}] = \begin{bmatrix} -1 & -h_j/2 & 0 & 0 \\ (s_4)_j^{i,\kappa} & (s_6)_j^{i,\kappa} & (s_2)_j^{i,\kappa} & (s_8)_j^{i,\kappa} \\ 0 & 0 & 0 & 0 \\ 0 & 0 & 0 & 0 \end{bmatrix} \quad \text{for } 2 \leq j \leq J$$

$$[C_j^{i,\kappa}] = \begin{bmatrix} 0 & 0 & 0 & 0 \\ 0 & 0 & 0 & 0 \\ 0 & 1 & -h_{j+1}/2 & 0 \\ 0 & 0 & 0 & 1 \end{bmatrix} \quad \text{for } 1 \leq j \leq J-1$$

$$[A_1^{i,\kappa}] = \begin{bmatrix} 1 & 0 & 0 & 0 \\ 0 & 1 & 0 & 0 \\ 0 & -1 & -h_2/2 & 0 \\ 0 & 0 & 0 & -1 \end{bmatrix}$$

$$[A_J^{i,\kappa}] = \begin{bmatrix} 1 & -h_J/2 & 0 & 0 \\ (s_3)_J^{i,\kappa} & (s_5)_J^{i,\kappa} & (s_1)_J^{i,\kappa} & (s_7)_J^{i,\kappa} \\ 1 & 0 & 0 & 1/\tilde{c}_{ii} - \eta_J \\ 0 & 1 & 0 & -1 \end{bmatrix}$$

The components of the right hand side vectors can be calculated from the following formulae

$$(r_1)_j^{i,\kappa} = f_{j-1}^{i,\kappa-1} - f_j^{i,\kappa-1} + h_j U_{j-1/2}^{i,\kappa-1} \quad \text{for } 2 \leq j \leq J$$

$$(r_2)_j^{i,\kappa} = \begin{cases} \text{as given by} \\ \text{momentum equation} \end{cases} \quad \text{for } 2 \leq j \leq J$$

$$(r_3)_j^{i,\kappa} = U_j^{i,\kappa-1} - U_{j-1}^{i,\kappa-1} + h_{j+1} V_{j+1/2}^{i,\kappa-1} \quad \text{for } 1 \leq j \leq J-1$$

$$(r_4)_j^{i,\kappa} = \Pi_j^{i,\kappa-1} - \Pi_{j+1}^{i,\kappa-1} \quad \text{for } 1 \leq j \leq J-1$$

$$(r_1)_1^{i,\kappa} = 0, \quad (r_2)_1^{i,\kappa} = 0, \quad (r_3)_J^{i,\kappa} = \frac{\tilde{g}_i - \tilde{c}_{ii} f_J^{i,\kappa-1} - (1 - \tilde{c}_{ii} \eta_J) \Pi_J^{i,\kappa-1}}{\tilde{c}_{ii}}$$

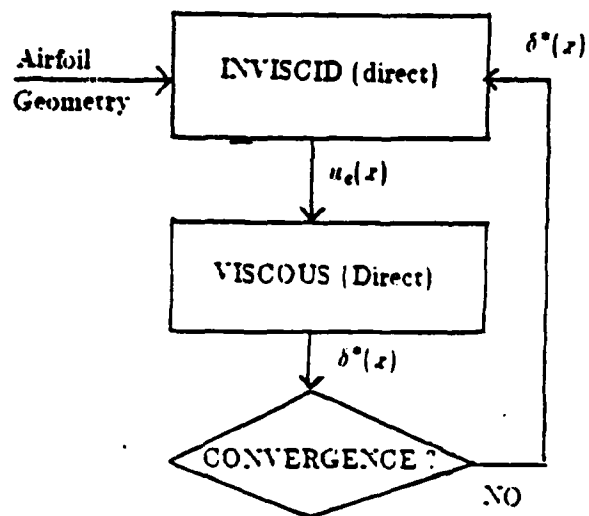
$$(r_4)_J^{i,\kappa} = 0$$

The numerical solution of the above system can again be achieved by Keller's block elimination method, which works very much like Gauss's algorithm, but, firstly, matrices are eliminated instead of scalars, and, secondly, quite a few manipulations can be saved because of sparse occupation.

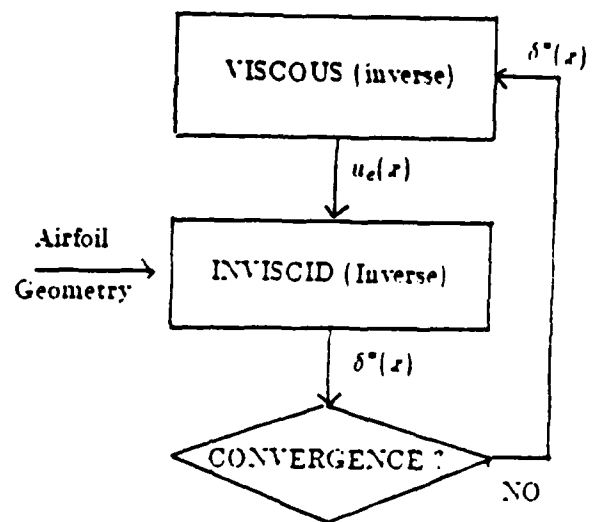
C. INTERACTION MODEL

The interaction model refers to the coupling of the boundary layer and the external inviscid flow. In principle, the interaction consists of thickening the effective airfoil shape by viscous displacement, which will result in a change of the surface pressure. Numerically the interaction between viscous and inviscid flow regions takes place via the boundary conditions only, which is the specification of either an impermeable displacement surface or a nonzero wall transpiration at the original surface in case of inviscid flow, respectively, the prescription of either pressure, or displacement thickness, or a linear combination of both in case of viscous flow. If the viscous effects on pressure remain small, then the interaction is called weak. However, situations, where viscous disturbances to the inviscid flow field are substantial, demand the application of strong interaction. In general, interaction models can be classified into four types, whereby the first three types provide loose coupling of viscous and inviscid regions:

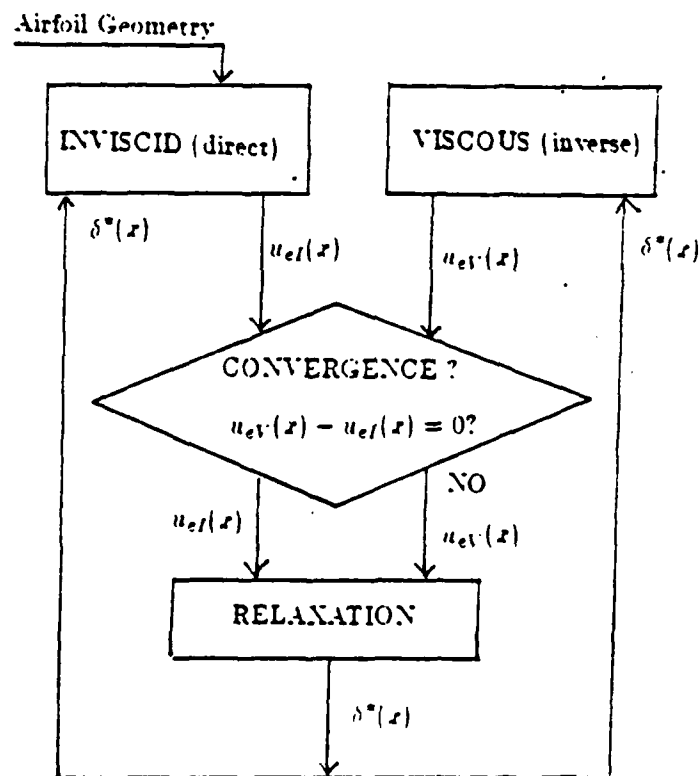
1. The direct interaction method combines a direct inviscid and direct viscous flow solver. This classical approach achieves a solution by iterative matching of boundary layer calculations with prescribed pressure and inviscid calculations with prescribed displacement thickness. The alternate treatment of pressure and displacement thickness leads to a local breakdown of the procedure when slight changes in pressure entail significant changes in displacement thickness (see Figure 4-2a).
2. In the inverse method the roles of the displacement thickness and pressure are interchanged. Hence the inviscid flow equations determine the displacement thickness distribution, which is imposed as boundary condition on the viscous flow calculation. The result of which is the pressure, which closes the cycle by being input to the inviscid flow computation. The hierarchical manner of solving the complete flow problem excludes this model just as the previous one from handling strongly interacting regions (see Figure 4-2b).
3. The semi-inverse interaction method is composed of a direct inviscid and an inverse viscous flow solver. Both parts of the scheme process the same input, i.e. displacement thickness, and generate the same output, i.e. pressure. After each cycle an updated displacement thickness is relaxed based on the deviation of the two pressure distributions, which should coincide upon convergence (see Figure



(a) DIRECT METHOD



(b) INVERSE METHOD



(c) SEMI-INVERSE

Figure 4.2 Direct, Inverse and Semi Inverse method.

4-2c). The existence of a definite hierarchy between boundary layer and the outer flow in the above mentioned methods gives rise to a limited rate of feedback between both regions. Strong interaction models incorporate the outer flow somehow in the boundary layer calculations, for example by the following interaction law:

4. Simultaneous or strong interaction methods solve the boundary layer equations subject to an interaction law as outer boundary condition, which retrieves the elliptic character of the outer flow. No definite assignment of displacement thickness and pressure can be made to viscous and inviscid region. Rather, both quantities are treated as unknowns, related by the interaction law. The procedure emphasizes simultaneous solution for both displacement thickness and pressure (Figure 4.2d).

The current interaction law is formulated in terms of displacement thickness δ^* and the external velocity u_e , the latter being related to pressure by Bernoulli's equation. The solution of the boundary layer equations in an iterative fashion makes use of an outer boundary condition, in which the total external velocity is written according to

$$u_e(x) = u_{ef}(x) + u_{e\delta}(x) \quad (4.31)$$

where $u_{ef}(x)$ is the inviscid external velocity and $u_{e\delta}(x)$ is the perturbation due to displacement effects. Using the thin airfoil concept, the perturbation velocity can be written as the Hilbert integral

$$u_{e\delta}(x) = \frac{1}{2\pi} \int_{x_0}^{x_*} \frac{\sigma(\xi)}{x - \xi} d\xi = \frac{1}{\pi} \int_{x_0}^{x_*} \frac{d}{d\xi} (u_e \delta^*) \frac{d\xi}{x - \xi} \quad (4.32)$$

The contribution due to viscous effects can be evaluated by means of the *blowing velocity* concept. Lighthill proved that the effect of boundary layers on the outer flow can be represented by a surface distribution of sources. The source strengths must be determined such that the virtual displacement surface becomes a streamline (see Figure 4.3)

$$\frac{d\delta^*(x)}{dx} = \frac{v(x, \delta^*)}{u_e(x)} \quad (4.33)$$

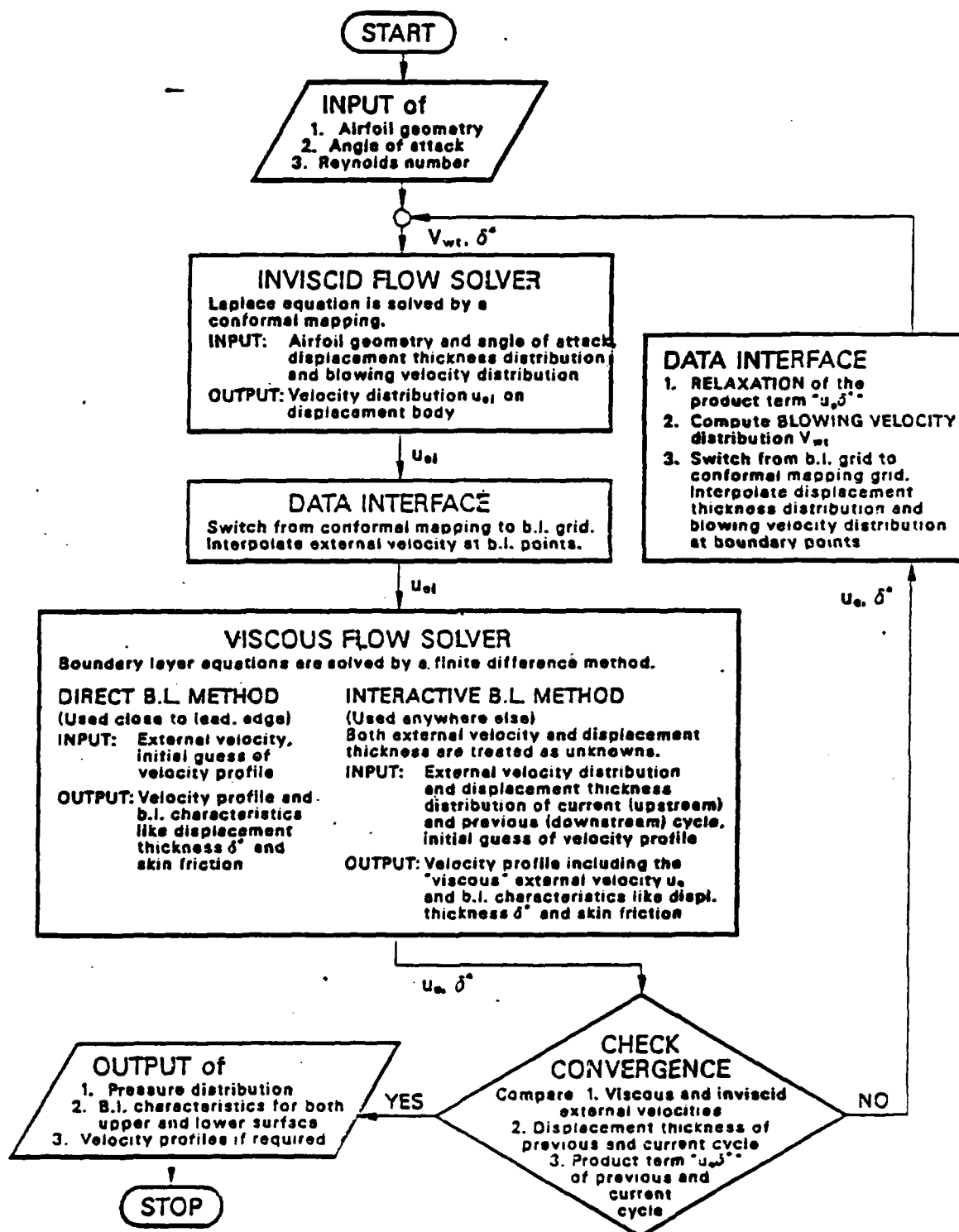


Figure 4.2d Viscous-Inviscid Interaction Method.

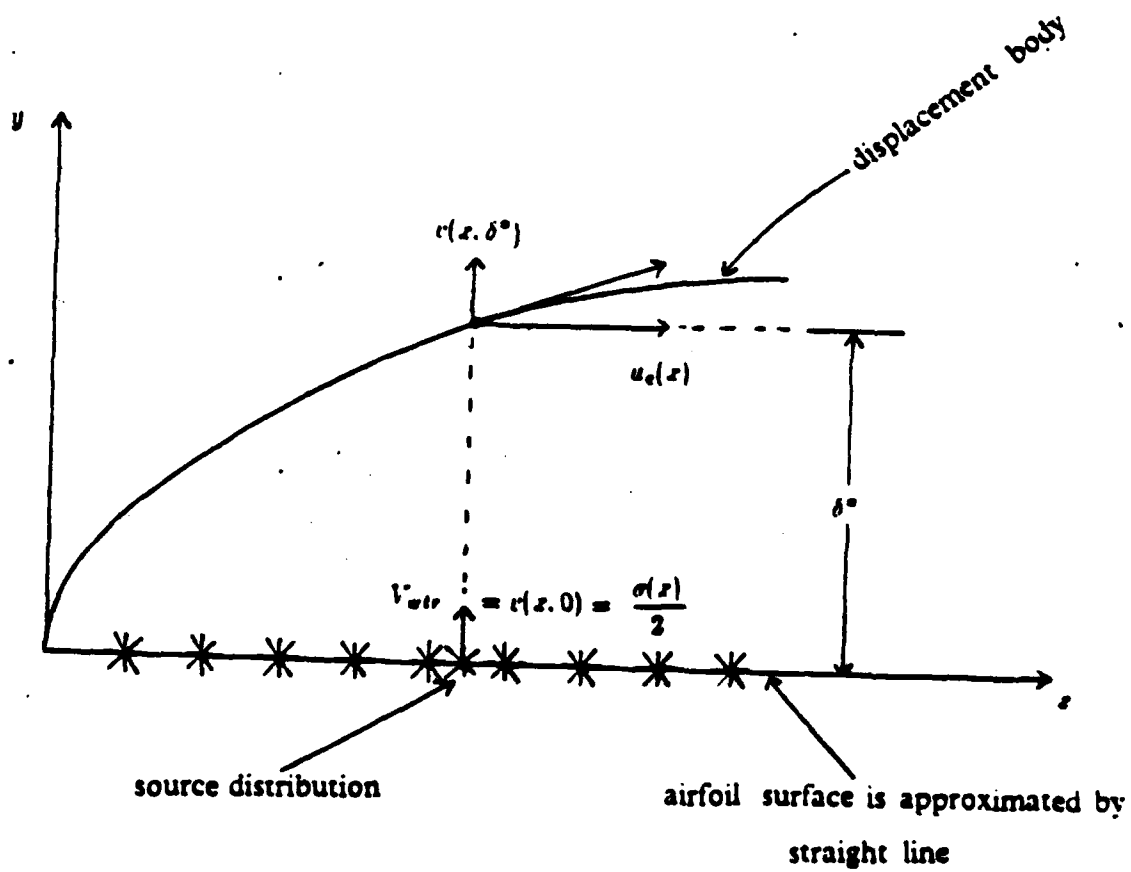


Figure 4.3 Concept of blowing velocity.

where $v(x, \delta^*)$ denotes the vertical velocity on the displacement surface. Since it is sufficient to approximate the correction term $u_e \delta$, we can use the thin airfoil approximation as follows:

1. The upper and lower surfaces of the airfoil will be considered as flat plates. This implies that the blowing velocity $v(x, 0)$ equals half of the local source strength
2. The displacement thickness is assumed to be so small that the horizontal velocity components of the inviscid flow do not vary across the boundary layer

$$\frac{\sigma(x)}{2} = v(x, 0) = v(x, \delta^*) - \int_0^{\delta^*} \frac{\partial v}{\partial y} dy = \frac{d}{dx}(u_e \delta^*) \quad (4.34)$$

The interaction region is limited to the finite region $x_b \leq x \leq x_e$ on either the upper or lower surface. The numerical implementation of the interaction law requires some discrete approximation of the above thin airfoil integral. Adopting the panel method approach, which concerns here a piecewise approximation of the continuous blowing velocity $d(u_e \delta^*)/dx$ to allow piecewise analytical integration, the integral can be written as a finite series

$$\frac{1}{\pi} \int_{x_b}^{x_e} \frac{d}{d\xi}(u_e \delta^*) \frac{d\xi}{x - \xi} = \sum_{k=1}^K c_{ik} (u_e \delta^*)^k \quad (4.35)$$

with $[c_{ik}]$ denoting a matrix of interaction coefficients defining the relationship between the boundary layer thickness and the external velocity. Recalling that the boundary layer calculation at a streamwise position involves Newton's iterations, the inviscid contribution can be included in the total external velocity of the previous Newton's iteration, leading to a generalized version of the interaction law

$$(u_e)^{i,\kappa} = (u_e)^{i,\kappa-1} + \sum_{k=1}^K c_{ik} [(u_e \delta^*)^{k,\kappa} - (u_e \delta^*)^{k,\kappa-1}] \quad (4.36)$$

Since displacement thickness does not belong to the dependent variables, $(\delta^*)^{i,\kappa}$, the displacement thickness of the streamwise position currently being solved, must be expressed in terms of dependent variables to make allowance for its unknown status.

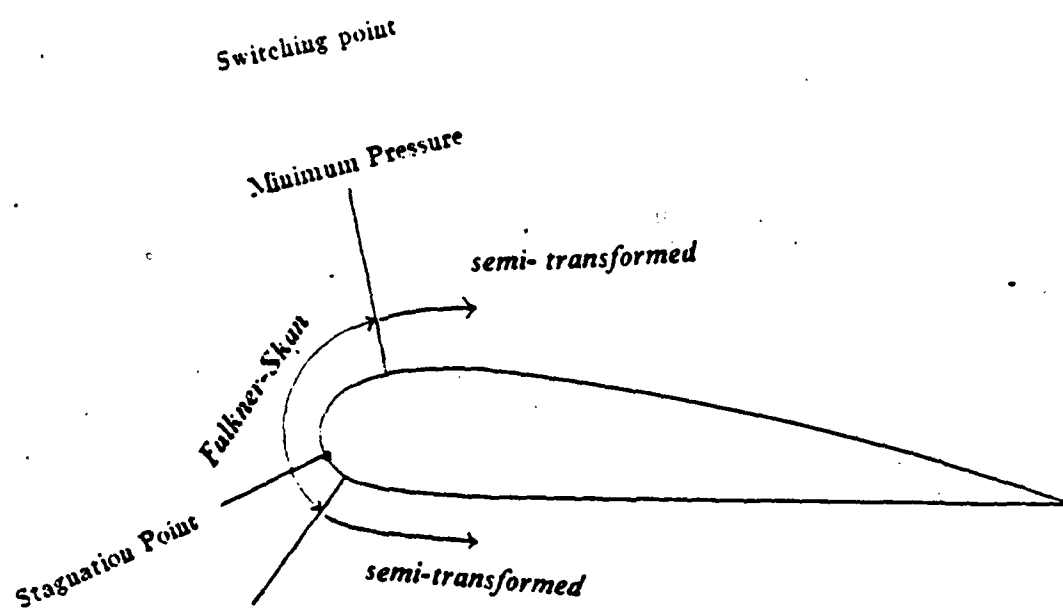


Figure 4.4 Application of the Direct and Interactive Method.

With $(\delta^*)^{i,\kappa}$ being replaced by $y_J - v_J^{i,\kappa}/(u_e)^{i,\kappa}$ and after separating known and unknown terms, the interaction law takes the form

$$(u_e)^{i,\kappa} (1 - c_{ii} y_J) + c_{ii} v_J^{i,\kappa} = g_i^\kappa \quad (4.37)$$

with

$$g_i^\kappa = (u_e)^{i,\kappa-1} + \sum_{\substack{k=1 \\ k \neq i}}^K c_{ik} [(u_e \delta^*)^{k,\kappa} - (u_e \delta^*)^{k,\kappa-1}] - c_{ii} (u_e y_J - v_J)^{i,\kappa-1}$$

Implementation of this relation necessitates a known right hand side, which can be evaluated only in approximate fashion, because the term $(u_e \delta^*)^{k,\kappa}$ is not known yet downstream of the current x-location. To ensure interaction also over this region, these terms are taken from the previous iteration updated by some relaxation formula. With $\tilde{c}_{ik} \sqrt{\nu x / u_0}$ and $\tilde{g}_i^\kappa = g_i^\kappa / u_0$ denoting the dimensionless interaction coefficient and right hand side, respectively, the actually coded interaction law can be written in terms of semi-transformed coordinates

$$\pi_J^{i,\kappa} (1 - \tilde{c}_{ii} \eta_J) + \tilde{c}_{ii} f_J^{i,\kappa} = \tilde{g}_i^\kappa \quad (4.38)$$

This equation is being used as an outer boundary condition in the viscous flow computation, and relates the unknown external velocity with the unknown displacement thickness of the i-th boundary layer station, whereas the displacement thickness has been expressed by the streamfunction and external velocity. Because of the elliptic character of the outer flow, which has been incorporated in the boundary layer via the interaction law, the solution requires a global iteration, consisting of several viscous sweeps to be performed over both the streamwise upper and lower surface.

Let the continuous function "external velocity times displacement thickness", denoted by D, be discretized at a finite number of streamwise positions, then the thin airfoil integral can be approximated by a finite series of weighted "D's" at the very locations

$$\frac{1}{\pi} \int_{x_1}^{x_K} \frac{dD}{d\xi} \frac{d\xi}{x_i - \xi} = \sum_{k=1}^K c_{ik} D_k \quad (4.39)$$

The weights are the interaction coefficients c_{ik} , with the first subscript indicating the streamwise position, where the correction term $u_{e\delta}$ is to be evaluated, and the second indicating the location, whose effect is accounted for. With a properly interpolated D-function, integration can be carried out analytically piece by piece. Provided the point under consideration does not fall within the limits of integration, D will be interpolated linearly. A piecewise linear function can be built up by overlapping triangular distributions, integration over which yields the coefficients whose $k \neq i$, $k \neq i-1$, $k \neq i+1$

$$c_{ik} = \frac{1}{\pi D_k} \int_{x_{k-1}}^{x_{k+1}} \frac{dD}{d\xi} \frac{d\xi}{x_i - \xi}$$

with $\frac{dD}{d\xi} = \begin{cases} \frac{D_k}{x_k - x_{k-1}} & \text{for } x_{k-1} \leq \xi \leq x_k \\ -\frac{D_k}{x_{k+1} - x_k} & \text{for } x_k \leq \xi \leq x_{k+1} \end{cases} \quad (4.40)$

$$c_{ik} = \frac{1}{\pi} \left[\frac{1}{x_k - x_{k-1}} \ln \left| \frac{x_i - x_{k-1}}{x_i - x_k} \right| - \frac{1}{x_{k+1} - x_k} \ln \left| \frac{x_i - x_k}{x_i - x_{k+1}} \right| \right] \quad (4.41)$$

A linearly interpolated D-function would lead to singular integrals for the coefficients $k = i$, $k = i-1$ and $k = i+1$. Therefore D will be approximated by a polynomial of degree 2 in the interval $x_{i-1} \leq \xi \leq x_{i+1}$. Splitting again into overlapping distributions, which this time are parabolic, and applying Cauchy's principal value technique permits integration of singular integrands. The coefficient at the middle of the inducing source distribution is given by

$$c_{ii} = \frac{1}{\pi D_i} \int_{x_{i-1}}^{x_{i+1}} \frac{dD}{d\xi} \frac{d\xi}{x_i - \xi} \quad (4.42)$$

with

$$\frac{dD}{d\xi} = \frac{D_i}{x_{i+1} - x_{i-1}} \left[\frac{x_{i+1} - \xi}{x_i - x_{i-1}} - \frac{x_i - \xi_{i-1}}{x_{i+1} - x_i} \right] - \frac{2(\xi - x_i)}{x_{i+1} - x_{i-1}} \left[\frac{D_i}{x_{i+1} - x_i} + \frac{D_i}{x_i - x_{i-1}} \right]$$

$$c_{ii} = \frac{1}{\pi} \left\{ \left[\frac{x_{i+1} - x_i}{x_i - x_{i-1}} - \frac{x_i - x_{i-1}}{x_{i+1} - x_i} \right] \frac{1}{x_{i+1} - x_{i-1}} \ln \left| \frac{x_i - x_{i-1}}{x_i - x_{i+1}} \right| + \frac{2}{x_i - x_{i-1}} + \frac{2}{x_{i+1} - x_i} \right\}$$

The coefficient at the right of the inducing source distribution is given by

$$c_{i,i-1} = \frac{1}{\pi D_{i-1}} \int_{x_{i-2}}^{x_{i-1}} \frac{dD}{d\xi} \frac{d\xi}{x_i - \xi} \quad (4.43)$$

with

$$\text{with } \frac{dD}{d\xi} = \begin{cases} \frac{D_{i-1}}{x_{i-1} - x_{i-2}} & \text{for } x_{i-2} \leq \xi \leq x_{i-1} \\ -\frac{D_{i-1}}{x_i - x_{i-1}} \frac{x_{i+1} - x_i}{x_{i+1} - x_{i-1}} + \frac{2(\xi - x_i)}{x_{i+1} - x_{i-1}} \frac{D_{i-1}}{x_i - x_{i-1}} & \text{for } x_{i-1} \leq \xi \leq x_{i+1} \end{cases}$$

$$c_{i,i-1} = \frac{1}{\pi} \left[\frac{1}{x_{i-1} - x_{i-2}} \ln \left| \frac{x_i - x_{i-2}}{x_i - x_{i-1}} \right| - \frac{x_{i+1} - x_i}{(x_i - x_{i-1})(x_{i+1} - x_{i-1})} \ln \left| \frac{x_i - x_{i-1}}{x_i - x_{i+1}} \right| - \frac{2}{x_i - x_{i-1}} \right]$$

The coefficient at the left of the inducing source distribution is given by

$$c_{i,i+1} = \frac{1}{\pi D_{i+1}} \int_{x_{i-1}}^{x_{i+2}} \frac{dD}{d\xi} \frac{d\xi}{x_i - \xi} \quad (4.44)$$

with

$$\text{with } \frac{dD}{d\xi} = \begin{cases} \frac{D_{i+1}}{x_{i+1} - x_i} \frac{x_i - x_{i-1}}{x_{i+1} - x_{i-1}} + \frac{2(\xi - x_i)}{x_{i+1} - x_{i-1}} \frac{D_{i+1}}{x_{i+1} - x_i} & \text{for } x_{i-1} \leq \xi \leq x_{i+1} \\ -\frac{D_{i+1}}{x_{i+2} - x_{i+1}} & \text{for } x_{i+1} \leq \xi \leq x_{i+2} \end{cases}$$

$$c_{i,i+1} = \frac{1}{\pi} \left[\frac{x_i - x_{i-1}}{(x_{i+1} - x_i)(x_{i+1} - x_{i-1})} \ln \left| \frac{x_i - x_{i-1}}{x_i - x_{i+1}} \right| - \frac{2}{x_{i+1} - x_i} - \frac{1}{x_{i+2} - x_{i+1}} \ln \left| \frac{x_i - x_{i+1}}{x_i - x_{i+2}} \right| \right]$$

As indicated above, the overall solution is approached in an iterative process, in which alternately viscous and inviscid flow equations are being solved:

1. Calculate the external velocity distribution u_{eI} in an inviscid flow field by means of the conformal mapping method. To account for the airfoil-thickening due to viscous displacement, specify a nonzero normal velocity (blowing velocity) at the airfoil surface.
2. March through the boundary layers of both streamwise upper and lower surface using the interaction law as outer boundary condition.
3. Check convergence and quit if the criterion satisfied.
4. If the convergence criterion is not met, prepare for another cycle. Update the product-term "external velocity times displacement thickness" on the basis of the deviation between inviscid and viscous external velocity distributions

$$(u_e \delta^*)^{i, \lambda+1} = (u_e \delta^*)^{i, \lambda} \left[1 + \omega \left(\frac{(u_e)^{i, \lambda}}{(u_{ef})^{i, \lambda}} - 1 \right) \right] \quad (4.45)$$

where λ denotes the counter of global iterations. Further, compute the blowing velocity (V_{wtr} = wall transpiration velocity) distribution, which serves as boundary condition for the inviscid flow solution

$$(V_{wtr})^i = \frac{d}{dx} (u_e \delta^*)^{i, \lambda+1} \quad (4.46)$$

and proceed with the first step.

D. TURBULENCE MODELLING

The presence of additional unknown shear stresses in turbulent flows requires modelling assumptions to balance the number of unknowns and equations. Eddy viscosity models, one of which is used in the present method. [Ref. 13.] relate turbulent shear stresses to mean flow quantities on an empirical basis. They draw their versatility from the convenience of maintaining the same approach and numerical formulation for both laminar and turbulent flows. According to this formulation for wall boundary layer flows, the turbulent kinematic eddy viscosity is defined by two separate formulas, one for the inner region being based on Van Driest's approach, and the other for the outer region being based on a velocity defect approach

$$\nu_t = \begin{cases} \left\{ 0.4 y \left[1 - \exp\left(-\frac{y}{A}\right) \right] \right\}^2 \left| \frac{\partial u}{\partial y} \right| \gamma_{tr} & \text{for } 0 \leq y \leq y_c \\ \alpha \int_0^\infty (u_e - u) dy \gamma_{tr} \gamma & \text{for } y_c \leq y \leq \delta \end{cases} \quad (4.47)$$

$$\text{where } A = 26\nu / \left(\nu \frac{\partial u}{\partial y} \right)_{max}^{1/2} \quad \text{and} \quad \gamma = \frac{1}{1 + 5.5(y/\delta)^6}$$

Continuity of the turbulent kinematic viscosity is established by defining y_c as the distance from the wall where expressions for inner and outer region do agree. Since transition is not an instantaneous process, an intermediate status of flow is assumed between the laminar and fully turbulent regions. This region is taken into account by introducing an intermittency factor, which smears out the step-shaped change from kinematic to eddy viscosity. The formula here is suggested by Chen and Thyson.

$$\gamma_{tr} = 1 - \exp \left[- \frac{u_e^3}{G_{\gamma_{tr}} \nu^2} R_{x_{tr}}^{-1.34} (x - x_{tr}) \int_{x_{tr}}^x \frac{d\xi}{u_e} \right] \quad (4.48)$$

where $R_{x_{tr}}$ denotes the transitional Reynolds Number $(u_e x / \nu)_{tr}$, i.e., Reynolds Number based on external velocity and streamwise location x_{tr} at onset of transition. A value of 1200 was originally assigned to the empirical constant $G_{\gamma_{tr}}$. However, numerical experiments seem to indicate that low Reynolds number flows can be better modelled by values below 1200 (further discussion in the next section). The parameter α in the outer region formula is obtained from

$$\alpha = \frac{0.0168}{F^{2.5}} = 0.0168 / \left[1 - \beta \frac{\partial u / \partial x}{\partial u / \partial y} \right]^{2.5}$$

where the nondimensional factor F denotes the ratio of total turbulence energy production to the shear-stress-related turbulence energy production, evaluated at the location of maximum shear stress

$$F = 1 - \left[\frac{(\overline{u'^2} - \overline{v'^2}) \partial u / \partial x}{-\overline{u'v'} \partial u / \partial y} \right]_{(-\overline{u'v'})_{max}} \quad (4.49)$$

The ratio of the time-averaged quantities above can be approximated by a function of $R_T = \tau_w / (-\overline{u'v'})_{max}$

$$\beta = \left[\frac{\overline{u'^2} - \overline{v'^2}}{-\overline{u'v'}} \right]_{(-\overline{u'v'})_{max}} = \begin{cases} \frac{6}{1 + 2R_T(2 - R_T)} & \text{for } R_T < 1 \\ \frac{1 + R_T}{R_T} & \text{for } R_T \geq 1 \end{cases} \quad (4.50)$$

Since this turbulence model is not validated for separated flow, eddy viscosities in regions of backflow correspond to those of adjacent upstream station at the same η -coordinate. Transition, if not available from other sources, currently is predicted by an empirical data correlation expressed in terms of the Reynolds Numbers based on momentum thickness and streamwise coordinate at onset of transition

$$R_{xtr} = 1.174 \left(1 + \frac{22400}{R_{xtr}} \right) R_{xtr}^{0.46} \quad (4.51)$$

E. DISCUSSION OF THE COMPUTER PROGRAM

1. Inviscid Flow Method

The inviscid flow method used in the interaction method is based on *conformal mapping* which can be divided into the transformation of the region outside the airfoil to the region outside a unit circle and to the solution of the equations in the transformed plane. The transformation was achieved in three parts which together represent the major computational effort.

In the first mapping, the airfoil is perturbed slightly to make the upper and lower surface trailing-edge points coincide. This is accomplished using a logarithmic mapping function and is necessary only in those cases in which the airfoil trailing edge has non-zero thickness.

In the second mapping, the trailing-edge corner is analytically removed by applying the Karman-Trefftz mapping.

In the last mapping, the resulting quasi-circular shape is mapped to a perfect circle using an iterated sequence of applications of the fast Fourier transform algorithm. The calculation of the flow in the transformed plane also makes use of Fourier analysis technique.

The major computational effort required in the inviscid flow method is due to the transformation. It is necessary to compute the transformation only once in the viscous inviscid flow interactions, so that the computational expense due to inviscid calculations can be held to a minimum. When the angle of attack increases, care must be taken since the displacement thickness can become fairly large, approaching 10% of the airfoil chord. In this case, use of the blowing velocity (equation 4.33) on the airfoil surface produces a dividing streamline from the leading-edge stagnation point which approximates the edge of the boundary-layer displacement thickness. The inviscid flow outside this dividing streamline is therefore the same as that past the solid body defined by this streamline. However, inside this dividing streamline, the inviscid flow is fictitious. In particular, the assumption that there is no pressure variation across this fictitious region becomes invalid as the magnitude of blowing velocity V_{wtr} increases. The approach adopted here is, therefore, to evaluate the velocity distribution directly on the displacement surface while still applying the blowing velocity on the

original airfoil surface. To avoid a discontinuity of the velocity between upper and lower surface, the Kutta condition is applied on the displacement surface. Requiring equal off-body pressures for the upper and lower trailing edge points, a quadratic equation can be solved for the unknown circulation.

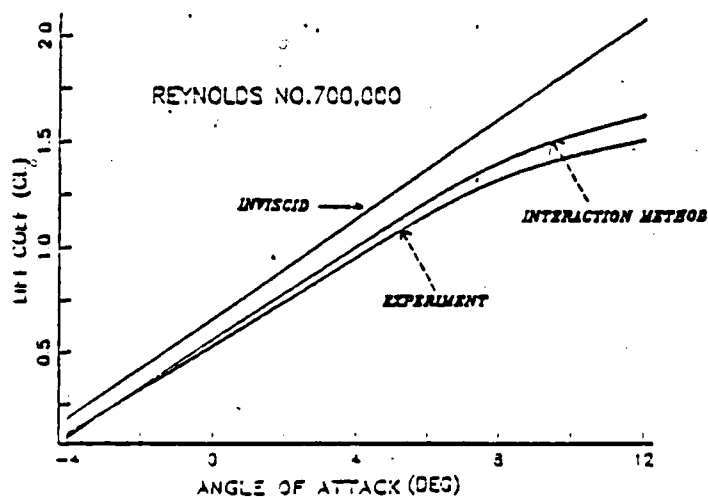
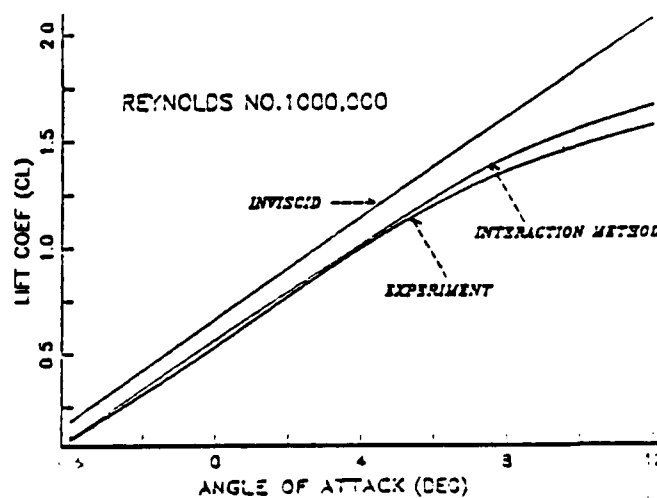
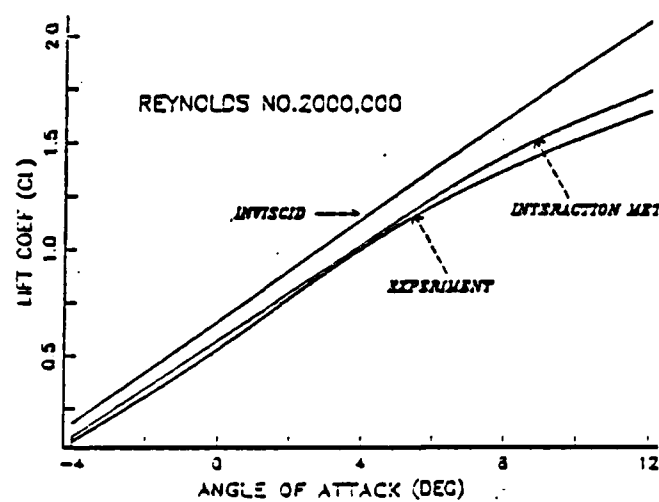
2. Interactive Viscous Flow Method

In this method, the boundary layer is transformed into Falkner-Skan and subsequently semi-transformed coordinates. The numerical solution of the transformed equations is performed using an implicit finite-difference technique, which is first-order accurate in the streamwise direction and second order accurate in the normal direction. In principle, the computer program calculates:

1. The inviscid pressure distribution for a specified angle of attack
2. The boundary layer, including the velocity profile, skin friction, momentum and displacement thickness either:
 1. subject to a prescribed pressure distribution, or
 2. subject to an interactive edge boundary condition. In this case, the external velocity will be a part of the boundary layer results.

These calculations are performed for a specified number of x -stations on the airfoil and in the wake, a number of sweeps is made on the airfoil in order to obtain a converged solution. The Cebeci-Smith two layer model is used here for computing the eddy viscosity ν_t , and the transitional flow region is modelled using equation 4.48. The method also employs a semi-empirical formula to predict the onset of transition. This criterion, equation 4.51, was proposed by Michel. The code offers two possibilities how to deal with transition:

1. The loci of transition are calculated by the code. In this case Michel's criterion is employed to predict the onset of transition. When laminar separation occurs upstream of the calculated point of transition, then Michel's Criterion is disregarded and the onset of transition is redefined at the point of laminar separation.
2. The begin of transition is specified by the user (fixed). The code has been modified to allow the onset of transition to be within or downstream of the laminar separation bubble. The previous version of the code always redefined transition at the point of laminar separation.



LIFT CURVE PLOT
FX 60-125

Figure 4.5 Lift curves of the Wortmann FX 60-126 airfoil at $Re = 700,000$,
1,000,000 and 2,000,000
(source of experimental results: Ref. 18).

F. DISCUSSION OF THE RESULTS

1. High Reynolds Number Flows

The computer program was first applied to high Reynolds-Number flows about the Wortmann airfoil FX 60-126. Figure 4.5 shows results for Reynolds Numbers from 700,000 up to 2000,000. It is seen that the lift predictions are in quite good agreement with experimental data.

2. Low Reynolds Number Flows

The subject of low Reynolds Number flows is important to a number of practical problems, including remotely piloted vehicles, wind turbines and propellers, sail planes, human powered vehicles, etc. Many boundary layer phenomena which have eluded accurate analytical prediction occur within this flow regime and are associated with laminar separation and subsequent transition of a laminar free shear layer. Figure 4.6 shows the phenomenological features of the boundary layer on a low Reynolds number airfoil.

When the Reynolds Number based on momentum thickness, R_{θ} , is sufficiently low, the boundary layer remains laminar up to, including, the point of minimum pressure or maximum suction. At some location between the minimum pressure and the theoretical point of laminar separation the Reynolds Number of the boundary layer attains a critical value. This is referred to as the transition Reynolds Number based on momentum thickness, $R_{\theta_{tr}}$.

The provision of reliable information of the flow characteristics of low Reynolds Number airfoils is hampered by the sensitivity of the flows, and particularly those involving separation and transition.

In recent years, several theoretical studies have led to the development of methods for predicting airfoil characteristics at low Reynolds Numbers, but there are no universal methods which can accurately predict and account for a separation bubble in the design of efficient low Reynolds Number airfoils.

The viscous inviscid interaction method was applied to the NACA 65-213 airfoil at a Reynolds number of 240,000. It was found that the calculation would fail to converge if transition was predicted by Michel's criterion (equation 4.51) and if the empirical constant $G_{\gamma_{tr}}$ was chosen to be 1200. Therefore it was decided to investigate the influence of the start of the transition and of the constant $G_{\gamma_{tr}}$ on the results by systematically varying both parameters. Table I of Appendix C shows the predicted lengths of the separation bubble which is obtained if transition is chosen to start at $x =$

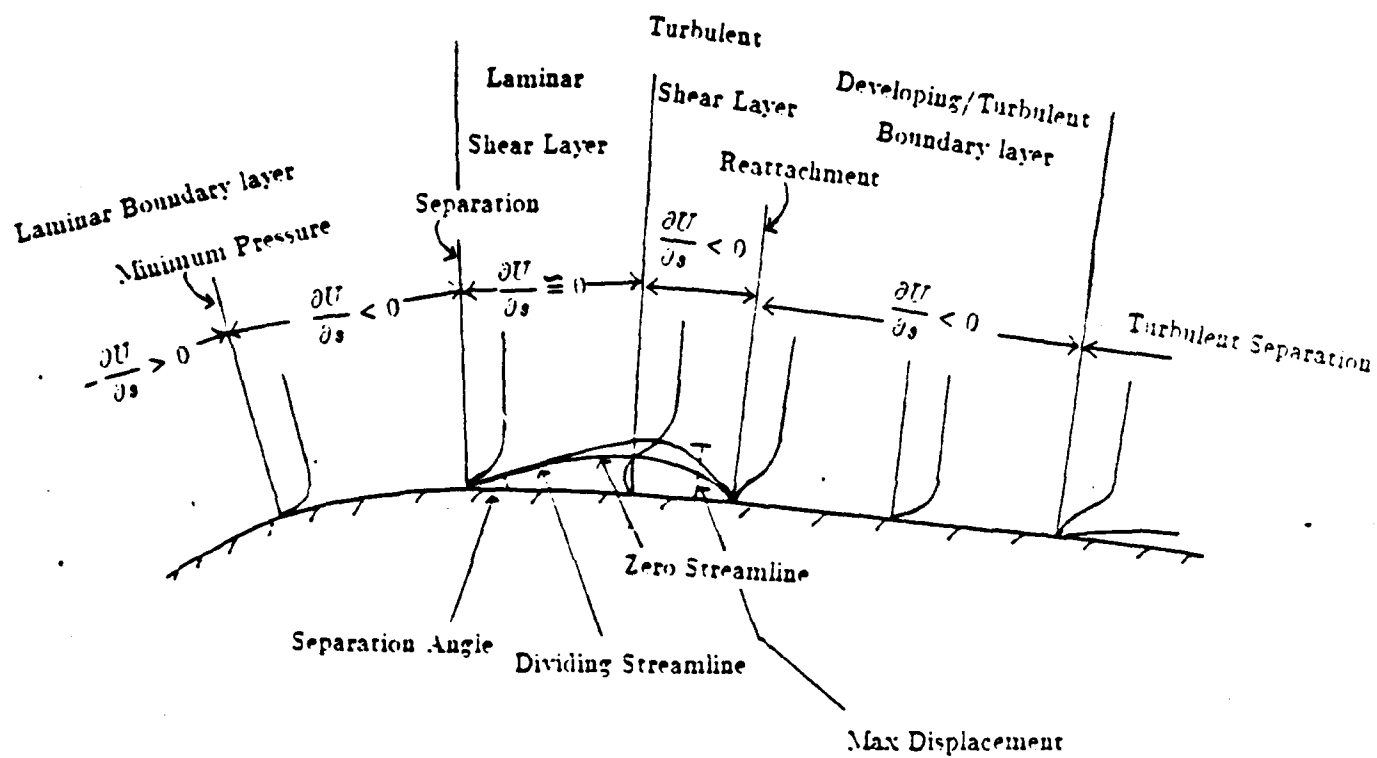


Figure 4.6 Phenomenological features of the boundary layer on the low Reynolds Number airfoil.

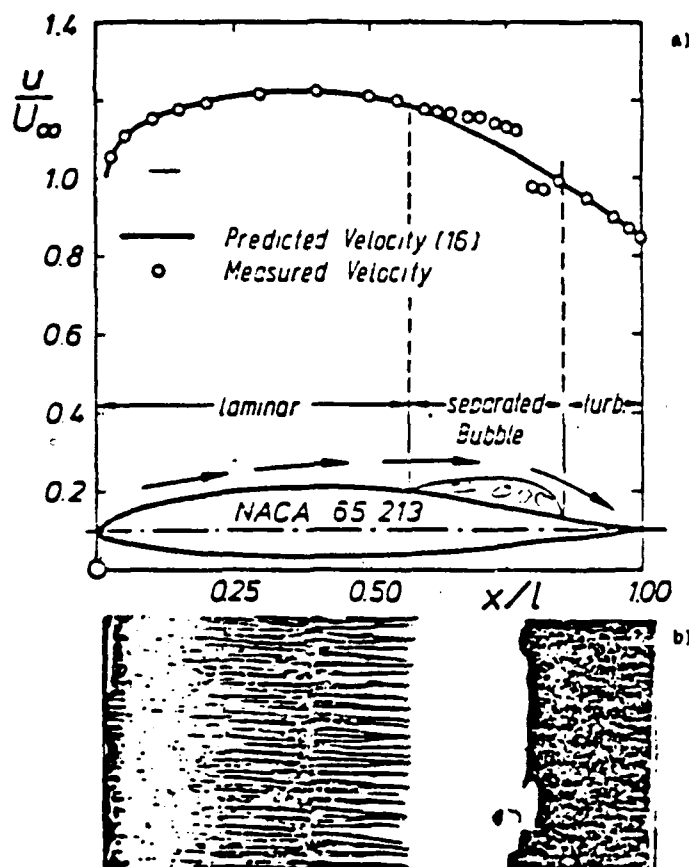


Figure 4.7 Experimental result for the NACA 65-213 (by Hoheisel et al.)
 $M_\infty = 0.1$, $Re_\infty = 240,000$, $Tu_\infty = 0.2\%$, $AOA = 0.0^\circ$
 (a) Velocity distribution and (b) Flow visualization.

65, 66, 67, 68, 69, 70, 72, 74, or 76 % of chord and if G_{ytr} is chosen as 10, 20, 40, 80, or 120. It is seen that there are significant changes in the length of the separation bubble depending on the chosen parameter combination. This effect is displayed more clearly in Figure 4.11 and 4.12.

An increase in G_{ytr} increases the transition length as well as the length of the separation bubble.

Hoheisel et al. [Ref. 14] performed detailed laser-Doppler velocimetry measurements of this airfoil at a Reynolds number of 240,000. Their results are shown in Figures 4.7, 4.9, and 4.10 and it was attempted to choose that parameter combination which would give the best agreement with the experimental results. If the begin of transition is chosen at 74 % of chord and if $G_{ytr} = 20$, then the results shown in Figures 4.13, 4.14 and 4.15 are obtained. It is seen that the boundary layer profiles, displacement and momentum thickness distributions upstream of the separation bubble are in excellent agreement, whereas considerable deviations are found in the bubble. Finally, Figure 4.16 through 4.20 show the computed boundary layer velocity profiles for different values of G_{ytr} ranging from 10 to 50.

SKIN FRICTION

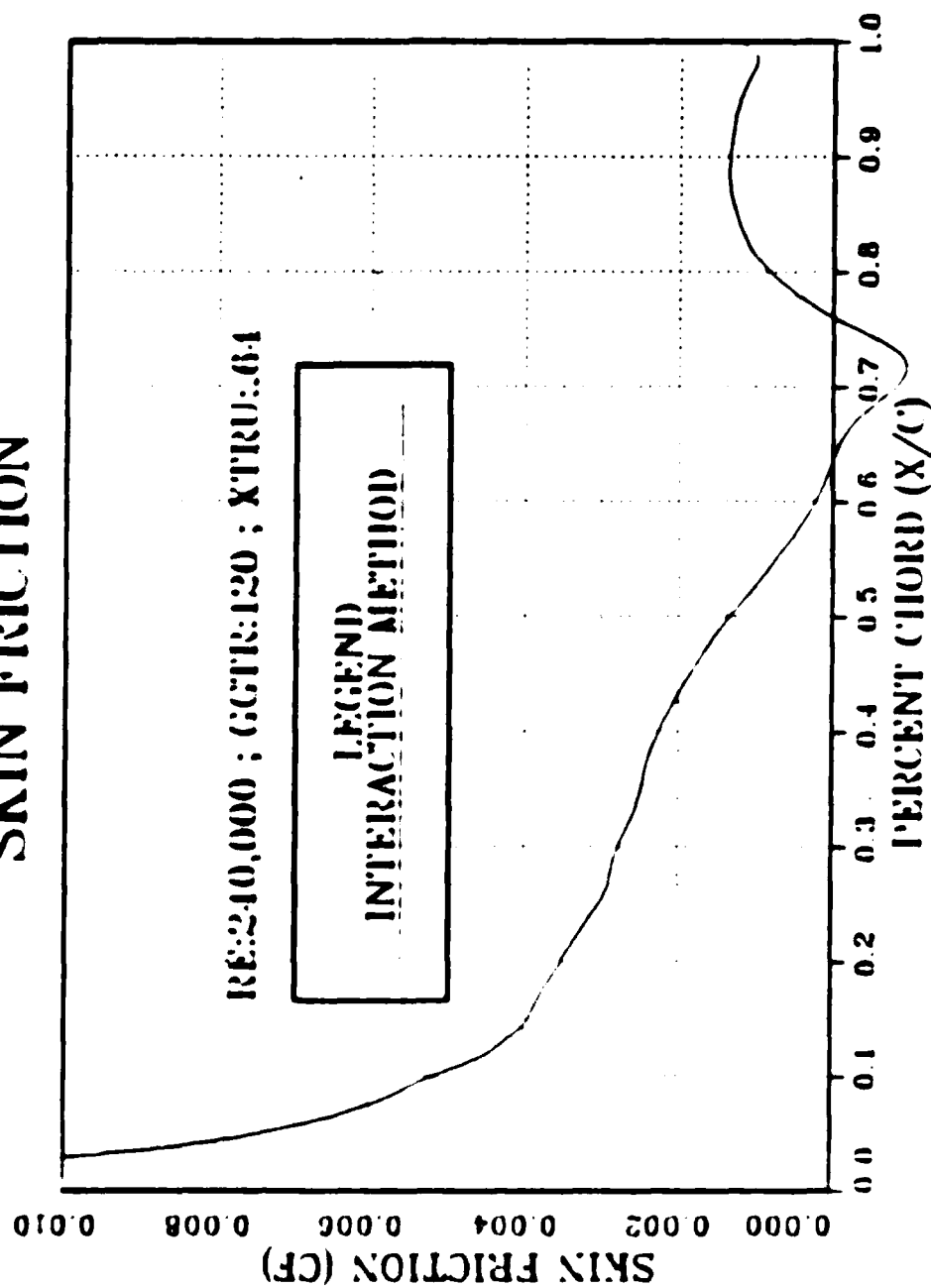


Figure 48 Skin friction distribution on the NACA 65-213 for $C_{yfr} = 120$ and $XTRU = 64$

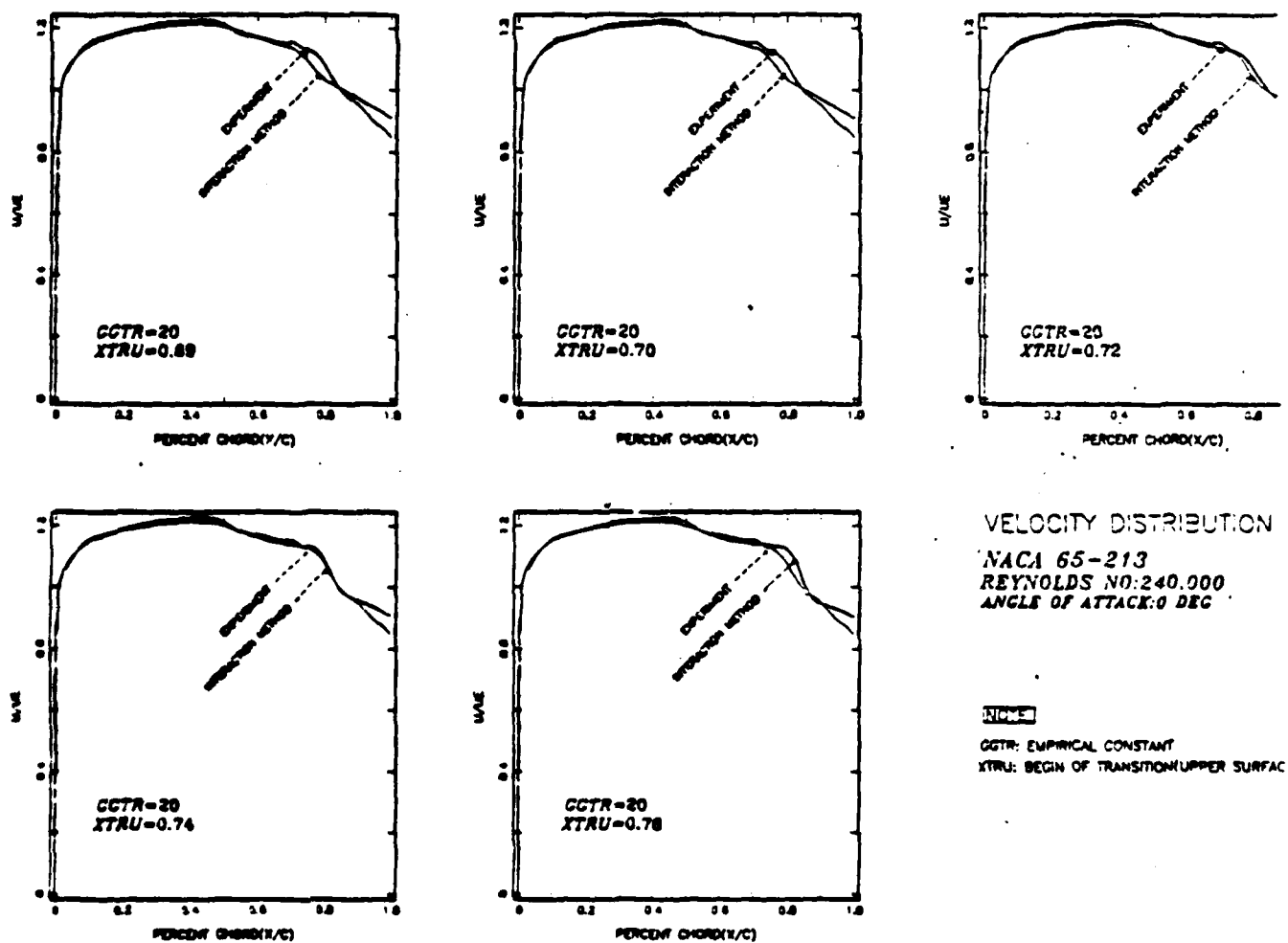


Figure 4.9 Effect of variation of $XTRU$ for $G_{7tr} = 20$ on the velocity distribution.

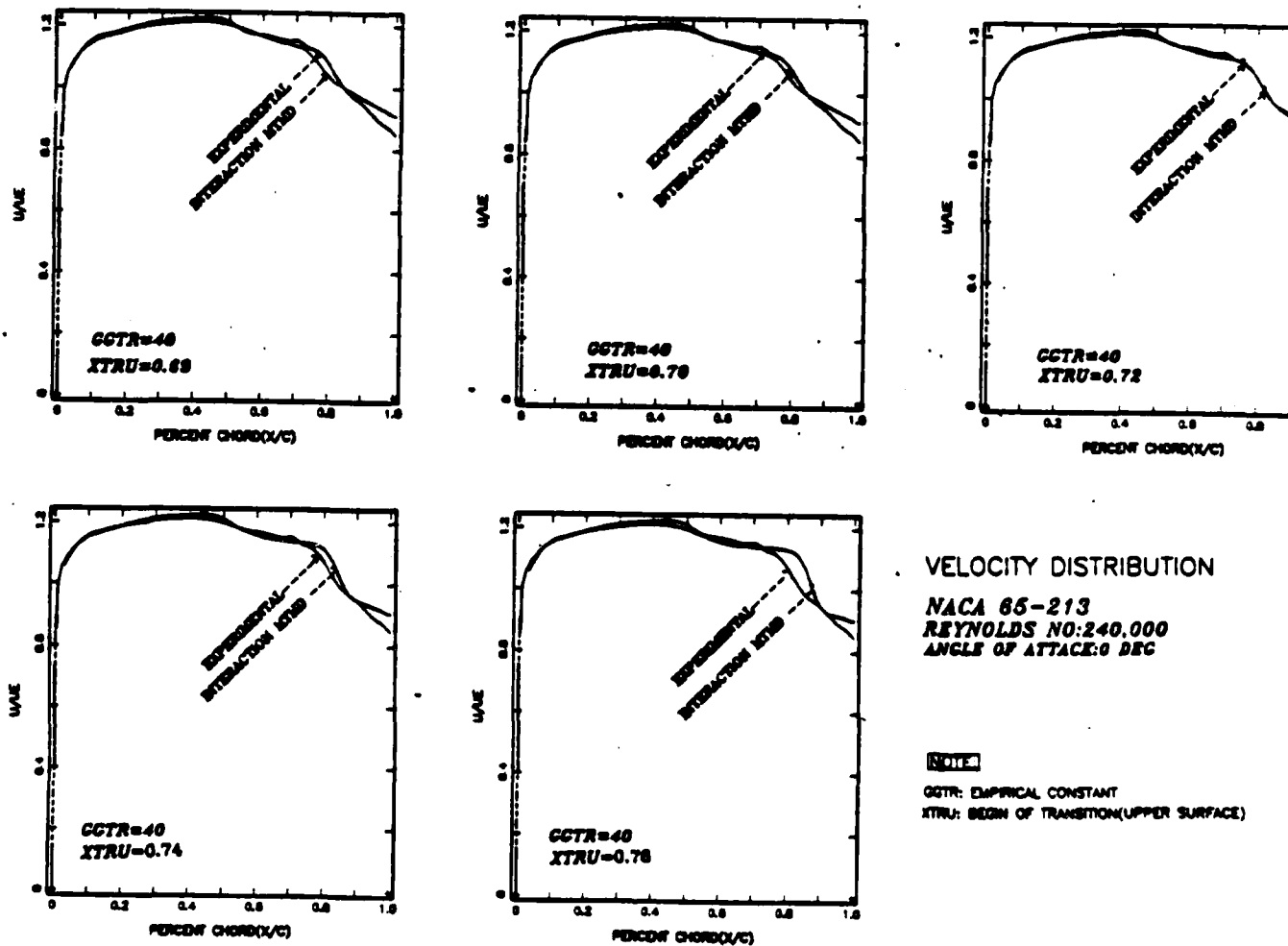


Figure 4.10 Effect of variation of XTRU for $G_{ytr} = 40$ on the velocity distribution.

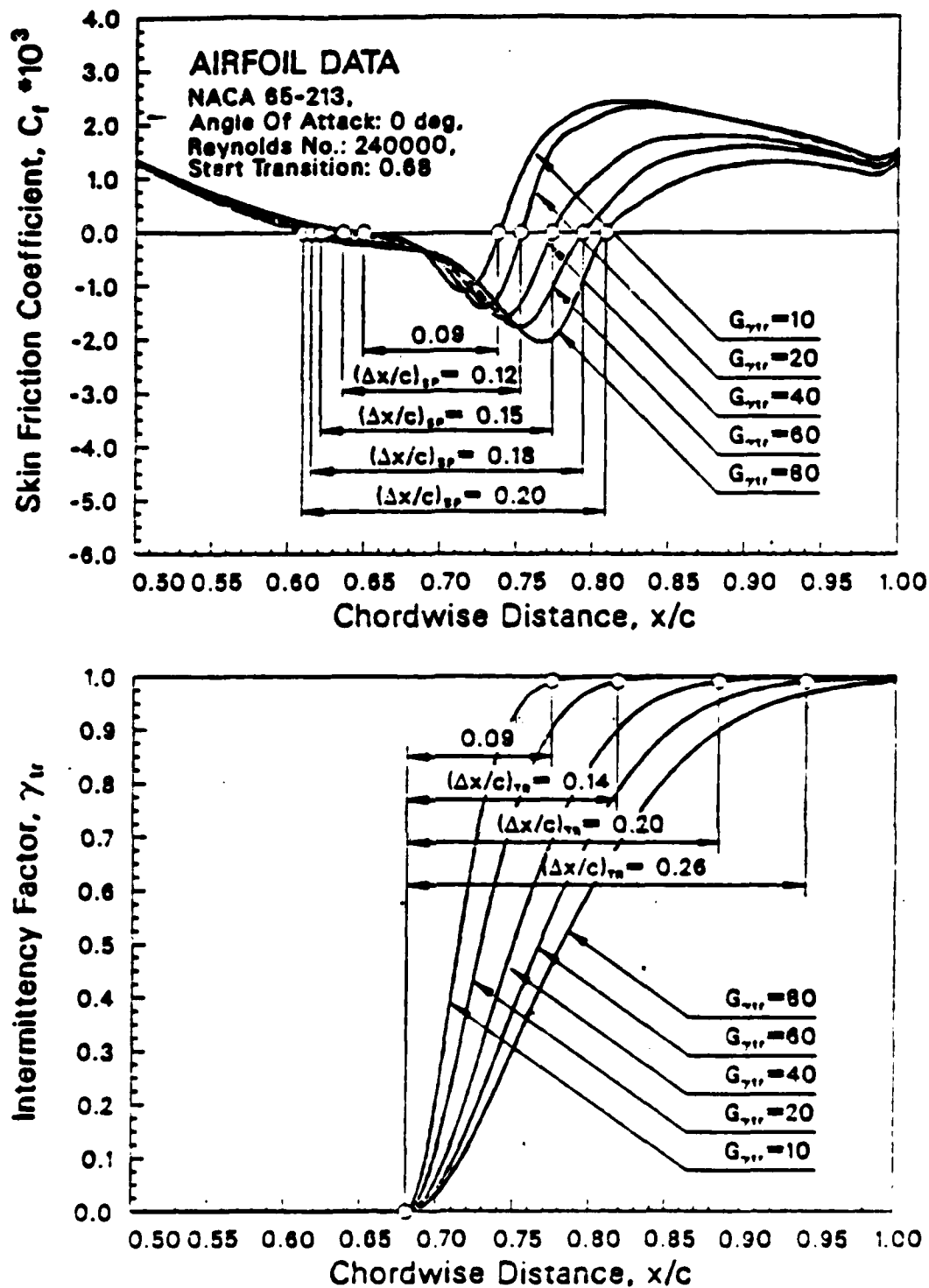


Figure 4.11 Effect of variation of $G_{\gamma_{tr}}$ for $NTRU = 0.68$ on the distributions of skin friction and intermittency factor.

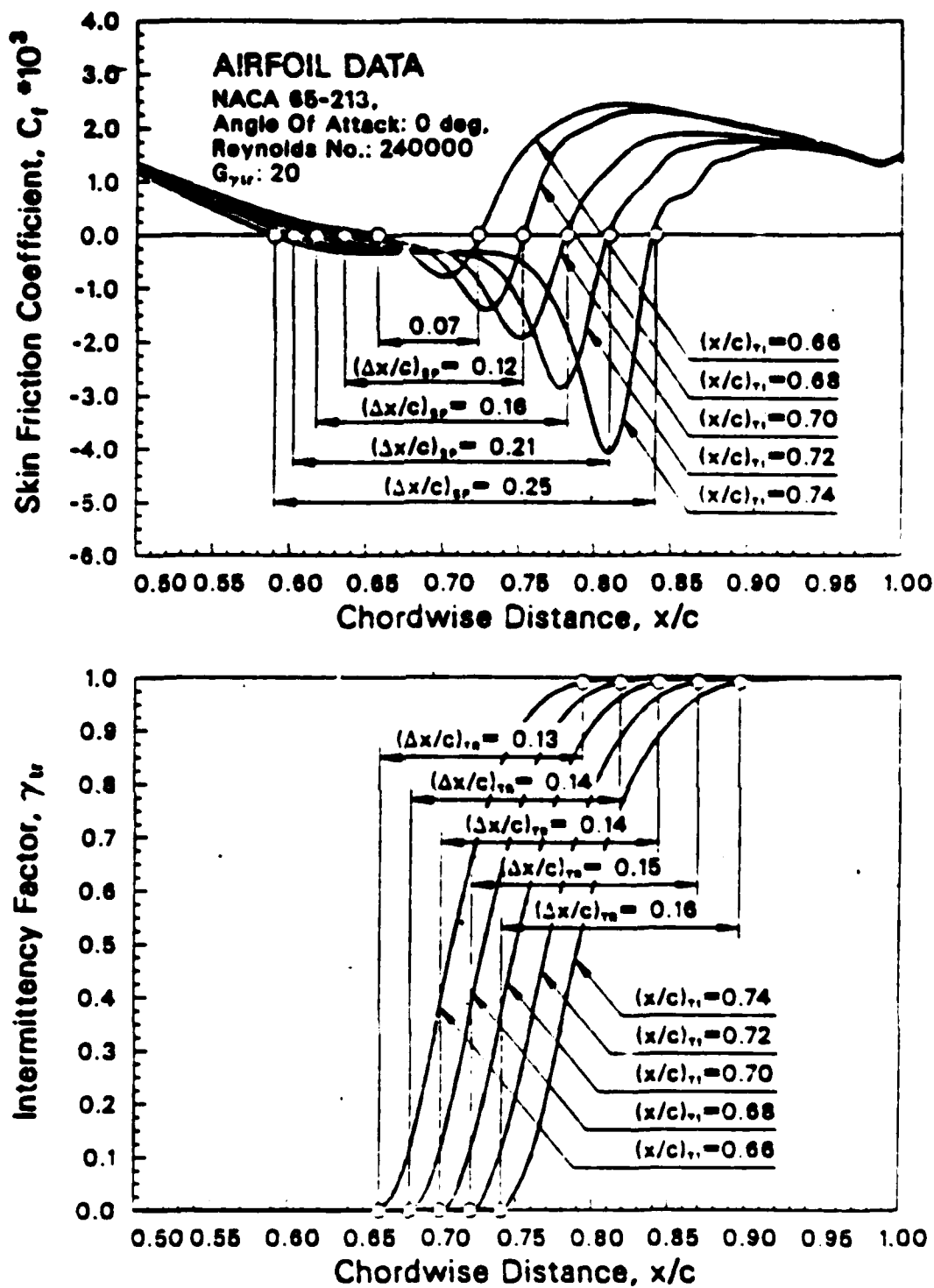


Figure 4.12 Effect of variation of NTRU (begin of transition) for $G_{\gamma_{tr}} = 20$ on the distributions of skin friction and intermittency factor.

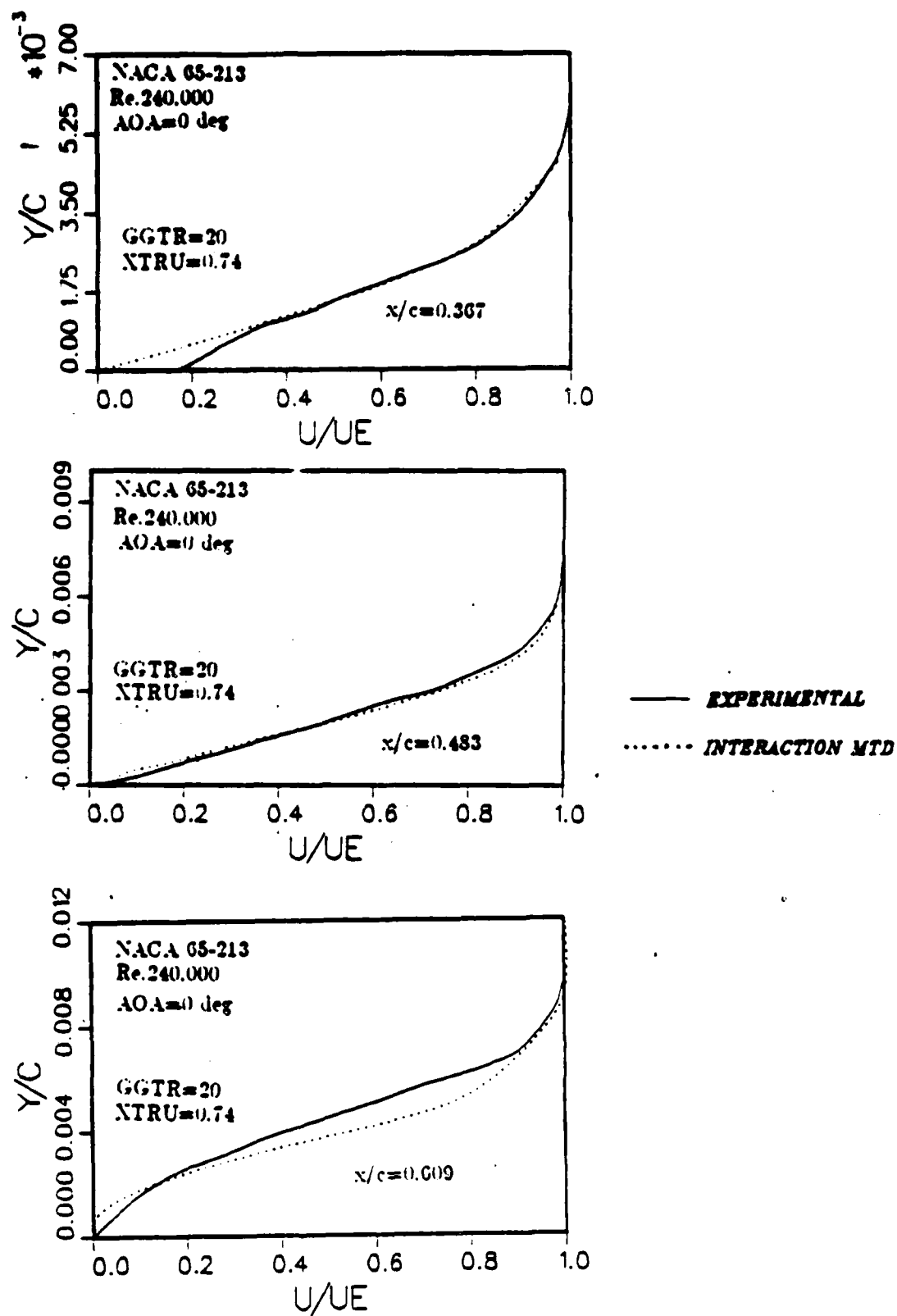


Figure 4.13 Velocity profiles in front of the bubble at $x/c = 0.367, 0.483$ and 0.609 .

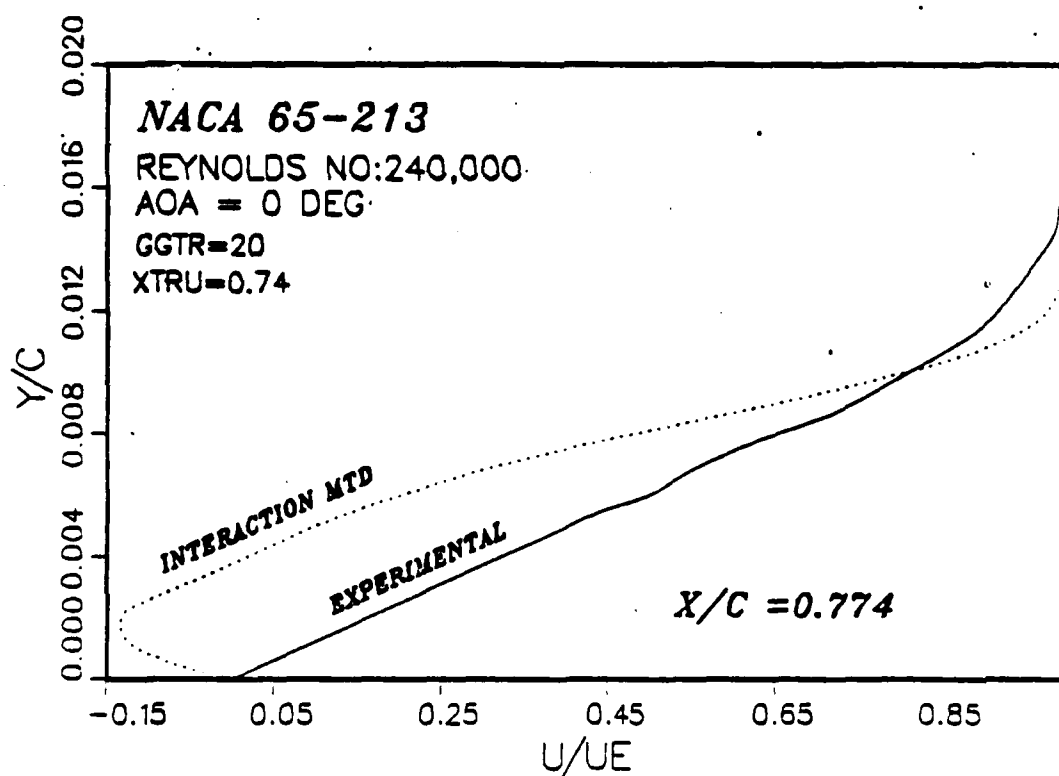
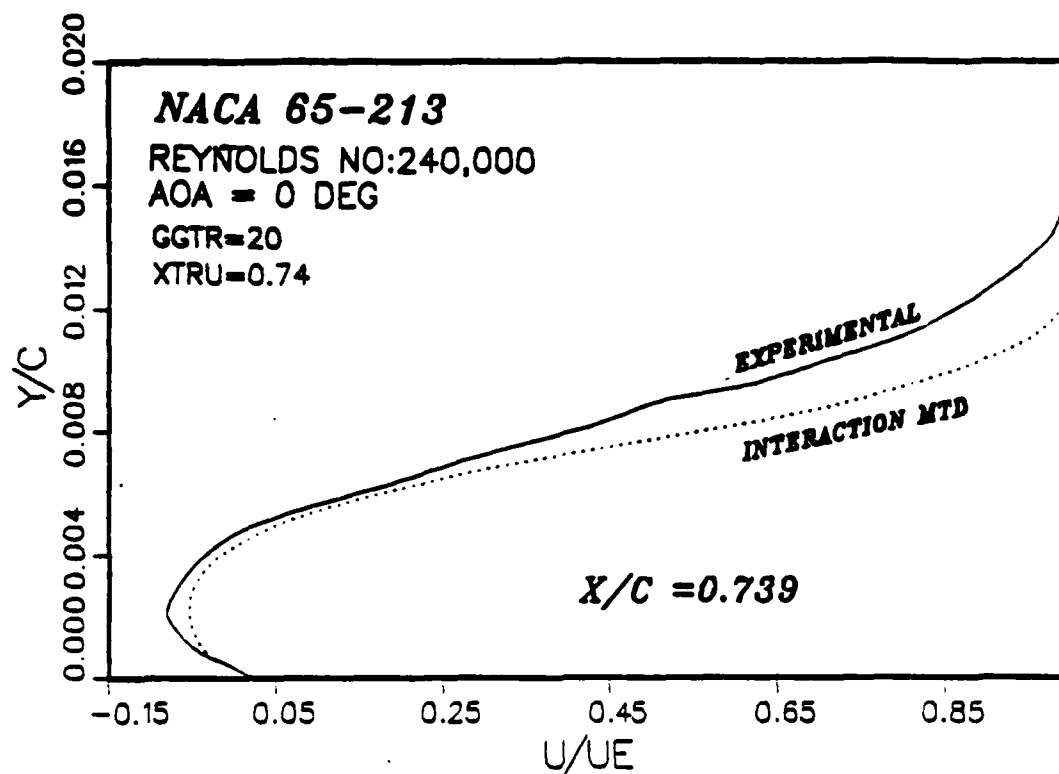


Figure 4.14 Velocity profiles in the bubble region at $x/c = 0.739$ and 0.774 .

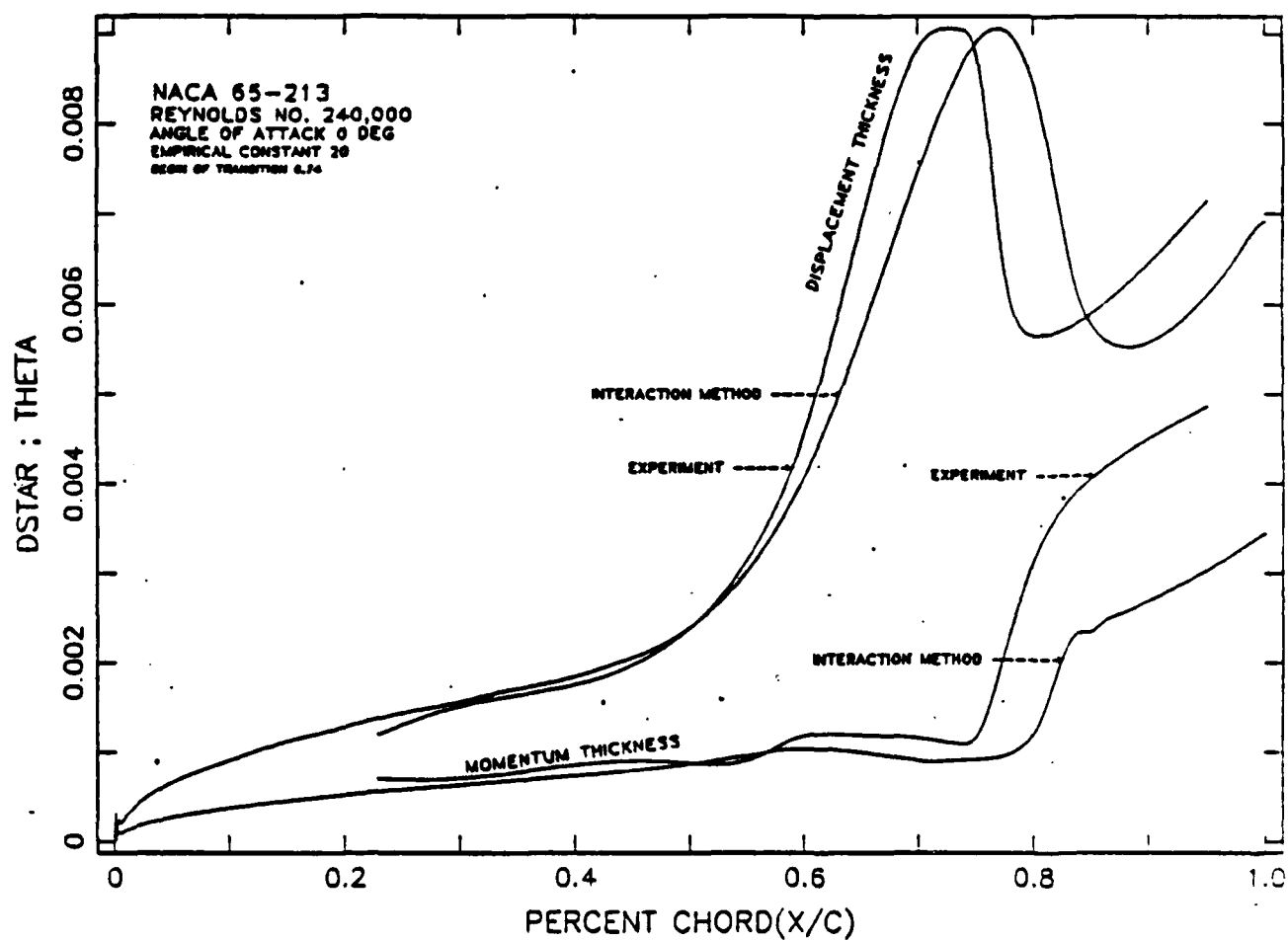


Figure 4.15 Comparison of δ^* and θ with experimental results.

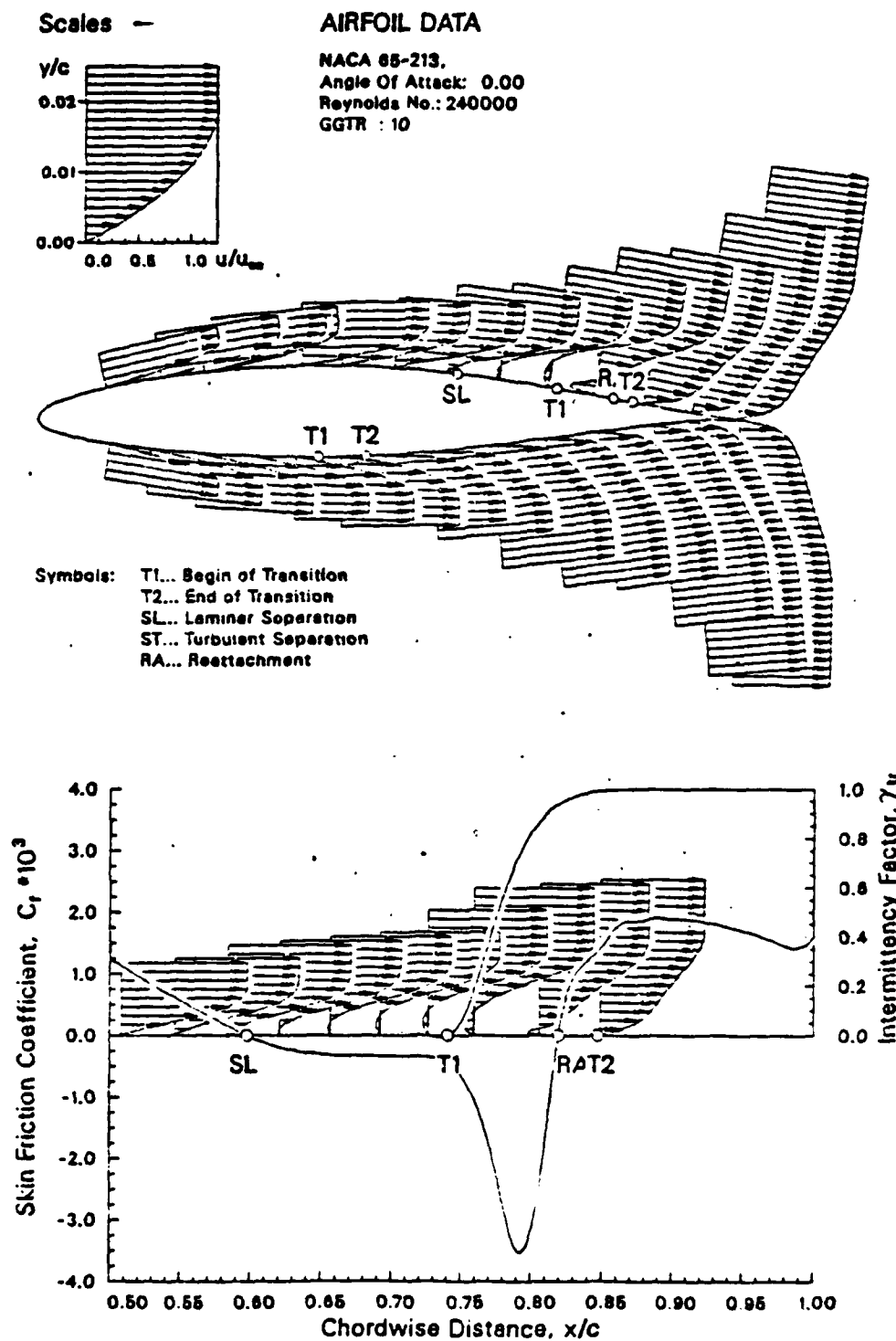


Figure 4.16 Boundary layer profiles on the NACA 65-213 at $Re = 240,000$
AOA = 0 deg and $G_{ytr} = 10$.

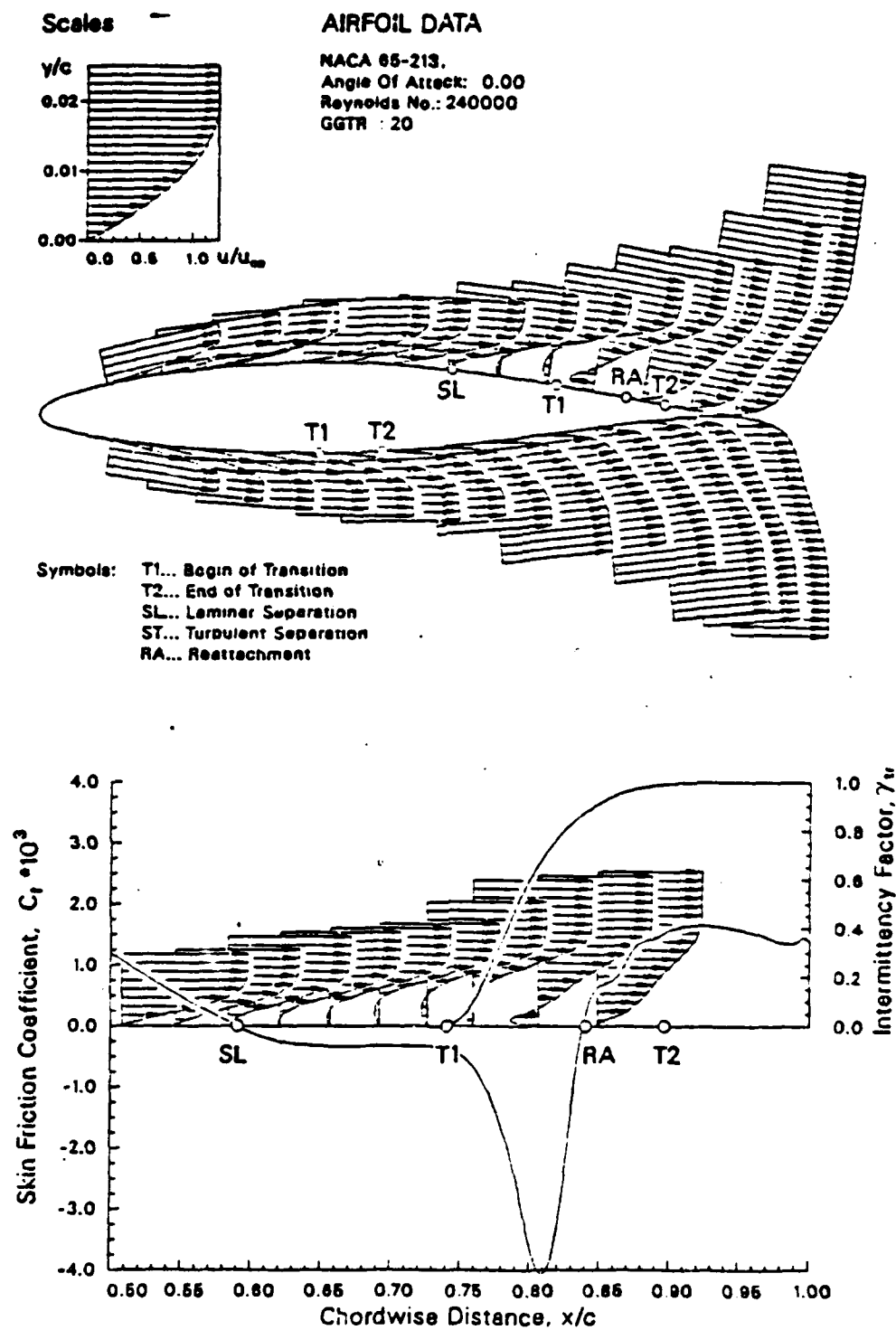


Figure 4.17 Boundary layer profiles on the NACA 65-213 at $Re = 240,000$
AOA = 0 deg and $G_{ytr} = 20$.

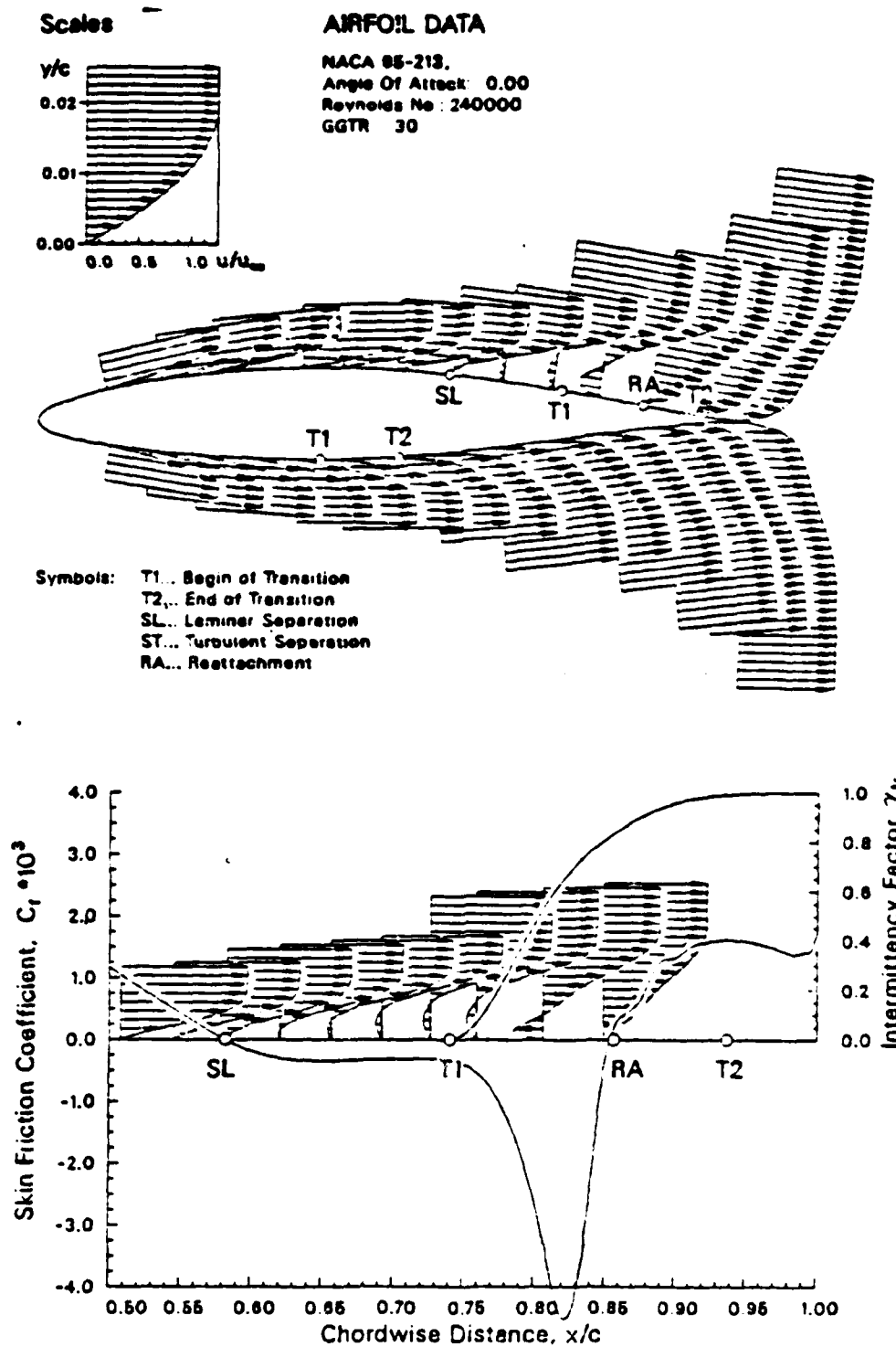


Figure 4.18 Boundary layer profiles on the NACA 65-213 at $Re = 240,000$
AOA = 0 deg and $G_{ytr} = 30$.

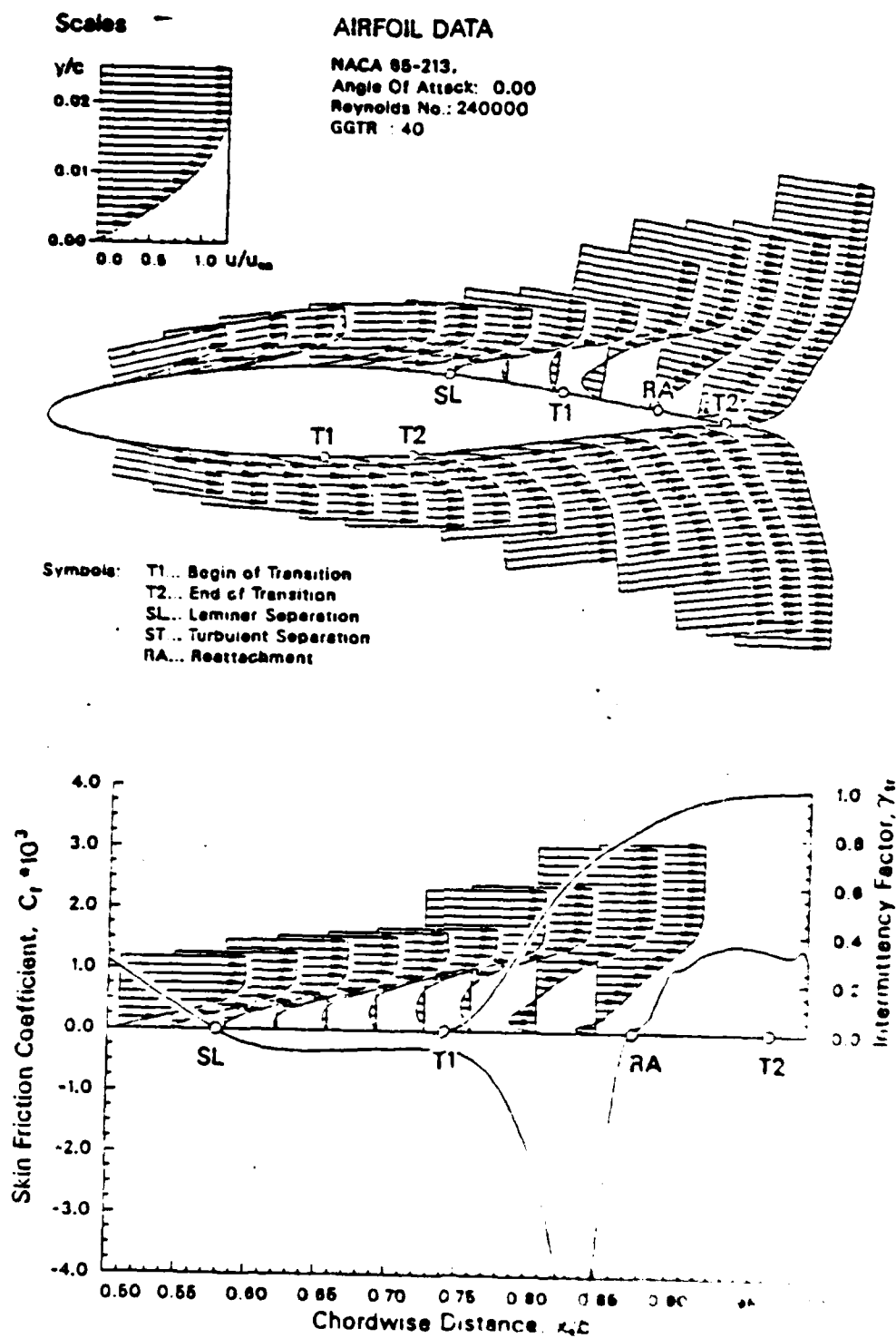


Figure 4.19 Boundary layer profiles on the NACA 65-213 airfoil
 AOA = 0 deg and $C_{xtr} = 0.0$

AD-A182 091

VISCOUS/INVISCID INTERACTION ANALYSIS OF THE
AERODYNAMIC PERFORMANCE OF THE NACA 65-213 AIRFOIL(U)
NAVAL POSTGRADUATE SCHOOL MONTEREY CA P H SUBROTO

2/2

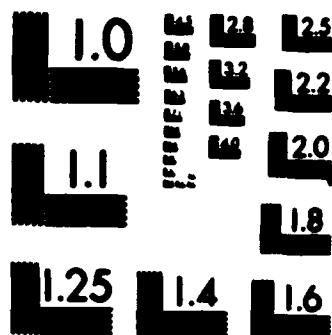
UNCLASSIFIED

MAR 87

F/G 20/4

NL





MICROCOPY RESOLUTION TEST CHART
NATIONAL BUREAU OF STANDARDS-1963-A

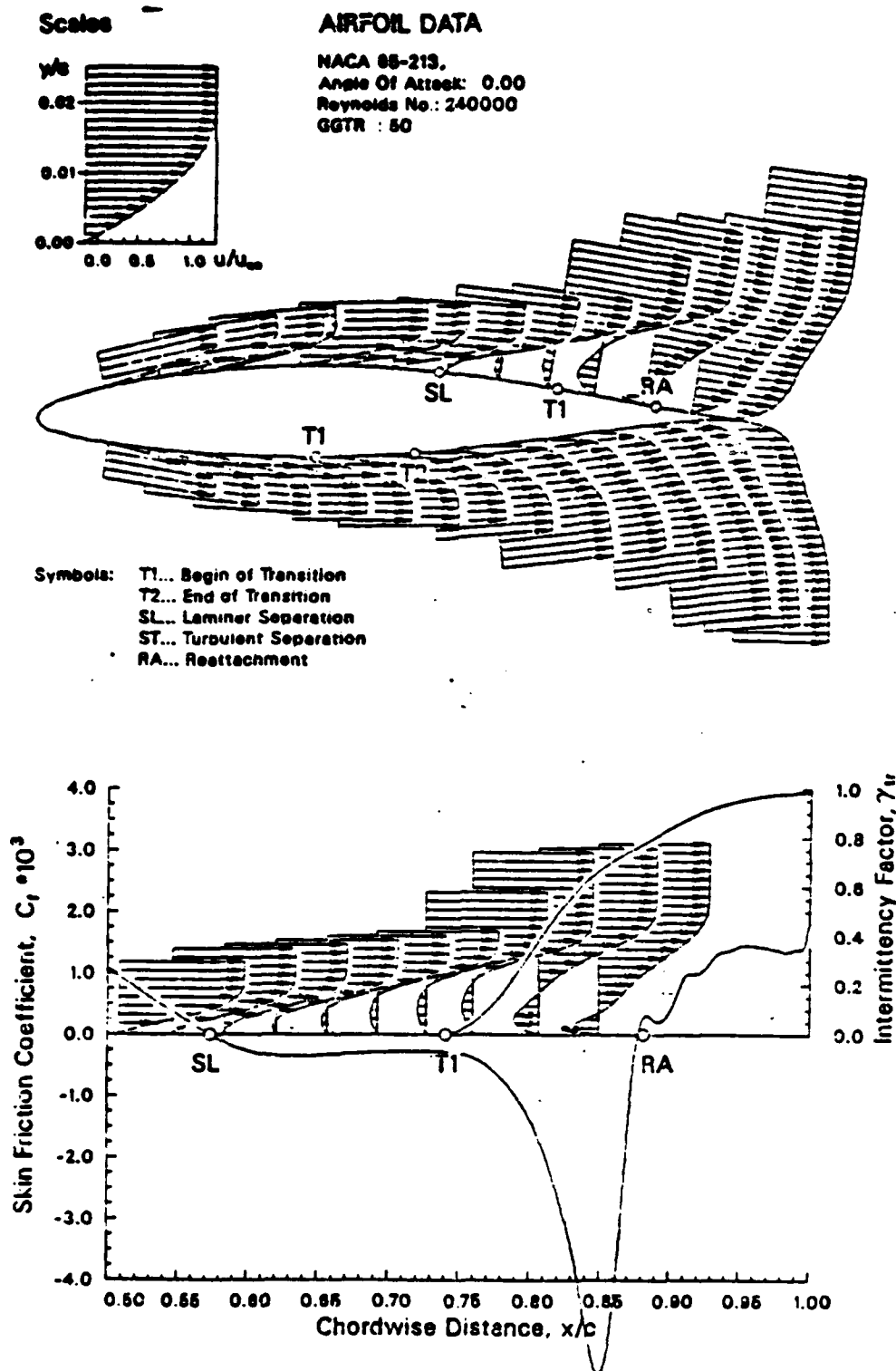


Figure 4.20 Boundary layer profiles on the NACA 65-213 at $Re = 240,000$
 $AOA = 0$ deg and $G_{ytr} = 50$.

V. CONCLUSION AND RECOMMENDATION

Cebeci's viscous inviscid interaction program was applied to the analysis of steady two dimensional incompressible flow past a NACA 65-213 airfoil at zero angle of attack at a Reynolds number of 240,000. Predicted boundary layer characteristics were found to be quite sensitive to the choice of boundary layer transition begin and length. Good agreement with the experimental results of *Hoheisel et al* could be obtained by proper choice of both transition begin and length. Further detailed measurements and calculations for other airfoils at low Reynolds number are recommended in order to further validate the predictive capability of the viscous inviscid interaction method.

APPENDIX A

FORTRAN PROGRAM

CSNOEXT

```
*****
*
* THIS PROGRAM CALCULATE THE PRESSURE DISTRIBUTIONS IN THE
* AIRFOIL AT ANY ANGLE OF ATTACK, BY USING PANEL METHOD IN
* 2-D, INVISCID, STEADY FLOW.
* IMPLEMENTATION OF VORTEX AND SOUCRE DISTRIBUTIONS ARE USED
* ALL VELOCITIES AND LENGTH ARE NORMALIZED BY FREE STREAM
* VELOCITY AND CHORD LENGTH RESPECTIVELY.
*
* WRITTEN BY : CAPT.INDAF PHUTUT SUBROTO
* NAVAL POSTGRADUATE SCHOOL
* MONTEREY, CA., OCTOBER 1986
*
*****
```

```
C
COMMON /NODE/ N
COMMON /AAA/ AA(100,100), AAX(100,100), AAY(100,100), AAT(100,100)
COMMON /BBB/ BB(100,100), BBX(100,100), BBY(100,100), BBT(100,100)
COMMON /STAR/ BSTAR(100), CSTAR(100)
COMMON /ALBE/ ALPA(100), BETA(100)
COMMON /VEL/ VI(100), VXI(100), VYI(100)
COMMON /XY/ X(100), Y(100), XB(100), YB(100)
COMMON /SSS/ S(100), SIGMA(100), SUMB(100)
COMMON /ANGLE/ AN, ANG, TPI, TH(100)
COMMON /PRESS/ CP(100)
```

```
C
C ----INPUT DATA : #NODE, # AOA ----
C
```

```
1 READ(5,1) NN, AN
  FORMAT(I10, F10.4)
  PI = 4.*ATAN(1.0)
  ANG = AN/180.*PI
  VXA = -COS(ANG)
  VYA = -SIN(ANG)
  TPI = .5/PI
  DO 10 I = 1, NN
    READ(5,5) XB(I), YB(I)
10 CONTINUE
5  FORMAT(2F10.5)
```

```
C
*****
*
* COMPUTE THE ANGLES AND LENGTHS OF EACH PANELS,
* CALCULATE THE COORDINATE OF CONTROL POINTS
*
*****
```

```
C
N = NN-1
SS = 0.0
DO 15 I = 1, N
  X(I) = .5*(XB(I) + XB(I+1))
  Y(I) = .5*(YB(I) + YB(I+1))
  TH(I) = ATAN2 (YB(I+1)-YB(I), XB(I+1)-XB(I))
  S(I) = SORT((XB(I+1)-XB(I))**2 + (YB(I+1)-YB(I))**2)
  SS = SS + S(I)
15 CONTINUE
```

```
C
*****
*
* COMPUTE TIME INDEPENDENT INFLUENCE COEFFICIENTS
*
```

```

*      FOR NORMAL, TANGENTIAL ,X AND Y DIRECTION      *
*      *      *      *      *      *      *      *      *
*****
C
DO 25 I= 1,N
  DO 25 J= 1,N
    IF(I .EQ. J) THEN
      AA(I,J) = 0.5
      BB(I,J) = 0.0
      AAX(I,J) = -0.5*SIN(TH(I))
      BBX(I,J) = 0.5*COS(TH(I))
      AAY(I,J) = 0.5*COS(TH(I))
      BBY(I,J) = 0.5*SIN(TH(I))
      AAT(I,J) = 0.0
      BBT(I,J) = 0.5
    ELSE
      A = -(X(I)-XB(J))*COS(TH(J)) - (Y(I)-YB(J))*SIN(TH(J))
      B = (X(I)-XB(J))**2 + (Y(I)-YB(J))**2
      C = SIN(TH(I)-TH(J))
      D = COS(TH(I)-TH(J))
      E = (X(I)-XB(J))*SIN(TH(J)) - (Y(I)-YB(J))*COS(TH(J))
      F = ALOG(1.0 + S(J)*(S(J)+2.*A)/B)
      G = ATAN2 (E*S(J), B+A*S(J))
      AA(I,J) = TPI*(.5*C*F - D*G)
      BB(I,J) = TPI*(.5*D*F + C*G)
      AAX(I,J) = TPI*(-.5*COS(TH(J))*F + SIN(TH(J))*G)
      BBX(I,J) = TPI*(-.5*SIN(TH(J))*F - COS(TH(J))*G)
      AAY(I,J) = BBX(I,J)
      BBY(I,J) = -AAX(I,J)
      AAT(I,J) = -BB(I,J)
      BBT(I,J) = AA(I,J)
    ENDIF
  25 CONTINUE
C
C
*****
*      SETUP MATRICES,SET GAMA=1.0, SOLVE THE SYSTEM      *
*      BY USING GAUSSIAN ELIMINATION WITH PARTIAL PIVOTING *
*      FOR TWO RIGHT HAND SIDES.      *
*****
C
DO 68 I =1,N
  SUMB(I) = 0.0
  DO 680 J =1,N
    680 SUMB(I) = SUMB(I) + BB(I,J)
    BSTAR(I) = -SUMB(I)
    CSTAR(I) = -VXA * SIN(TH(I)) + VYA * COS(TH(I))
    AA(I,N+1) = BSTAR(I)
    AA(I,N+2) = CSTAR(I)
  68 CONTINUE
C
  CALL GAUSS(2)
C
DO 500 I =1,N
  ALPA(I) = AA(I,N+1)
  BETA(I) = AA(I,N+2)
500 CONTINUE
C
C
C
C
---- MEET KUTTA CONDITIONS ,SOLVE FOR VORTEX STREGNTH(GAMA)
      USING QUADRATIC EQUATION ----
C
AX1 = 0.0
AXN = 0.0
AY1 = 0.0
AYN = 0.0
BX1 = 0.0
BXN = 0.0

```



```

BY1 = 0.0
BYN = 0.0
DO 510 J = 1,N
  AX1 = AX1 + AAX(1,J)*ALPA(J)+BBX(1,J)
  AXN = AXN + AAX(N,J)*ALPA(J)+BBX(N,J)
  AY1 = AY1 + AAY(1,J)*ALPA(J)+BBY(1,J)
  AYN = AYN + AAY(N,J)*ALPA(J)+BBY(N,J)
  BX1 = BX1 + AAX(1,J)*BETA(J)
  BXN = BXN + AAX(N,J)*BETA(J)
  BY1 = BY1 + AAY(1,J)*BETA(J)
  BYN = BYN + AAY(N,J)*BETA(J)
510 CONTINUE
C
  EE = AX1**2+AY1**2 - AXN**2-AYN**2
  PP = AX1*BX1+AY1*BY1 - AXN*BXN-AYN*BYN +(AXN-AX1)*VXA
  + (AYN-AY1)*VYA
  QQ = BX1**2+BY1**2-BXN**2-BYN**2 +2.*(BXN-BX1)*VXA +2.*
  + (BYN-BY1)*VYA
C
  R = PP*PP - EE*QQ
  GAMA1 = (-PP + SORT(R))/(EE)
  GAMA2 = (-PP - SORT(R))/(EE)
  IF(ABS(GAMA1) .GT. ABS(GAMA2)) THEN
    GAMA = GAMA2
  ELSE
    GAMA = GAMA1
  ENDIF
C
  ---- SOLVE THE SOURCE STRENGTH SIGMA(J) ----
  DO 550 J = 1,N
    SIGMA(J) = GAMA*ALPA(J) + BETA(J)
550 CONTINUE
  CALL CPRESS(GAMA)
C
  ---- PRINT LIFT COEFFICIENT AND MOMENT COEFFICIENT ABOUT
  LEADING EDGE ----
C
  CFX = 0.0
  CFY = 0.0
  CM = 0.0
  DO 110 I = 1,N
    DX = XB(I+1) - XB(I)
    DY = YB(I+1) - YB(I)
    CFX = CFX + CP(I)*DY
    CFY = CFY - CP(I)*DX
    CM = CM + CP(I)*(DX*X(I)+DY*Y(I))
110 CONTINUE
  CL = CFY*COS(ANG) - CFX*SIN(ANG)
  CD = CFX*COS(ANG) - CFY*SIN(ANG)
  WRITE(8,120) CL
  WRITE(8,125) CD
  WRITE(8,130) CM
120 FORMAT(//,15X,'CL      = ',F10.5)
125 FORMAT(//,15X,'CD      = ',F10.5)
130 FORMAT(//,15X,'CMLE     = ',F10.5)
  PRINT*,"COMPUTATION COMPLETED"
  STOP
  END
*****
*
* SUBROUTINE GAUSS
* SOLVE SIMULTANEOUS EQUATION WITH TWO RIGHT HAND SIDES
* BY GAUSS ELIMINATION WITH PARTIAL PIVOTING
* SOLUTIONS STORES IN COLUMNS NEQNS+1 AND NEQNS+2 OF
* MATRIX AA(NEQNS,NEQNS+2).
* (AA) = COEFFICIENT OF AUGMENTED MATRIX
*

```

```

*      NEQNS = NUMBER OF EQUATIONS      *
*      NRHS  = NUMBER OF RIGHT HAND SIDES *
*****
C      SUBROUTINE GAUSS(NRHS)
C
COMMON /NODE/ NEQNS
COMMON /AAA/ AA(100,100), AAX(100,100), AAY(100,100), AAT(100,100)
NP      = NEQNS+1
NTOT    = NEQNS+NRHS
C
C      GAUSS REDUCTION
C
DO 40 I = 2,NEQNS
C
C      SEARCH FOR LARGEST ENTRY IN (I-1)TH COLUMN
C      ON OR BELOW MAIN DIAGONAL
C
IM      = I-1
IMAX    = IM
AMAX    = ABS(AA(IM,IM))
DO 10 J = I,NEQNS
IF(AMAX .GE. ABS(AA(J,IM))) GO TO 10
IMAX    = J
AMAX    = ABS(AA(J,IM))
10 CONTINUE
C
C      SWITCH (I-1)TH AND IMAXTH EQUATIONS
C
IF(IMAX .NE. IM) GO TO 30
DO 20 J = IM,NTOT
TEMP    = AA(IM,J)
AA(IM,J) = AA(IMAX,J)
AA(IMAX,J) = TEMP
20 CONTINUE
C
C      ELIMINATE (I-1)TH UNKNOWN FROM ITH THRU
C      (NEQNS)TH EQUATIONS
C
30 DO 40 J = I,NEQNS
R        = AA(J,IM)/AA(IM,IM)
DO 40 K = I,NTOT
AA(J,K) = AA(J,K)-R*AA(IM,K)
40 CONTINUE
C
C      BACK SUBSTITUTION
C
DO 70 K = NP,NTOT
AA(NEQNS,K) = AA(NEQNS,K)/AA(NEQNS,NEQNS)
DO 60 L = 2,NEQNS
I        = NEQNS+1-L
IP       = I+1
DO 50 J = IP,NEQNS
50 AA(I,K) = AA(I,K)-AA(I,J)*AA(J,K)
60 AA(I,K) = AA(I,K)/AA(I,I)
70 CONTINUE
RETURN
END
C
*****
*      SUBROUTINE CPRESS
*      CALCULATE PRESSURE COEFFICIENTS AND TOTAL VELOCITY
*      AT MID POINTS (CONTROL POINTS)
*
*****
C      SUBROUTINE CPRESS(GAMA)

```

C

```

COMMON /AAA/ AA(100,100),AAX(100,100),AAY(100,100),AAT(100,100)
COMMON /BBB/ BB(100,100),BBX(100,100),BBY(100,100),BBT(100,100)
COMMON /PRESS/ CP(100)
COMMON /MODE/ N
COMMON /ANGLE/ AN,ANG,TPI,TH(100)
COMMON /SSS/ S(100),SIGMA(100),SUMB(100)
COMMON /VEL/ VI(100),VXI(100),VYI(100)
COMMON /XY/ X(100),Y(100),XB(100),YB(100)
WRITE(8,5)
5  FORMAT(//,15X,'NACA 23012' )
   WRITE(8,6) N
   WRITE(8,7) AN
6  FORMAT(15X,'NUMBER OF PANELS =' ,I3)
7  FORMAT(15X,'ANGLE OF ATTACK =' ,F7.4)
   WRITE(8,20)
   DO 12 I = 1,N
     SUMM = 0.0
     DO 13 J = 1,N
       SUMM = SUMM + AAT(I,J)*SIGMA(J)+GAMA*BBT(I,J)
13  CONTINUE
     VI(I) = SUMM + COS(TH(I)-ANG)
     CP(I) = 1.0 - VI(I)**2
     WRITE(8,30) I,X(I),Y(I),VI(I),GAMA,SIGMA(I),CP(I)
     WRITE(6,31) X(I),-CP(I)
12  CONTINUE
20  FORMAT(//,3X,'PNL(I)',3X,'X(I)',7X,'Y(I)',6X,'VEL(I)',5X,
1   'GAMA',5X,'SIGMA(I)',4X,'CP(I)' //)
30  FORMAT(2X,I3,5X,F8.5,3X,F8.5,3X,F8.5,3X,F8.5,3X,F8.5,3X,F8.5)
31  FORMAT(2F10.5)
   RETURN
   END

```

C

APPENDIX B PROGRAM OUTPUT

SOURCE AND VORTEX PANEL SOLUTION
NACA 23012
NUMBER OF PANELS = 34
ANGLE OF ATTACK = 12.0000

PNL(I)	X(I)	Y(I)	VEL(I)	GAMMA	SIGMA(I)	CP(I)
1	0.97500	-0.00350	-0.89112	0.39035	2.28747	0.20590
2	0.92500	-0.00965	-0.88365	0.39035	2.31831	0.21917
3	0.85000	-0.01695	-0.88620	0.39035	2.40999	0.21464
4	0.75000	-0.02580	-0.88782	0.39035	2.41656	0.21177
5	0.65000	-0.03335	-0.87216	0.39035	2.42538	0.23933
6	0.55000	-0.03920	-0.85087	0.39035	2.43692	0.27602
7	0.45000	-0.04325	-0.82394	0.39035	2.44450	0.32113
8	0.35000	-0.04470	-0.77104	0.39035	2.47951	0.40549
9	0.27500	-0.04370	-0.71339	0.39035	2.50195	0.49107
10	0.22500	-0.04125	-0.66069	0.39035	2.54546	0.56348
11	0.17500	-0.03735	-0.57694	0.39035	2.60630	0.66714
12	0.12500	-0.03210	-0.46811	0.39035	2.65463	0.78087
13	0.08750	-0.02765	-0.36096	0.39035	2.64815	0.86971
14	0.06250	-0.02435	-0.25392	0.39035	2.62380	0.93553
15	0.03750	-0.01985	-0.00657	0.39035	2.65274	0.99996
16	0.01875	-0.01470	0.41263	0.39035	2.58301	0.82974
17	0.00625	-0.00615	1.41005	0.39035	2.67224	-0.98825
18	0.00625	0.01335	2.61069	0.39035	-0.18981	-5.81568
19	0.01875	0.03140	2.59588	0.39035	-1.31312	-5.73860
20	0.03750	0.04260	2.32749	0.39035	-1.62967	-4.41720
21	0.06250	0.05355	2.17813	0.39035	-1.84536	-3.74423
22	0.08750	0.06115	2.07578	0.39035	-2.00811	-3.30887
23	0.12500	0.06810	1.90685	0.39035	-2.23615	-2.63608
24	0.17500	0.07345	1.74625	0.39035	-2.40177	-2.04941
25	0.22500	0.07550	1.63801	0.39035	-2.46583	-1.68307
26	0.27500	0.07575	1.55856	0.39035	-2.50044	-1.42910
27	0.35000	0.07345	1.45669	0.39035	-2.55339	-1.12194
28	0.45000	0.06775	1.35494	0.39035	-2.58751	-0.83586
29	0.55000	0.05940	1.27629	0.39035	-2.61244	-0.62891
30	0.65000	0.04915	1.20826	0.39035	-2.62994	-0.45989
31	0.75000	0.03720	1.13842	0.39035	-2.65075	-0.29600
32	0.85000	0.02380	1.07219	0.39035	-2.65258	-0.14958
33	0.92500	0.01300	1.01371	0.39035	-2.57577	-0.02761
34	0.97500	0.00460	0.89101	0.39035	-2.59479	0.20611

CL = 1.57532

CD = -0.63272

CMLE = -0.41146

APPENDIX C

TABLE I

TABLE 2
EFFECT OF GGTR AND XTRU ON THE BUBBLE LENGTH

	GGTR = 10	20	40	80	120
XTRU = .64	.6567-.6745	.6567-.6920	.6567-.7093	.6567-.7263	.6387-.7593
XTRU = .65	.6567-.6920	.6745-.7093	.6567-.7263	.6387-.7429	.6387-.7752
XTRU = .66	.6745-.7093	.6567-.7093	.6567-.7263	.6387-.7593	.6204-.7908
XTRU = .67	.6745-.7093	.6745-.7093	.6387-.7429	.6204-.7752	.6204-.8207
XTRU = .68	.6567-.7263	.6387-.7593	.6387-.7593	.6204-.8060	.6020-.8489
XTRU = .69	.6387-.7429	.6387-.7593	.6204-.7752	.6020-.8350	.5834-.8876
XTRU = .70	.6387-.7593	.6204-.7752	.6204-.8060	.6020-.8623	.6204-.8060
XTRU = .72	.6204-.7908	.6204-.8060	.6020-.8350	.5834-.8752	.5647-.9216 .9415-.9740 (turb)
XTRU = .74	.6020-.8060	.6020-.8350	.5834-.8623	.5647-.9319	-
XTRU = .76	.6020-.8350	.5834-.8623	.5647-.8752	-	-

NACA 65-213

Reynolds No.

= 240,000

AOA

= 0.0 deg

XTRU

= Begin of transition (Upper Surface)

XTRL

= Begin of transition (Lower Surface fixed at 0.4)

GGTR

= Empirical Constant ($G_{\gamma_{tr}}$)

APPENDIX D

TABLE II

TABLE 3
EFFECT OF GGTR AND XTRU ON THE SHAPE FACTOR(H)
AT POINT OF ZERO SKIN FRICTION

	GGTR = 10	20	40	80	120
XTRU = .64	2.830	2.780	2.726	2.7423	2.722
XTRU = .65	2.7262	2.745	2.684	2.7024	2.7013
XTRU = .66	2.586	2.624	2.660	2.691	2.682
XTRU = .67	2.604	2.657	2.5941	2.653	2.78
XTRU = .68	2.95	2.478	2.39	2.6478	2.589
XTRU = .69	2.877	2.776	2.644	2.5554	2.5844
XTRU = .70	2.5524	2.523	2.534	2.5152	2.478
XTRU = .72	2.54	2.583	2.60	2.487	2.480
XTRU = .74	2.575	2.609	2.692	2.669	-
XTRU = .76	2.624	2.667	2.82	-	-

NACA 65-213
 Reynolds No. = 240,000
 AOA = 0.1 deg
 H = 0.0
 XTRU = Begin of transition (Upper Surface)
 XTRL = begin of transition (Lower Surface fixed at 0.4)
 GGTR = Empirical Constant (G_{yr})

APPENDIX E

TABLE III

TABLE 4
EFFECT OF GGTR AND XTRU ON THE DRAG COEFFICIENT (CD)

	GGTR = 10	20	40	80	120
XTRU = .64	TE:.01025 WK:.01064	.01015 .01054	.010029 .010423	.009876 .010274	.009813 .010225
XTRU = .65	TE:.01022 WK:.01062	.01013 .01052	.010022 .010416	.009900 .010301	.009785 .010193
XTRU = .66	TE:.01010 WK:.01049	.010112 .01050	.010018 .010398	.009845 .010248	.009741 .010149
XTRU = .67	TE:.01016 WK:.01055	.01010 .01050	.00926 .010316	.009785 .010185	.009816 .010236
XTRU = .68	TE:.01016 WK:.01055	.009980 .010383	.009944 .010338	.009846 .010246	.009865 .010312
XTRU = .69	TE:.01001 WK:.01050	.010015 .010405	.009948 .010339	.009886 .010316	.010014 .010467
XTRU = .70	TE:.01011 WK:.01049	.010015 .010403	.009900 .010334	.009964 .010382	.010173 .010729
XTRU = .72	TE:.01008 WK:.01047	.00997 .010352	.009981 .010380	.010034 .010481	.010644 .011202
XTRU = .74	TE:.01004 WK:.01042	.01005 .010405	.010017 .010411	.010489 .010947	- -
XTRU = .76	TE:.00999 WK:.01037	.010024 .010434	.010222 .010672	- -	- -

NACA 65-213

Reynolds No.

AOA

TE

WK

XTRU

XTRL

GGTR

= 240,000

= 0.0 deg

= Cd at the trailing edge

= Cd at the wake

= Begin of transition (Upper Surface)

= Begin of transition (Lower Surface fixed at 0.4)

= Empirical Constant (G_{yu})

APPENDIX F **TABLE IV**

TABLE 5
EFFECT OF GGTR AND XTRU ON THE LIFT COEFFICIENT (CL)

	GGTR = 10	20	40	80	120
XTRU = .64	.1550	.1555	.1559	.1562	.1560
XTRU = .65	.1557	.15602	.1565	.1569	.1571
XTRU = .66	.1571	.15630	.1573	.1581	.1589
XTRU = .67	.1568	.15692	.1588	.1598	.1599
XTRU = .68	.1570	.1588	.1594	.1609	.1630
XTRU = .69	.1580	.15963	.1609	.1632	.1693
XTRU = .70	.1596	.16072	.1625	.1677	.1800
XTRU = .72	.1624	.16464	.1687	.1815	.2074
XTRU = .74	.1671	.1708	.1784	.2045	-
XTRU = .76	.1740	.1805	.1910	-	-

NACA 65-213

Reynolds No.

AOA

XTRU

XTRL

GGTR

= 240,000

= 0.0 deg

= Begin of transition (Upper Surface)

= Begin of transition (Lower Surface fixed at 0.4)

= Empirical Constant ($G_{\gamma_{tr}}$)

LIST OF REFERENCES

1. John D. Anderson Jr., *Fundamental of Aerodynamics*, McGraw Hill, 1984
2. Arnold M. Kuethe and Chuen-Yen Chow, *Foundations of Aerodynamics*, third edition, John Wiley & Sons, 1976
3. John J. Bertin and Michael L. Smith, *Aerodynamics For Engineers*, Prentice Hall, 1979
4. Jack Moran, *An Introduction to Theoretical and Computational Aerodynamics*, John Wiley & Sons, 1984
5. H. Schlichting, *Boundary Layer Theory*, 7th edition, McGraw Hill, 1979
6. T. Sarpkaya, *Viscous Flow*, Naval Postgraduate School, 1973
7. M.J. Kim and D.T. Mook, *Application of Continuous Vorticity Panels to General Unsteady Incompressible Two-Dimensional Lifting Flows*, Journal of Aircraft, Vol.23, No.6, 1986
8. Tuncer Cebeci, *Numerical and Physical Aspects of Aerodynamic Flows II*, Springer-Verlag, 1983
9. I.H. Abbot and A.E. von Doenhoff, *Theory of Wing Section*, Dover Publication, 1958
10. W.J. Feiereisen and M. Acharva, *Modeling of Transition and Surface Roughness Effects in Boundary-Layer flows*, AIAA Journal, Vol.24, No.10, October 1986
11. R.L. Davis and J.E. Carter, *Counterrotating Streamline Pattern in a Transitional Separation Bubble*, AIAA Journal, Vol.24, No.5, May 1986
12. V.N. Vatsa and J.E. Carter, *Analysis of Airfoil Leading-Edge Separation Bubbles*, AIAA Journal, Vol.22, No.12, December 1984
13. Tuncer Cebeci and P. Bradshaw, *Momentum Transfer in Boundary Layers*, Hemisphere Publ. Co., 1977
14. H. Hoheisel, M. Hoeger (Institute fur Entwurfsaerodynamik, Braunschweig, W.Germany) and P. Meyer, G. Koerber (Institut Franco-Allemand de Recherches de Saint-Louis, France), *A Comparison of Laser-Doppler Anemometry and Probe Measurements within the Boundary Layer of an Airfoil at Subsonic Flow*. Presented at the Second International Symposium on Applications Laser Anemometry to Fluid Mechanics. Lisbon, Portugal, 1984.

15. R.E. Melnik, R.R. Chow, H.R. Mead, and A. Jameson. *An Improved Viscid Inviscid Interaction Procedure for Transonic Flow over Airfoils*. NASA Contractor Report 3805, July 1984
16. R.L. Davis and J.E. Carter, *Analysis of Airfoil Transitional Separation Bubbles*. NASA Contractor Report 3791, October 1985
17. R.D. Zucker, *The Current Aerodynamic Analysis*, Naval Postgraduate School. 1979
18. D. Althaus and F.X. Wortmann, *Stuttgarter Profilkatalog I*, Vieweg 1979.

INITIAL DISTRIBUTION LIST

	No. Copies
1. Defense Technical Information Center Cameron Station Alexandria, VA 22304-6145	2
2. Library, Code 0142 Naval Postgraduate School Monterey, CA 93943-5002	2
3. Chairman, Dept. of Aeronautics, Code 67 Naval Postgraduate School Monterey, California 93943-5000	6
4. Dr. Tuncer Cebeci Professor, Center for Aerodynamic Research, California State University Long Beach, California 90840	1
5. Dr. B.J. Habibie Ketua BPPT Jl. Thamrin No.8 Jakarta, Indonesia	1
6. Dirdik Mabes TNI-AU Jl. Gatot Subroto Jakarta, Indonesia	1
7. Komandan Koharmatau Lanuma Husein Sastranegara Bandung, Indonesia	1
8. Dirpers Mabes TNI-AU Jl. Gatot Subroto Jakarta, Indonesia	1
9. Office of the Defence Attache Embassy of the Republic of Indonesia 2020 Massachusetts Avenue, N.W. Washington, D.C.20036	2
10. Komandan Skadron 31 Lanuma Halim Perdanakusuma Jakarta, Indonesia	1
11. Perpustakaan AAU Lanuma Adisucipto Yogyakarta, Indonesia	1

- | | | |
|-----|-----------------------------------------------------------------------------------------------------------------|---|
| 12. | Lembaga Ilmu Pengetahuan Indonesia (LIPI)
Jl. Gatot Subroto
Jakarta, Indonesia | 1 |
| 13. | Major Tarigan
SMC 2782
Naval Postgraduate School
Monterey, California 93943 | 1 |
| 14. | Major Soerjono
SMC 2155
Naval Postgraduate School
Monterey, California 93943 | 1 |
| 15. | Subroto, Phutut Hadi
Skadron 31, Halim AFB
Jakarta, Indonesia | 4 |
| 16. | Paik, Seung Woock
982-1, Sin-Jung 4 Dong
Kang-Seo Ku (150-02)
Seoul, Korea | 1 |
| 17. | Perpustakaan SMP Negeri Wanadadi
Banjarnegara, Jawa Tengah
Indonesia | 1 |
| 18. | Perpustakaan SMA Negeri
Banjarnegara, Jawa Tengah
Indonesia | 1 |
| 19. | Agus Budiyanto
Fak. Teknik Jur. Sipil
NIM. I.0180101
Universitas Sebelas Maret
Surakarta, Indonesia | 1 |

END

7-87

DTIC